~~SOME~~ REACTIONS IN GAS SOLID SYSTEMS

A thesis

submitted in part fulfillment of the requirements

of the Degree of Doctorate of Philosophy

of the

University of London

by

Ernest Frederick McFarlane B.Sc.

Department of Physical and Inorganic Chemistry

Imperial College of Science and Technology

October 1960.

ABSTRACT

The kinetics of the oxidation of evaporated lithium films and the nitridation of both solid and molten bulk lithium have been investigated.

Oxidation was studied using a constant pressure technique over the range 10^{-4} - 10^{-2} m.m. Hg and between 78°K and 323°K. The results were consistent with a modified Mott and Cabrera theory of very thin film formation. The rate was proportional to $p^{\frac{1}{2}}$ indicating dissociative O_2 adsorption. A linear dependence of activation energy on the reciprocal oxide thickness was found as predicted by the theory, the value of the maximum activation energy at infinite thickness being 17 kcal.mole^{-1}. An estimation was made of the total number of metal sites/unit area of interface from which the metal ion penetrates the oxide lattice. Above a certain thickness and temperature, breakaway of the oxide layer occurs regenerating the "original" metal surface for further oxidation, due to stresses set up by incongruent substrate/epitaxial lattice parameters and vacancy formation at the metal/oxide interface. A mechanism for O_2 sorption to account for the $p^{\frac{1}{2}}$ relationship has been proposed based upon the existence of surface kink sites.

The nitridation of solid lithium was examined at constant pressure between 273°K and 433°K, over the range 20 to 600 m.m. Hg. A nucleation period with an increasing rate was found, followed by linear uptake. The nucleation period obeyed a power law indicating two or three dimensional growth of nuclei. The activation energy was zero and the rate was proportional to $p^{1.6}$. A mechanism, leading to these results, has been proposed, based on the generation of cracks in the nitride crust (under the stresses predicted by the Pilling-Bedworth rule), which remained statistically constant in number and effective dimensions, and through which a mixture of Poiseulle and Knudsen gas flow to the metal interface occurs.

The kinetics of the nitridation of molten lithium, studied at constant pressure between 500 and 638°K over the range 10.43 to 44.44 cm. Hg, conformed approximately to the parabolic law. The rate was independent of pressure, but dependent on temperature with an activation energy of 15.42±0.34 kcal.mole^{-1}, consistent with an outward diffusion of Li^+ ions - soluble in the Li_3N lattice - as the rate determining process.

ACKNOWLEDGEMENTS

I wish to express my thanks to Professor R.M. Barrer for the provision of research facilities in the Department of Physical and Inorganic Chemistry of Imperial College where this work was carrid out between September 1957 and October 1960.

My thanks are due to Drs. P.W.M. Jacobs and P.M. Gundry for their helpful discussions and advice.

I am indebted to Johnson Mathey Ltd. and the United Kingdom Atomic Energy Authority for the supply of lithium.

I also wish to acknowledge the award of a maintenance grant by the United Kingdom Atomic Energy Authority.

I should like to express my gratitude to all the members of the College Technical Staff for their unfailing assistance, and to my follow students, in particular the occupants of Room 124, whose discussions and companionship have greatly added to the pleasure of the work.

I owe an inestimable debt of gratitude to my supervisor and mentor Professor F.C. Tompkins for his stimulating discussions and guidance throughout this work.

Finally I wish to acknowledge the part played by my wife, without whose patience and unflagging encouragement this thesis could not, in the first place, have been attempted.

E.F. McFarlane

CONTENTS

Page

Abstract

Acknowledgements

1. Introduction 1

1.1. The Lithium Oxidation System 1
1.2. Laws of Oxidation Kinetics 1

1.2.1. The Logarithmic Laws 2
1.2.2. The Parabolic Law 5
1.2.3. The Rectilinear Law 8
1.2.4. The Pilling Bedworth Principle 9
1.2.5. The Cubic Law 11

1.3. Theory and Mechanism 13

1.3.1. General Considerations 13
1.3.2. Formation of Coherent Uniform Layers 17
1.3.3. Oxide Layers Subject to Flaws and Mechanical Imperfections 40

1.4. Literature Survey of Previous Investigations on Alkali and Alkaline Earth Elements 44

1.4.1. Oxidation of Alkali Metals 44
1.4.2. Oxidation of Alkaline Earth Metals 48
1.4.3. Nitridation of Lithium 56
1.4.4. Nitridation of the Alkaline Earth Elements 59

2. Experimental 64

2.1. Oxidation of Evaporated Lithium Films 64

2.1.1. Apparatus 64
2.1.2. Experimental Procedure 73

2.2. Nitridation of Bulk Lithium 81

2.2.1. Apparatus 81
2.2.2. Experimental Procedure 86

Contents continued.

	Page
3. Results and Discussion	89
3.1. Oxidation of Evaporated Lithium Films	89
3.1.1. Qualitative Observations	89
3.1.2. Kinetics of Sorption	91
3.1.3. Dependence of the Rate on Temperature	93
3.1.4. Dependence of Rate on Pressure	110
3.1.5. The Point of Breakaway	113
3.1.6. Discussion	115
3.2. Nitridation of Bulk Solid Lithium	137
3.2.1. Nucleation Period	137
3.2.2. Linear Uptake	139
3.2.3. Dependence of Rate on Pressure	143
3.2.4. Dependence of Rate on Temperature	147
3.2.5. Appearance of Reaction Product	149
3.2.6. Conclusions and Discussion	150
3.3. Nitridation of Molten Lithium	155
3.3.1. Kinetics of Nitridation	155
3.3.2. Dependence of Rate on Temperature	157
3.3.3. The Dependence of Rate on Pressure	160
3.3.4. Appearance of the Reaction Product	161
3.3.5. Discussion	162

1 INTRODUCTION

1.1. The Lithium Oxidation System.

Although there have been a large number of kinetic studies on the oxidation and nitridation of many metals there have been relatively few investigations of the alkali metals and in particular of lithium itself, which has interesting and unique features.

First, it has the simplest electronic structure of any metal, a comparatively small ionic radius of approximately 0.6 Å (1) and a relatively low work function (2.48 eV) (2).

Secondly, as the first member of its group, it resembles both Group IA members and the alkaline earths other than Be, the so-called "diagonal relationship". Thus, Li alone of the alkali metals but in common with the Group II elements forms a stable nitride by direct combination of the elements. It has extreme chemical reactivity and exists in the solid phase over a comparatively small range of temperature.

The complications involved in the manufacture, handling and storage of Li in the pure state and the consequent difficulties in obtaining clean reaction surfaces, due to its high reactivity, may well account for the comparatively few quantitative investigations.

1.2. Laws of Oxidation Kinetics.

Since the oxidation of metals commences at the surface, with the formation of a film, separation between the original participants of the reaction is rapidly brought about.

Some transport phenomena, through the film, is thus necessary, in order for reaction to proceed.

Recent developments of solid state theory have provided an understanding of many of the basic mechanisms of the transport process, and thus made possible theoretical interpretations of the oxidation laws found in practice.

Due to the effect of the barrier film, different kinetics are found to hold over different ranges of oxide thickness, and also of temperature and pressure.

The methods of investigation in most common use are either manometric, where the decrease of gas pressure or volume is measured, or gravimetric where increases in weight are observed. Results are thus usually expressed as increments in weight W per unit surface area at time t.

1.2.1. The Logarithmic Laws.

In logarithmic uptake, the rate is extremely fast initially, but after a comparatively short time, of perhaps a few minutes or hours, the rate falls to a very low value, at which oxidation can be regarded as having ceased. This type of behaviour is therefore often referred to as protective oxidation. With Al reacting with dry O_2, for instance, Hart (3) found that oxidation proceeds rapidly to a thickness of about 30 Å after which the rate is negligibly slow. Tamman (4) first proposed an equation in which the thickness of the oxide film at moderate temperatures is an exponential function of the time.

$$t = ae^{b\theta} \qquad (1)$$

where t is the time, θ the film thickness, and a and b constants. In this work the film thicknesses were observed by interference colours produced by the very thin films. This procedure was criticised on optical grounds by Evans (5) and Dunn (6), however, and the relationship was therefore of doubtful validity until it was verified for the oxidation of Zn below 400°C by Vernon, Ackeroyd and Stroud (7), using a more conventional technique.

Subsequent to these early experiments, many cases of an exponential dependence, under specific conditions of temperature and time, have been reported in the literature. The logarithmic equation in its more usual form,

$$X = k\ln(at + 1) \qquad (2)$$

where X is the thickness of the film at time t, k and a are constants, a having the dimension $(\text{time})^{-1}$, has been found applicable to the oxidation of copper (4, 8, 9, 10, 11), Zinc (4, 7), cadmium (4), lead (4), tin (4), manganese (4), iron (4, 12, 13, 14, 15), nickel (4, 16), aluminium (8, 17, 3), titanium (18) and tantalum (19).

This law referred to as the direct logarithmic law, usually applies at moderate to low temperature and results in relatively thin films. Thus Tylecote (11) has confirmed that the equation holds for films below a thickness of 10^5 Å.

The second form of logarithmic law, known as the inverse

log law, was first proposed by Mott on theoretical grounds in 1947 (20), and further developed by Mott and Cabrera in 1948 (21). The theory predicts the following relationship

$$\frac{1}{X} = A - B\ln t \qquad (3)$$

where A and B are constants.

This law has been found to be valid experimentally, only in ranges of oxide film thickness of 100 Å or less, as predicted theoretically, and usually at low temperatures in the region of "very thin films". There is an initial very rapid rate of oxidation, followed by a rapid decrease in rate, thereby resulting in a protective oxide layer. It has been found by Roberts and Tompkins, for example, in the nitridation of evaporated calcium films (22). Other investigators have shown it to hold for the oxidation of aluminium over a certain range (3), for the low temperature oxidation of copper (23), (24) and of iron (24) and of barium (25).

The third log. law of relatively minor importance is the asymptotic log. law. It has been found to be valid only for very few systems; e.g. for the corrosion of pure aluminium (26) in solutions of KCl following the earlier work of Bengough et al. for the corrosion of zinc and iron (27, 28, 29, 30, 31). U.R. Evans (32) has given a theoretical basis for this law, which has the form:

$$W = k_1(1-e^{-k_2 t}) \qquad (4)$$

where W = weight increase at time t and k_1, k_2 are constants. This is a true asymptotic law, since W approaches a limiting

value, k_1 as t becomes infinitely large. Evans has shown, (33) however, that a logarithmic form is insensitive to small deviations and sometimes variations of the constants can lead to one law approximating another over various ranges. Care is thus needed in differentiating between them. Of the various theoretical treatments and mechanisms which have been proposed to account for an exponential dependence of the growth rate, the two foremost are those of Mott (21), which is confined to thin and very thin oxide layers of stoichiometric composition, and of Evans, which is based on mechanical imperfections (33, 34)..

1.2.2. The Parabolic Law.

The parabolic or square root law was first proposed by Tamman (35) in 1920 and independently by Pilling and Bedworth in 1923 (36). If a continuous coherent surface film of oxide is formed and the temperature is high enough for a diffusion process to be rate controlling the rate is inversely proportional to the thickness of the film:

$$\frac{dX}{dt} = \frac{1}{2}\frac{k_p}{X}, \qquad (5)$$

which gives on integration,

$$X^2 = k_p t + c, \qquad (6)$$

where X is the film thickness at time t, and k_p is the parabolic rate constant. The integration constant is zero since X = 0 at t = 0. It is sometimes necessary to add a constant, other than that of integration, to fit the

experimental results, as when plots of X^2/t do not intersect the zero point. In such circumstances,

$$X^2 = k_p t + c' . \qquad (7)$$

Although it has been shown experimentally that c' is often negligibly small, its presence can be ascribed to initial disturbing phenomena which are not included in the theory. Some of these have been enumerated by Gulbransen (37); they are the effect of:

(1) the decrease in roughness or surface area as the reaction proceeds,

(2) the heat evolved in the reaction on the rate of reaction,

(3) the solution of oxygen in the metal,

(4) the concentration of impurities in the oxide during the early stages of reaction,

(5) changes in oxide composition, and

(6) the influence of potential fields at the gas interface due to adsorbed oxygen ions.

If the reaction in the initial stages is controlled by boundary effects at either of the interfaces and only later becomes diffusion controlled, then as shown by Evans (38), a more general equation is obtained.

Assuming that oxygen is moving inwards through the film, its concentration in excess of that value representing equilibrium in the metal, being C_i at the metal/oxide interface and C_o at the oxide/oxygen interface, then the rate of transport is proportional to $\frac{(C_o - C_i)}{X}$ and the

oxidation rate to C_i. In a steady state,

$$\frac{dX}{dt} = K_p(C_o - C_i)/X,$$

and by the mass action law

$$\frac{dX}{dt} = K_c C_i$$

where K_p is a physical constant, and K_c is a chemical constant.

Eliminating C_i gives,

$$\frac{dX}{dt} = \frac{K_p K_c C_o}{XK_c + K_p},$$

On integrating,

$$\tfrac{1}{2}K_c X^2 + K_p X = K_p K_c C_o t + K^1$$

or

$$K_1 X^2 + K_2 X = K_3 t + K^1 \qquad (8)$$

which approximates to the simple parabola when X is large, and to a linear equation when X is small. This is known as the "mixed parabolic equation" and includes the possibility that two different processes can be rate-determining during the progress of the reaction.

Obedience to the parabolic law has been reported in a large number of systems, and it appears likely that over some range of temperature and pressure the oxidation of most metals conforms with it. It is usually found to hold in regions of temperature higher than those for which the log. laws are applicable and for much thicker films. It confers a moderate degree of protection on metals since the diffusion time eventually becomes so large that further oxidation may

become negligible. However, with thick films mechanical breakdown becomes likely leading to flaking away and cracking, with the possible consequent renewal of oxidation and corrosion.

Of the various mechanisms proposed for the parabolic law in terms of fundamental concepts, the first and also the most elegant and complete theory is that of Wagner (39, 40). An excellent agreement has been obtained between the experimental and predicted values in a number of cases (40).

1.2.3. The Rectilinear Law

The simplest relationship in accord with experimental results is the rectilinear law. This corresponds to a zero order rate equation,

$$\frac{dX}{dt} = k \qquad (9)$$

or

$$X = kt + k' \qquad (10)$$

It never leads to protective oxidation since the layers formed offer no resistance to reaction. Where the oxygen concentration is very low, linear oxidation might be expected when the rate is controlled by the rate of replenishment of oxygen to the reacting surface. This state of affairs occurs when the film is / capable of growing at a much faster rate than that at which oxygen is being supplied, particularly when the oxide film is thin and the rate of transport of material through it is large. In such circumstances, a change of kinetics would be expected on raising the pressure until the rate of oxygen replenishment becomes larger than the transport rate.

A process in which oxygen has continual free access to the metal surface would give the linear law; as for example, when volatile oxides are formed at the temperature of the experiment. This has been observed for molybdenum (41) and thorium (42) at high temperatures.

Should strains be present in the epitaxial layer spalling or flaking away of the oxide layer may result. This leads to periods of slowing down as the film thickens, then speeding up as the film spalls, exposing new metal surface, thereby giving a roughly linear law over a period of time (43). At lower temperatures oxygen may have direct access to the metal when the oxide layer is porous, as Pilling and Bedworth pointed out, (36) for the oxidation of calcium wire.

1.2.4. The Pilling Bedworth Principle.

Pilling and Bedworth introduced the concept of the oxide/metal volume ratio defined as

$$\frac{\text{molecular volume of oxide}}{\text{atomic volume of metal}},$$

each being referred to equivalent amounts of metal. On this basis they divided the metals which develop oxide films into two classes:

(1) those comprising light metals, where the volume of the oxide is less than the metal volume consumed in producing it, i.e. when the volume ratio is less than unity, and

(2) those where the volume ratio is greater than unity i.e. where the volume of the oxide produced is greater than the

metal consumed. Results of calculations based on density measurements and crystallographic data, show that the normal oxides of all the alkali and alkaline earth metals, other than berylium, belong to the first group, while all the heavy metals, including some fairly light metals, (aluminium, beryllium and titanium), belong to the second class (44). The authors argued that when the volume ratio was less than unity a porous oxide film must result, which would be unprotective and lead to a rectilinear growth. On the other hand, those oxides with a volume ratio greater than unity would form a compact and protective layer. In arriving at these conclusions they assumed that the oxygen moved inwards towards the metal, consequently, the oxide is constrained to occupy the volume of the metal consumed; this effect gives rise to stresses which can be relieved only by the oxide developing porosity. However, it is now known, from radioactive tracer and chemical marker experiments (45, 46, 47), that in many cases the cation moves outwards to the oxide/oxygen interface. In these circumstances, with the oxide layer growing at the oxide/oxygen interface unconstrained by the volume of the metal consumed at the metal interface, Vermilyea (48) suggests that the Pilling Bedworth principle is invalid. Certainly there are a number of deviations from the principle, particularly at low temperatures, including the results of some of the present work.

1.2.5. The Cubic Law.

Occasionally a cubic relationship,

$$X^3 = kt \qquad (11)$$

has been found to hold. This law appears to be well substantiated in the oxidation of zirconium (49, 50) and titanium (51), and various workers have found good agreement in some temperature ranges for the oxidation of copper (52, 23). However, other workers (53) studying the oxidation of some copper alloys, nickel and stainless steel have reported that values of the exponent "n" in the equation $X^n = kt$ vary from 2.5-4. The fact that the value of the exponent is often only approximately 3, and indeed in some cases may vary widely about this value, has lead Evans (54) and other authorities to regard the cubic equation as representing an intermediate region in a more general equation that fortuitously approximates to a cubic law; whilst others e.g. Uhlig (55) and Mott and Cabrera (21) believe that the cubic law is sufficiently well established to warrant a theoretical interpretation.

1.2.6. Sigmoid Forms.

The last form of growth curve that has been observed experimentally is the sigmoid form, recognized by a curve which is concave upwards in the initial period, when weight increase is plotted as the ordinate and time as the abscissae. This behaviour is usually found at low oxygen pressures.

Tylecote (52) found it to be valid in the oxidation of copper in the temperature range 200-800°C. It is explained by an initial slow nucleation period where isolated nuclei are formed at points on the metal surface, followed by lateral growth of the nuclei until a more or less uniform surface layer is formed. Since it is energetically easier for nuclei to grow than to be formed initially, this leads to an acceleratory period until the surface is completely covered, after which a transition to one of the usual laws occurs. If this is a parabolic law then the rate decreases and a curve concave downwards is produced, giving a sigmoid curve. The existence of nuclei related to and oriented with the grains of the substrate metal, growing laterally to cover the surface, has been clearly demonstrated by the work of Bénard and Bardolle (56) on the oxidation of iron. Similar evidence has been presented by Gulbransen et al. (57), from electron optical studies of oxidation of iron surfaces at low pressures.

1.3. Theory and Mechanism.

1.3.1. General Considerations.

The growth of an oxide layer is only possible if transport of matter, as ions, and transport of charge by both ions and electrons, can occur through the intervening oxide lattice to the reaction front. According to Frenkel, Schottky and Wagner (58, 59), for ionic crystal lattices, and Wagner (60, 61) for semiconducting oxides, sulphides and nitrides, transport of matter and charge takes place through the medium of defects in the structure. The existence of deviations from the ideal crystal lattice is necessary in order that the lattice, in its equilibrium condition, should have minimum free energy. For a crystal at $0^{\circ}K$, no thermal vibrations in the lattice are possible, but on raising the temperature such vibrations cause atoms to jump from the normal lattice sites to take up interstitial positions thereby creating defects. This leads to an increase in the internal energy of the crystal. However the free energy is comprised of two terms of opposite sign

$$\Delta F = \Delta H - T\Delta S$$

and although the enthalpy term ΔH has increased due to formation of defects the entropy term ΔS has also increased since the number of distinguishable configurations of the system having the same energy has been raised. The number of defects in all crystals increases rapidly as the temperature is raised (62). Two types of defect are, in

general, possible in ionic crystals:

(1) Frenkel defects, where an ion leaves its lattice point and moves through the crystal to take up an interstitial site, sufficiently distant so that there is negligible interaction between them.

(2) Schottky defects. These are created by ions near the surface of the crystal moving to build up new layers of the lattice at the surface. To preserve electrical neutrality, equal numbers of cation and anion vacancies must be created. When cation and anion differ widely in size, leaving large interstitial sites, Frenkel defects will be favoured, whereas, when cation and anion radii are comparable, Schottley disorder is more likely.

Wagner, Schottky and others have extended these concepts to semiconducting crystals, such as oxides and sulphides, by proposing that further lattice disorder may be produced by deviations from stoichiometry. They consider that certain oxides are stable with either an excess or deficit of one component, and Wagner (40) has enumerated the following types of disordered structure. An excess of metal may be present as cations in interstitial positions giving free electrons, as shown, e.g. for ZnO, Fig.1.1. Since an excess of metal is equivalent to a deficit of non-metal, there may be instead, anion vacancies and free electrons, (anion defect n-type semi-conductor).

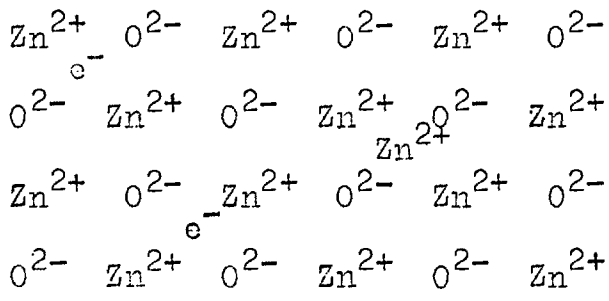


Fig. 1.1. Lattice deffects in zinc oxide. (Interstitial cation n-type semi-conductor)

If there is a metal deficit, there may be either cation vacancies and positive holes, or interstitial anions and positive holes, (p-type). Energetically, anions in interstitial sites in oxides, are not favoured due to the large anion radius.

Provided sufficient activation energy is available, matter and electronic transport can occur by ions jumping through interstitial sites or into adjacent vacancies and by electrons filling adjacent positive holes, in the full band. Fig. 1.2.

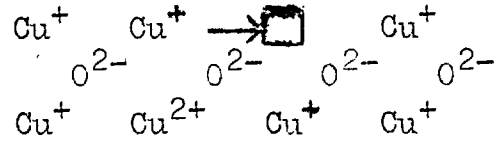


Fig. 1.2. Lattice defects in cuprous oxide (vacant copper site indicated by a square; positive hole represented by a divalent copper ion).

1.3.1.1. Motivating Force in Transport.

For each mode of migration of electrically charged particles the motivating force is the electrochemical potential of the particle. The electrochemical potential η

is composed of the chemical potential μ and the electrical potential V. If these values are expressed in the same units, e.g. electron volts, one obtains for the potential gradients of a species of particles i,

$$\text{grad.}\eta_i = \text{grad.}\,\mu_i + Z_i \text{grad.} V, \qquad (1)$$

where Z_i is the valency or charge born by the species. If B_i is the mobility of a defect species i, D_i is the self diffusion coefficient, R. the gas constant, then by Einstein's relation (63)

$$D_i = B_i RT$$

Putting $n_i(x)$ the concentration of defects at the point of abscissa x, and grad.$\eta_i(x)$ the corresponding electrochemical potential gradient, the following general expression for the flux of defect particles i at point x is obtained, since the flux of particles = mobility x concentration of particles x electrochemical potential gradient.

$$J_i(x) = -\frac{D_i}{RT}\, n_i(x) \times \text{grad.}\,\eta_i(x) \qquad (2)$$

Resolving the electrochemical potential into its chemical part μ and electrical part V,

$$\eta_i(x) = \mu_i(x) + N_i Z_i e V(x), \qquad (3)$$

thus
$$J_i(x) = -\frac{D_i}{RT}\, n_i(x)\left\{\text{grad.}\,\mu_i(x) + N_i Z_i e E(x)\right\}, \qquad (4)$$

where N_i is avogadro's number and $E(x) = \text{grad.}\, V(x)$, the electrical field at the point x.

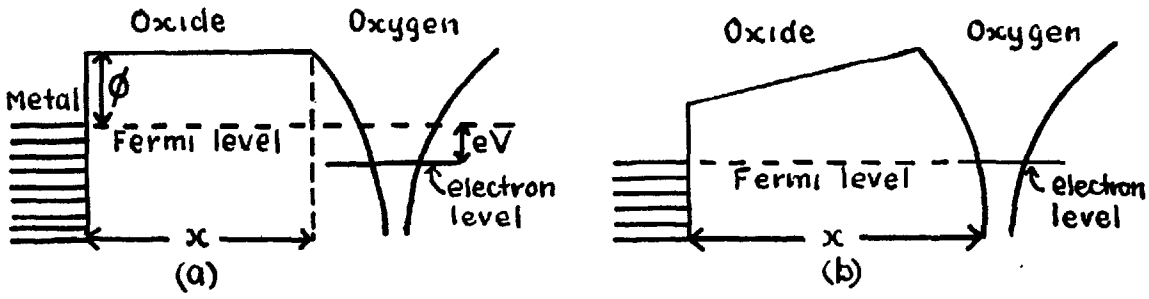
1.3.2. Formation of Coherent Uniform Layers.

Equation (4) is a perfectly general relationship, but it is important to know whether the chemical potential or electrical field in the braces is predominant under certain circumstances. At high temperatures and with thick oxide layers, matter is transported, in general, under the influence of the chemical potential gradient (pure diffusion). At much lower temperatures, and with very thin films, the electrical potential gradient due to the spatial separation of electrical charges, is the important factor. Such charges are situated in semi-conductors near the phase boundaries in a region known as the interfacial layer, or space charge layer. In the first case, the kinetics depend on the first term in the braces and conform to the parabolic law. In the second case, they depend on the second term, since, at low temperatures, diffusion under the action of a chemical potential gradient becomes negligible.

1.3.2.1. Low Temperature - Thin Film Region.

At sufficiently low temperatures a chemisorbed layer of oxygen atoms, only, is formed, following dissociation of the oxygen molecule on collision with the surface (64). Charge transfer results from the metal to the adsorbed oxygen atoms, if the energy levels of the oxygen atoms lie below the Fermi level of the metal. The oxygen atoms thus act as trapping states for electrons. The oxygen layer is

FIG. 1.3.



Electronic energy levels in the metal oxide and oxygen (a) before and (b) after exchange of electrons and attainment of steady state.

FIG. 1.4.

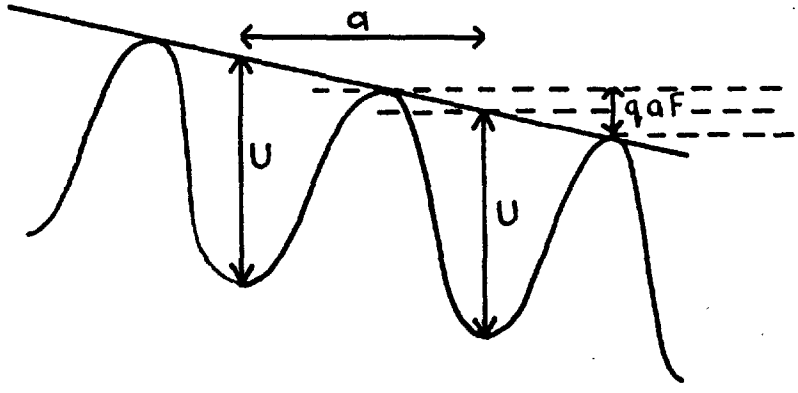
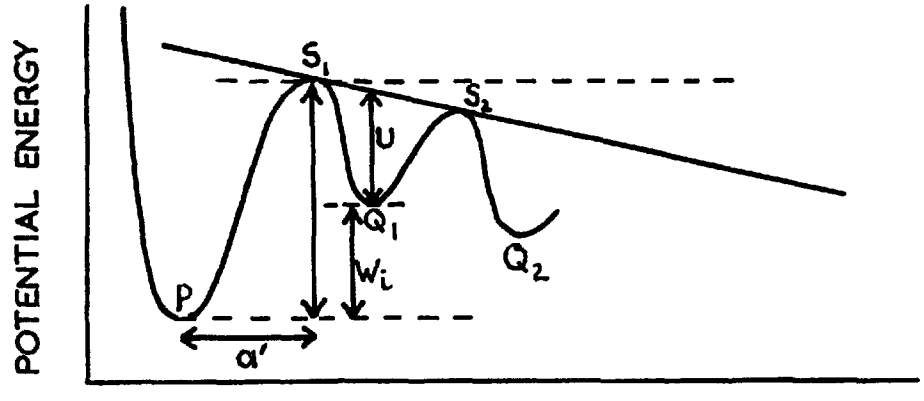


FIG. 1.5.



Potential energy of an interstitial ion in neighbourhood of metal/oxide interface.

then negatively charged and a high field is set up. For further growth of oxide into a three dimensional layer higher temperatures are necessary to provide sufficient activation energy for ion movement, assisted by the potential gradient across the oxide barrier. Further oxygen adsorption must occur at the outer surface of this oxide layer, the requirement being that electrons must penetrate the oxide barrier layer. Mott (65) proposes two mechanisms; at higher temperatures penetration occurs by thermionic emission, and at lower temperatures by the quantum-mechanical tunnel effect. By this process anions are formed at the oxide/oxygen interface, and an equivalent number of cations at the metal/oxide interface. Mott and Cabrera (21) consider the growth of an interstitial cation n-type semi-conducting oxide layer. (Fig.1.3.) Denoting the concentration of ions and electrons in the oxide, at a distance x from the metal/oxide interface, by $n_i(x)$ and $n_e(x)$ respectively, the energy to remove an ion from its position in the metal to an interstitial position in the oxide by W_i, and the energy to remove an electron into the oxide conduction band as $\emptyset$, (see fig.1.3.) then $(W_i + \emptyset)$ is the heat of solution of a metal atom in the oxide (assuming complete dissociation). At the interface, the concentration $n_i(o)$ of interstitial ions is given by

$$n_i(o) = N_i \exp(-W_i/kT), \qquad (5)$$

where N_i is the number of interstitial positions per unit

volume in the oxide. Similarly the concentration $n_e(o)$ of electrons is

$$n_e(o) = N_e \exp(-\phi/kT), \qquad (6)$$

where $N_e = 2(2\pi mkT/h^2)^{3/2}$, Also if $n_i(x)$, $n_e(x)$ are the numbers at any distance x from the interface, the product $n_i(x)\, n_e(x)$ must be constant (mass action law); thus at large distances $n_i(x)$ and $n_e(x)$ are equal, say to n, where

$$n = \sqrt{(N_i N_e)} \exp\left\{-\tfrac{1}{2}(W_i + \phi)/kT\right\}. \qquad (7)$$

At intermediate distances these quantities can be deduced from Boltzmann's law:

$$n_i(x) = n \exp(-eV/kT),$$
$$n_e(x) = n \exp(eV/kT),$$

where V is the electrostatic potential, and from Poisson's equation

$$\frac{d^2V}{dx^2} = \frac{4\pi e}{\kappa}\left\{n_i(x) - n_e(x)\right\},$$

assuming ions carry unit charge.

Substituting for n_i and n_e, this gives

$$\frac{d^2V}{dx^2} = \frac{8\pi ne}{\kappa} \sinh\left(\frac{eV}{kT}\right) \qquad (8)$$

where κ is the dielectric constant. If x is large, and V consequently small, equation (8) then becomes

$$\frac{d^2V}{dx^2} = \frac{V}{X_o^2},$$

where

$$X_o = \sqrt{\{\kappa kT/8\pi nc^2\}}. \qquad (9)$$

The solution is

$$V = \text{const.}\ \exp(-x/X_o). \qquad (10)$$

We must therefore distinguish between systems where $x \gg X_o$ or $x \ll X_o$, where X_o is the thickness of the space charge layer set up at the boundaries of the film. When $x \gg X_o$ we may regard the quantities n_i and n_e as being equal throughout the oxide layer whereas when $x \ll X_o$ the space charge set up in the material has little effect and one can thus discuss the motion of ions and electrons separately.

1.3.2.1.1. $x \ll X_o$.

In this region, electrons pass through the film by a mechanism, (thermionic emission or tunnel effect) which transforms adsorbed oxygen atoms into O^- ions in a time small compared with that of ionic motion, thereby setting up a field between the negatively charged adsorbed layer and the positive cations formed at the metal/oxide interface. A steady state will quickly be reached, where as many electrons pass in one direction as the other. The electrostatic potential V set up across the layer is clearly independent of the thickness so that $F = V/x$. Since V is 1 or 2 volts in practice, F is of the order of 10^7 V $cm.^{-1}$ for a film 50 Å thick. Such enormous fields are capable of pulling cations interstitially through the oxide layer at temperatures where ordinary diffusion processes could not operate.

The motion of interstitial cations under these fields

can be treated as follows.(20). Suppose that an ion has to surmount a potential barrier U, in order to move from one interstitial site to another. In the absence of a field, the chance per unit time that it will do this, is given by $\nu \exp(-U/kT)$ with the lattice vibration frequency $\nu \sim 10^{12}$ sec^{-1}. The field will, however, lower the barrier by $\frac{1}{2}$ qaF, where q is the charge on the ion (see Fig. 1.4), for motion in the direction of the field, increasing the probability of motion to $\nu \exp\{-(U-\frac{1}{2}qaF)/kT\}$. In the opposite direction, the chance of movement is decreased by the same factor. Thus the velocity of drift becomes

$$\mu = \nu a \exp(-U/kT)\{\exp(\tfrac{1}{2}qaF/kT) - \exp(-\tfrac{1}{2}qaF/kT)\}. \quad (11)$$

For small values of F this reduces to

$$n \cong (\nu a^2 q/kT)F \exp(-U/kT), \quad (12)$$

which is proportional to the field. This is the case when $qaF \ll kT$, i.e. when $x \gg X_1$, where $X_1 = \frac{qaV}{kT}$. X_1 is 50-200 atomic layers at room temperature.

On the other hand, when $x \ll X_1$, i.e. for large F,

$$n \cong \nu a \exp(-U/kT) \exp(\tfrac{1}{2}qaF/kT) \quad (13)$$

giving an exponential dependence.

(a) $x < X_1 \ll X_0$. (equation 13)

The fields here are so large that the rate of ation movement is no longer proportional to the field. The motion of the ions is therefore overwhelmingly in one direction, thus there is no local equilibrium between metal

and oxide. Every ion which escapes from the metal is pulled right across the film, and none recombine with the metal. Two rate controlling processes are therefore possible:

(i) the rate of electron supply to the adsorbed oxygen atoms, and

(ii) the rate at which ions are released from the metal.

(a)(i)

At very low temperatures, where the only mechanism for electron transfer is the tunnel effect, Mott (65) considers that the rate of tunnelling, in certain circumstances, may be the rate controlling process. It is now evident that the conditions he proposed were unjustifiable, but the theory has recently been revived in a new form by Hauffe and Ilschner (66). They consider that in the region of extremely thin films, the fields are so great that the rate of arrival of cations at the oxide oxygen interface is greater than the rate of arrival of electrons. This does not imply that the actual velocity of the individual electrons is less than that of ions, but rather that the enormous fields acting on the readily available ions are capable of drawing a larger number per unit area per unit time through the film than the number of electrons tunnelling through unit area per unit time.

The proportion of electrons tunnelling through a rectangular barrier of height ϕ is given by the usual quantum mechanical formula (67),

$$p = \exp\left\{-\ 4\pi x\sqrt{2m(\phi - E)}/h\right\}, \qquad (14)$$

where x is the thickness of the barrier, h is Plank's constant, E is the kinetic energy of the electron and m is its rest mass. The number of electrons in the metal, with energies between any limits, can be obtained from Fermi-Dirac statistics and therefore the number tunnelling through, is the product of these two terms integrated over the range of energies considered. The integral is complicated but results in an equation of the form,

$$\frac{dx}{dt} = K \exp(-x/\bar{X}), \qquad (15)$$

where K is slightly temperature dependent and varies slowly with x,

and $$\bar{X} = h/4\pi\sqrt{2m\phi} \qquad (16)$$

having a value between 1-2 Å. This equation shows that the rate falls off very rapidly for $x > \bar{X}$.

Integrating (15)

$$x = \bar{X} \ln(Kt/\bar{X} + \text{const.}) \qquad (17)$$

giving a logarithmic law of growth.

As the film thickens, the field decreases until a point is reached where the rate controlling process becomes the rate of release of ions from sites at the metal surface. This is the second possibility mentioned above.

(a)(ii)

The potential energy of an ion in the surface layer of the metal is plotted in Fig. 1.5, (21). P represents the potential of ions in special sites, such as kink sites in

steps or emergent screw dislocations, that is, an ion ready to move into the oxide as the surface layer of metal dissolves. The heat of solution for a positive ion, W_i, and the activation energy for diffusion, U, are shown in the diagram. It is convenient to set $W = W_i + U$. By analogy with equation (13), the chance per unit time that the atom at P will escape over the barrier to Q_1, where a' is the distance to the top of the barrier from P, in the presence of strong fields, is

$$\nu \exp(-W/kT) \exp(qa'F/kT). \qquad (18)$$

The rate of growth of the film is thus

$$\frac{dx}{dt} = N'\Omega\nu \exp(-W/kT) \exp(qa'F/kT) \qquad (19)$$

where N' is the number of ions per unit area surface in sites such as P, Fig. 1.5. N' is difficult to estimate at present. Equation (19) may be written

$$\frac{dx}{dt} = u \exp(X_1/x) \qquad (20)$$

where $X_1 = qa'V/kT$, $u = u_o \exp(-W/kt)$ and $u_o = N'\Omega\nu$ X_1 is of the order 10^{-6}–10^{-5} cm; $u_o \sim 10^4$ cm.sec.$^{-1}$ or less. Hence growth is extremely rapid for small x. An important consequence of formula (20) is that, for constnat V, growth up to a certain limiting thickness occurs, even at low temperatures, where u is negligibly small; this will be the case when the solubility of metal ions in the oxide is negligible. Assuming growth has virtually stopped when one layer of atoms is added in 10^5 seconds, so that

$\frac{dx}{dt} = 10^{-13}$, then this occurs at a thickness, X_L, for which $\exp(X_L/X_1 - W/kT) = 10^{-17}$. Substituting for X_1 this gives, since 17 ln 10 = 39

$$X_L = Va'q/(W-39kT). \qquad (21)$$

Thus there exists a critical temperature W/39k; for temperatures below this temperature, the film grows rapidly up to some critical thickness and then stops; above this temperature there is no limiting thickness and the rate of growth is described by some other type of law.

For $x \ll X_1$, an approximate integration of equation (20) can be made, leading to the inverse logarithmic law, of type

$$\frac{X}{x}1 = A - \ln t. \qquad (22)$$

At temperatures so low that tunnel effect is the only mechanism for electron transfer, growth by any process, can not proceed beyond a thickness of approximately 50 Å, as calculated by Mott (65).

(b) $x > X_1 \ll X_o$.

This is an intermediate region where it is assumed that temperatures are sufficiently high for electron transfer to occur either by tunnel effect, or thermionic emission, and where ion movement occurs without the need for enormously large fields, but yet the film thickness is not great enough for the Wagner mechanism to hold. This is the region for which equation (12) holds.

(b) (i) Parabolic Law for Thin Films (21).

Here the number of ions crossing unit area per unit time is

$$n_i v_i F = n_i v_i \, V/x,$$

where v_i is the mobility of an ion. The rate of growth is thus $\frac{dx}{dt} = A/x$, where

$$A = n_i v_i V \Omega = n_i D_i \Omega (eV/kT), \qquad (23)$$

and D_i is the diffusion coefficient of an interstitial ion.

From equation (12), $n_i = a^{-3} \exp(-W_i/kT)$,

and $D_i = \nu a^2 \exp(-U/kT)$.

The film thus grows according to a parabolic law. The constant A in (23), valid for thin films, where $x \ll X_o$, is quite different from the parabolic rate constant for thick films, where $x \gg X_o$ (Wagner's mechanism).

(b) (ii) Cubic law for Thin Films (21).

Up to this point, we have considered n-type semiconductors with interstitial cations, e.g. ZnO. For these oxides n_i depends on the metal/oxide steady state and is therefore independent of film thickness. For oxides having cation vacancies, such as Cu_2O, which take up excess oxygen, n_i refers to the number of cation vacancies. These will be formed at the oxide/oxygen interface on adsorption of oxygen by the process shown in Fig. 1.6. W_i is now the energy required to move the positive ion from A to B. Since $n_i = (N/a) \exp(-W_i/kT)$, the concentration, n_i, is

proportional to the number, N, of such negative ions per unit area. N is related to the field, F, by the Coulomb formula

$$N = \frac{K.F}{4\pi e} = \frac{K.V}{4\pi e}\frac{1}{x}, \qquad (24)$$

showing that N is proportional to x^{-1}, therefore n_i in formula (23) is now proportional to x^{-1}. This gives a cubic oxidation law;

$$x^3 = 3A't, \qquad (25)$$

where the constant A' is proportional to $\exp\{-(W_i+U)/kT\}$, U being the activation energy for diffusion in the oxide.

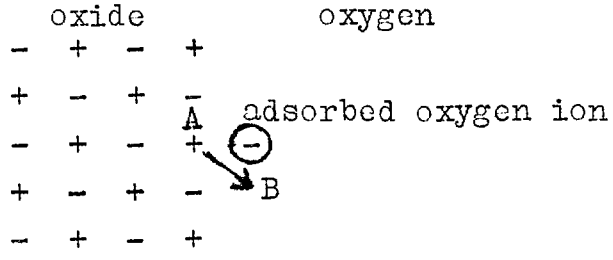


Fig. 1.6. Showing the process by which a vacant cation site is created in the vicinity of an adsorbed oxygen ion.

(b) (iii) Uhlig's Theory for Logarithmic Growth, based on Space Charge Considerations.

It is known that the direct log law holds up to film thickness of several thousand Å in some cases, at higher temperatures than dealt with hitherto. Uhlig (55) has therefore suggested that the rate of thermionic electron emission into the conduction band of the oxide against a varying more negative, or less positive, space charge is the rate controlling process. He produces evidence that the rate controlling process is at the metal oxide interface,

viz.,

(1) different oxidation rates have been observed on different lattice planes, of metals having cubic habit (68, 12).

(2) The activation energy, for oxidation of iron in CO_2 and H_2O, exhibits a discontinuity at the transformation temperature from the α (b.c.c.) to the γ (f.c.c.) lattice (69).

(3) The activation energy for the oxidation of Ni (70) and several alloys (71) exhibit discontinuities at the Curie temperature.

When contact is made between a metal and semi-conductor, all the electronic energy levels of the semi-conductor are altered relative to those of the metal by an amount equal to the contact potential difference. If the electron affinity of oxide is higher or the work function lower than that of the metal, the semi-conductor gains excess negative charge and the metal positive charge until the Fermi levels are equal and further transfer is prevented. Thicker oxides formed beyond the space charge layer are thus electrically neutral and grow according to the Wagner mechanism. For dissimilar metals, the electric charge constitutes a double layer, of atomic dimensions at the interface, but for semi-conducting oxides, with filled energy bands, and few electrons excited into the conduction band, excess charge associates itself with lattice vacancies or impurity levels, as bound or "trapped" electrons (72), giving rise to a

space charge. The number of these sites is restricted, so that the space charge may extend over several thousand Å. Measurements of Volta potential, on oxidizing metals at elevated temperatures (73, 74), show, at first, a decreasing positive potential for thin films, then an increasing negative potential extending over thousands of Å. This increasingly negative space charge tends to impede the rate of escape of electrons, causing a slowing down of the oxidation process. Uhlig was lead to propose the existence of a thin uniform charge density layer in the oxide, near the metal/oxide interface, with a much thicker diffuse charge density layer extending beyond this into the oxide. Solving Poisson's equation for the potential determining electron release, at the metal/oxide interface, in terms of film thickness and the density of trapped electrons in the thin uniform space charge layer, close to the metal, and substituting this potential in the equation for electron current across the contact boundary in crystal rectifiers, (75), an equation for the rate of growth is obtained; the integrated form being,

$$x = k_o \ln\left(\frac{t}{\tau} + 1\right), \qquad (26)$$

since the rate of growth is proportional to the electron current. This is a direct log. law. k_o is the log. rate constant and τ is a constant. He then assumes, that beyond a certain thickness, the trapping sites are only partially occupied by electrons, and a diffuse charge

density barrier layer extends for a relatively large distance into the growing oxide. In accord with Mott and Gurney's (76) treatment of metal/semi-conducting contacts a value for the concentration of excess negative charge is obtained, which in the same way as before, leads to a direct log. law with different constants k_o' and γ'. In the diffuse region, the log. rate constant is greater than that in the uniform region and thus a discontinuity in the rate law is to be expected at a certain thickness. This has been observed in a number of cases (7, 11, 12). By assuming that the negative charge density in the diffuse layer falls off in accordance with a Boltzmann distribution a cubic law results.

(b) (iv) Hauffe and Ilschner's Theory of the Parabolic and Cubic Law for Thin Films.

These authors (66) criticise Motts derivation in that he has used a simplification in his model which is only valid at best for bad semi-conductors of n-type, where the concentration of interstitial defects is small, i.e. that the concentration of defects is constant in the oxide layer. However, since the boundary processes are rapid compared to migration in the bulk, a stationary state is set up, with defect concentrations of different orders of magnitude at the boundaries, creating thereby a large concentration fall across the oxide layer. They obtain the same result without making this simplification, thus:

Setting $E(x) = \frac{V}{x_1}$ in equation (4) in its equivalent form:

$$J_o = - D_o\left\{\text{grad } n_o + Zn_o \frac{eV}{kT} \frac{1}{x_1}\right\} \qquad (27)$$

where n_o is the concentration of interstitial ions, and x_1 is the variable thickness of the oxide layer. In the stationary state J_o must be constant for all x, i.e. div $J_o = 0$. Hence

$$\frac{d^2 n_o}{dx^2} + \frac{1}{x_1} \frac{eV}{kT} Z \frac{dn_o}{dx} = 0 \qquad (28)$$

the solution of which is

$$n_o(x) = n_o^* - \alpha e^{\left\{-\frac{1}{x_1} Z \frac{eV}{kT} x\right\}} \qquad (29)$$

Now $n_o^{(o)}$ can be neglected in comparison with $n_o^{(i)}$, and kT in comparison with eV, where $n_o^{(o)}$ and $n_o^{(i)}$ are the defect concentrations at the oxide/oxygen interface and the metal/oxide interface respectively. Further $\alpha \sim n_o^{(i)}$ and $n_o^* \sim n_o^{(i)}$, independently of x_1. Substituting (29) in (27) gives for the ionic flux crossing the oxide layer,

$$J_o \sim - D_o n_o^{(i)} Z \frac{eV}{kT} \frac{1}{x_1}. \qquad (30)$$

Since, as before $\frac{dx_1}{dt}$ is proportional to J_o,

$$\frac{dx_1}{dt} = k_1'/x_1 \qquad (31)$$

i.e. a parabolic law identical to Mott's, with

$$k_1' = \Omega D_o n_o^{(i)} Z \; eV/kT \qquad (32)$$

These authors (77, 78) also derive a cubic relationship for p-type conductors assuming that the field, as a first approximation, is conditioned only by the distribution of positive holes in the space charge region.

1.3.2.2. Thick Films and High Temperatures.

1.3.2.2.1. $x \gg X_0$.

(a) Wagner's Theory. (78, 39, 40).

At high temperatures, the second term in the brackets in equation (4) may be cancelled, since the reaction can now proceed in a region of thickness where space charge effects are negligible; and, as shown by equation (1C), the concentrations of ion and electron defects can be considered equal. The greater bulk of the oxide layer is therefore neutral, and the rate controlling process is that of diffusion under the chemical potential gradient. Wagner assumed that diffusion of electrically neutral atoms and molecules could be neglected. Under these conditions equation (4) simplifies to

$$J_i(x) = - \frac{D_i}{RT} n_i(x) \text{ grad } \mu_i(x), \qquad (33)$$

In the absence of space charges and externally applied electrical fields, there must be some mechanism operating during mass flow to maintain electrical neutrality. This mechanism reduces the velocity of the considerably more mobile electron defects in the diffusion field arising from the difference of chemical potential, and also allows

equivalent numbers of ions and electron defects to pass unit cross section , perpendicular to the direction of diffusion. This type of mass migration, giving rise to currentless flow, is called ambipolar diffusion (78).

By postulating that the total current of cations and anions (indices 1 and 2 respectively), is given by $J_{1+2} = J = \frac{1}{q}(\frac{dn}{dt})$, where q is the cross sectional area, t the time in seconds, n is expressed as equivalents of substances 1 and 2, and noting that $\mu_i = RT\ln a_i$, and D_i^* is a function of a_i, Wagner's formula for parabolic oxidation is obtained:

$$\frac{dn}{dt} = \frac{q}{\Delta x}\left[C_{eq}\int_{a_2^{(i)}}^{a_2^{(o)}}\left(\frac{Z_1}{|Z_2|}D_1^* + D_2^*\right) d\ln a_2\right]. \qquad (34)$$

Here Z_1 and Z_2 are cation and anion valencies.
$C_{eq} = Z_1C_1 = Z_2C_2$ is the concentration of metal and non-metal ion in equivalents per cm^3 and Δx is the thickness of the oxide layer at any time. Furthermore $a_2^{(o)}$ and $a_2^{(i)}$ are the thermodynamic activities of non-metal at the oxide/oxygen and metal/oxide interfaces respectively. D_1^* and D_2^* are the self diffusion coefficients of the two ionic species in the lattice.

If the mobility, B, of lattice defects, is substituted for the self diffusion coefficient in equation (34) using the Einstein relation $D^* = B \times RT$, and if the total conductivity, σ, of the oxide layer is expressed in terms of the transference numbers t_1, t_2 and t_3 of cations, anions

and electrons (or holes) respectively, Wagner's other general equation results:

$$\frac{dn}{dt} = \frac{A}{\Delta x}\left[\frac{300}{96,500}\frac{RT}{|Z_2|Ne}\int_{a_2^{(i)}}^{a_2^{(o)}}(t_1+t_2)t_3\sigma\, d\ln a_2\right] \qquad (35)$$

The quantity in brackets has been named by Wagner "The rational rate constant" and is the reaction rate in equivalents per square cm. per sec, for a layer of the oxide 1 cm. thick (40). The defect diffusion coefficient, D_i, in the general transport equation (4), can not be substituted for the self diffusion coefficient D_i^*, because in order for defects to migrate, an activation energy for interstitial hopping is necessary, i.e.

$$D_i = \text{const } e^{-E_M/RT},$$

whereas for self diffusion, which is usually determined experimentally, using radioactive tracers, the radioactive material not only requires the activation energy E_M for interstitial migration, but also an activation energy of defect formation. Therefore

$$D_i^* = \text{const. } e^{-(E_M+E_F)/RT}$$

$$\frac{D_i^*}{D_i} = e^{-E_F/RT}, \text{ or } D_i > D_i^*. \qquad (36)$$

Since the lattice defect concentration in oxides is strongly affected by the neighbouring metal or gas phase, it is

necessary to determine self diffusion coefficients of oxides for use in formula (34) in equilibrium with either oxygen or metal. The appropriate condition is determined by the type of conduction operating in the oxidation system.
(1) For p-type oxide layers, the self diffusion coefficient of cations in the oxide in equilibrium with the oxygen partial pressure prevailing during oxidation, must be used.
(2) For n-type, the self diffusion coefficient of anions or cations in the oxide in equilibrium with the metal phase must be used.

(b) Treatment of the Parabolic Law According to Hoar and Price (79).

These authors have given a simplified treatment by drawing an analogy between the transport due to ions and electrons through the oxide layer and the flow of current through a cell; the film providing both the electrolyte for ionic transport, and the external circuit for electronic conduction. The e.m.f. of the cell is derived from the decrease in free energy of the reaction (E_o).

The cathodic reaction at the film/gas interface is represented by:- $X + e^- = X^-$ or $O_2 + 4e^- = 2O^=$.
The anodic reaction is:- $Me = Me^+ + e^-$. The total resistance (electronic and electrolytic) of an area A cm^2 of film of thickness Δx cm., acting as both an electrolytic and a metallic path is:-

$$R = \left(\frac{1}{\sigma_{electrolytic}} + \frac{1}{\sigma_{electronic}}\right) \frac{\Delta x}{A} \qquad (37)$$

where σ is the specific conductance of the species in $\Omega^{-1}cm.^{-1}$ If the transport numbers of the cations, anions and electrons are τ_c, τ_a and τ_e respectively, then:-

$$R = \left(\frac{(\tau_a+\tau_c+\tau_e)}{(\tau_a+\tau_c)\sigma} + \frac{(\tau_a+\tau_c+\tau_e)}{\tau_e \sigma} \right) \frac{\Delta x}{A}$$

$$= \frac{\Delta x}{(\tau_a+\tau_c)\tau_e \sigma A} \qquad \text{since } \tau_a+\tau_c+\tau_e = 1.$$

If the film consists of η gram equivalents, and is formed in t seconds and the rate of growth is equivalent to the current, I (amp), then Faraday's and Ohm's laws yield,

$$\frac{d\eta}{dt} = \frac{I}{F} = \frac{E_o}{Rf},$$

hence

$$\frac{d\eta}{dt} = \frac{(\tau_c+\tau_a)\tau_c \sigma A E_o}{96{,}500 \Delta x}, \qquad (38)$$

which is the simplest form of Wagner's equation. $\frac{d\eta}{dt}$ is proportional to the parabolic rate constant k_p, given by

$$\frac{d\eta}{dt} = \tfrac{1}{2} V_{eq} \left(\frac{Z}{M}\right)^2 k_p, \qquad (39)$$

for an oxide Me_2O, where V_{eq} = volume of 1 g-equivalent of the oxide, Z = valency of oxygen ion and M = the atomic weight of oxygen.

The theory does not require a uniform concentration gradient, but only a constant concentration difference across the film. Reasonable agreement is obtained between calculated and observed values of the rate constants.

This simple treatment, however, does not take into account the variation of σ with pressure which becomes

important with cation deficit semi-conductors. This can be seen by the application of the law of mass action to the equilibrium at the oxide/oxygen interface creating cation and electron vacancies. For example, with Cu_2O,

$$(O_2) + 4e^- = 4\square Cu^+ + 4\square e^- + Cu_2O, \qquad (40)$$

where $\square Cu^+$, $\square e^-$, represent cation vacancies and electron vacancies.

If other disorder equilibria are negligible, the concentrations of the ion and electron defects are equal.

i.e. $$C_{\square Cu^+} = C_{\square e^-}$$

thus $$\frac{p_{O_2}}{C^4_{\square Cu^+} \times C^4_{\square e^-}} = \text{constant};$$

and since the concentrations of Cu^{++}, $O^=$, and bound electrons are virtually constant, then

$$C_{\square Cu^+} = C_{\square e^-} = (\text{const } p_{O_2})^{\frac{1}{8}}. \qquad (41)$$

Assuming that the conductivity is proportional to the concentration of defects then $\sigma = \sigma_o p_{O_2}^{1/n}$, where n = 8 and σ_o is the conductivity at a pressure p_{O_2} = 1 atmosphere. $\sigma = \text{constant } p_{O_2}^{1/7}$ has been found experimentally for this system (80).

In order to take this into account, the oxide layer can be regarded as made up of a series of thin slices of thickness dx; the interfaces of each slice have their own electrochemical potentials, E_x and $E_x + dE_x$, (i.e. electrode

potentials due to a negative component, X). Assuming that the activity of the X^{i-} ions approximates that for Me_mX_n, of stoichiometric composition, and is virtually constant, the potentials E_X depend only on the pressure p_X of the gas X_y. E_X being given by

$$E_X = \frac{RT}{ZF} \ln p_X + \text{a constant}, \qquad (42)$$

where $Z = iy$ is the valency factor.

If I is the current flowing through the thin slice due to the potential difference dE_X between its surfaces, then by Ohm's law,

$$dE_X = \frac{I dx}{(\gamma_a+\gamma_c)\gamma_e \sigma_o p_X} 1/n_A \qquad (43)$$

Combining with equation (42),

$$\frac{RT}{ZF} p_X^{(1/n-1)} dp_X = \frac{I\ dx}{(\gamma_a+\gamma_c)\gamma_e \sigma_o A}, \qquad (44)$$

Since I is constant throughout the oxide layer integration of (44) gives

$$\frac{nRT}{ZF} (p_X^{1/n}(s) - p_X^{1/n}(m)) = \frac{I \Delta x}{(\gamma_a+\gamma_c)\gamma_e \sigma_o A}, \qquad (45)$$

where $p_X(s)$ is the pressure of gas at the external surface of the oxide film, and $p_X(m)$ is the dissociation pressure of Me_mX_n at the film/metal interface. Thus

$$\frac{d\eta}{dt} = \frac{I}{F} = \frac{(\gamma_a+\gamma_c)\gamma_e \sigma_o A}{96,500 x} \times \frac{1.983nT}{23066Z} (p_X^{1/n}(s) - p_X^{1/n}(m)) \qquad (46)$$

Since the chemical potential of the diffusing species is a linear function of $\ln p_X$, equation (46) reduces approximately

to Wagner's equation (35). Evans (81) has shown that the two treatments are thermodynamically equivalent.

1.3.3. Oxide Layers Subject to Flaws and Mechanical Imperfections.

1.3.3.1. Movement through Pores.

So far mechanically perfect layers have been considered; in these uniform movement through the lattice occurs. However, this represents an approximation, since movement is possible through discrete pores; such as,

(1) grain boundaries,

(2) disorder at intersecting slipplanes,

(3) axes of screw dislocations,

(4) lines representing edge dislocations.

Such movement may occur at temperatures too low for ordinary lattice migration and may hold up to greater thicknesses than those dealt with previously. If the pores are large enough for oxygen molecules to diffuse to the metal interface, ultimately blockage may occur at the base of the pores. Similarly if the pores are smaller, anion movement is possible and in this case, as well as for cation movement outwards, the pores may again become blocked. Evans considers two separate cases (82),

(1) Self blockage of pores, where only the pores themselves will block. This is more likely when the Pilling-Bedworth volume ratio is less than unity.

(2) Mutual blockage of pores, where the compressional stresses in a blocked pore may produce blocking in neighbouring pores; this is more likely when the volume ratio is greater than unity.

(a) Asymptotic equation due to self blockage.

If the rate of oxygen uptake is determined by the number of pores remaining open

$$\frac{dW}{dt} = k_1 N,$$

where W is the amount of oxygen per unit area, and N is the number of pores per unit area at time t.

Assuming $$-dN = k_2 dW,$$

then $$\frac{dN}{N} = -k_2 k_1 dt = -k_3 dt.$$

On integration, $$\frac{N}{N_o} = e^{-k_3 t},$$

where N_o is the number of pores per unit area.

Since $$\frac{dW}{dt} = k_1 N$$

then $$\frac{dW}{dt} = \text{const.} e^{-k_3 t},$$

which on integration may be put in the form

$$W = k_4'(1-e^{-k_3 t}), \qquad (1)$$

a true asymptotic equation such that $W \rightarrow k_4$ as $t \rightarrow \infty$.

(b) Direct logarithmic equation due to mutually blocking pores.

If the compressional stress in one pore exerts a pressure on neighbouring pores, then some of these may become blocked. Hence in considering the effect of dW on -dN, the value, N, must be taken into account, since it determines the number of pores existing within an effective distance,

i.e. $$-dN = k_2 N\, dW \quad \text{or} \quad \ln(N/N_o) = -k_2 W.$$

Since, as before,

$$\frac{dW}{dt} = k_1 N,$$

then $$\frac{dW}{dt} = k_3 e^{-k_2 W},$$

and $$e^{k_2 W} dW = k_3 dt,$$

which gives, with W = 0 at time t = 0,

$$k_3 t = \frac{1}{k_2}(e^{k_3 W} - 1).$$

This can be expressed as

$$Kt + 1 = e^{k_2 W}$$

or $$W = K' \ln(at + 1), \qquad (2)$$

a direct log equation.

1.3.3.2. Formation of Cavities (83).

Even when the oxide is capable of transmitting ions or vacancies, the area available for transmission may decrease with time due to vacancies condensing at the metal/oxide interface, either when cations migrate outwards leaving vacancies at the metal interface, or when vacancies migrate inwards. Evans has deduced what he calls "the New Logarithmic Law" based on this concept. It is essentially a modification of the parabolic law due to a decreasing area of reaction interface.

Vacancies condensing at the metal interface, reduce the area to ϕ times its original amount ($\phi < 1$) so that dW/dt is

reduced from $k_6 \frac{dx}{dt}$ to $k_7 \phi \frac{dx}{dt}$. Here $\frac{dx}{dt}$ represents the thickening rate according to a parabolic law in absence of cavities, and k_7 is the ratio of weight per unit area to thickness. The chance that a vacancy may be retained at the interface is now presumed to be proportional to the number of sites available, consequently,

$$-d\phi = k_8 \phi dW,$$

or

$$\ln\phi = - k_8 W + k_9,$$

giving

$$\phi = k_{10} e^{-k_8 W},$$

so that

$$\frac{dW}{dt} = k_7 \phi \frac{dx}{dt} = k_{11} t^{-\frac{1}{2}} e^{-k_8 W}.$$

Thus

$$e^{k_8 W} = 2k_8 k_{11} t^{\frac{1}{2}} + 1,$$

and if $W = 0$ at $t = 0$, $k_8 W = \ln(K(t^{\frac{1}{2}} + 1/K))$,

which may be written as $W = k' \ln (a(t^{\frac{1}{2}} + k''))$, (3)

the "New Logarithmic Law".

If $1/K \ll t^{\frac{1}{2}}$ the above equation reduces to

$$k_8 W = \ln(K^2 t)^{\frac{1}{2}},$$

or

$$W = \frac{1}{2k_8} \ln(K^2 t), \quad (4)$$

and if $K^2 t \gg 1$, this equation is indistinguishable from the direct logarithmic law given in section 1.3.3.1.b. The presence of oxides of a second metal in an alloy, collecting at the metal interface, should produce similar conditions.

1.4. Literature Survey of Previous Investigations on Alkali and Alkaline Earth Elements.

1.4.1. Oxidation of Alkali Metals.

1.4.1.1. Oxidation of Lithium.

In the present work a systematic study has been made of the kinetics of oxidation of evaporated lithium surfaces with pure dry oxygen at low temperatures and pressures in the region of very thin films.

Except for a few general qualitative observations on the reaction (84), little previous work has been done. It has been stated that the metal does not react with dry air below 100°C (85), that it burns in dry air at 200°C (86) or 250°C (87) with a white flame, forming the monoxide (Li_2O), and that the metal can be distilled in dry air without reaction (87).

The reaction product consists entirely of the monoxide Li_2O. Deliberate attempts (87) to produce higher oxides by heating the metal in air or oxygen have yielded only traces of peroxide Li_2O_2. The peroxide when prepared by other methods is relatively unstable, decomposing at 300°C into the monoxide and oxygen (88).

Tyzack and Longton (89) have studied the variation of the ignition temperature of distilled and filtered bulk lithium with oxygen pressure over the range 0-760 mm.Hg. and at temperatures between 25-900°C. Below the ignition

temperature the rate was immeasurably small. Ignition occurred suddenly and spontaneously at well defined temperatures and was markedly pressure dependent. Over the pressure range 100-500 mm.Hg. the ignition temperature has a minimum value of 630-650°C. At pressures below and above this range, it increases linearly to over 800°C. Visual observation suggested that reaction proceeded in the vapour phase.

1.4.1.2. Oxidation of other Alkali Metals.

The oxidation of multi-distilled evaporated sodium films has been studied by Cathcart, Hall and Smith (90), from rates of uptake by pressure decrease, in a constant volume system, from 200 mm.Hg pressure. The oxidation rate was small between -79°C and 48°C giving a highly protective oxide. The rate curves qualitatively agreed with those predicted by the Cabrera-Mott theory (21). The average thickness of the Na_2O film at -79°C was 50 Å, and 1500 Å at 48°C after 40,000 minutes. At 48°C the shape of the rate curve changed after 25,000 to 30,000 minutes to an accelerating curve.

Further oxidation studies on potassium and rubidium have been reported by Cathcart and Smith (91), with similar results. Rate measurements were made with potassium between -79°C and -20°C, and with rubidium at -79°C and -50°C. The film thickness attained by potassium at -50°C and -79°C was not greater than 100 Å, and remained protective even after 100,000

minutes duration of oxidation. At -20°C a transition from protective to non-protective behaviour occurred.

With rubidium, protective behaviour was exhibited, at first, at -50°C and -79°C, but at both temperatures a transition occurred later to a non-protective film, after about 25,000 to 30,000 minutes at -79°C but after only 100 minutes at -50°C.

The rates of reaction above the critical temperatures were too fast to be measured. Combustion of both metals occurred at room temperature, if oxygen was added to the fresh metal surface, but not if an oxide film was allowed to develop at a lower temperature, although there was a continuous uptake over several days. Thus for these three alkali metals, the transition temperature varied inversely with the electropositive character of the element. Previously Holt and Sims (87) observed a remarkable reduction in the oxidation rates of Na and K when exposed to carefully dried oxygen. Similarly Herrington (92) reported that no visible oxide film formed on quiescent sodium amalgam in dry oxygen, but that complete oxidation of the sodium was obtained by gentle agitation to break up the invisible film on the surface. More recently, Moyer (93) reported a very slow rate of reaction for the low pressure oxidation of sodium.

Howland and Epstein (94) found a parabolic rate of growth of thick crusts on sodium below the melting point

in air of varying moisture content. Conditions were ill defined and the crusts were almost certainly a complex mixture of sodium hydroxide and oxide. Highly purified lithium and sodium tarnishes less rapidly in air than freshly cut surfaces of the commercial product.

Tyzack, Steele and Longton (95) studied the oxidation of Na at constant pressure over a pressure range 0-700 mm. between 25°C and 400°C. The reaction rate below the ignition temperature was too slow to be measured and too fast to be followed above the ignition point. The ignition temperature was markedly pressure dependent (cp. lithium), with a minimum value of 260°C in the pressure range 250-600 mm.Hg. Outside these limits, raising or lowering the pressure, increases the ignition temperature to as much as 400°C. They concluded that the reaction proceeded in the vapour phase.

1.4.2. Oxidation of Alkaline Earth Metals.

(a) Beryllium.

Gulbransen and Andrew (114) studied the oxidation of Be between 350 and 950°C and found a parabolic law with an activation energy of 50.3 kcal/mole. The parabolic rate constant was the smallest found with any metal. The oxide film had an even greater depressent effect on the vapour pressure than did nitride films. The vapour pressure decreased with the square root of the oxide thickness; a film of 99 micrograms /cm^2, for instance, lowering the vapour pressure 100 fold. The pressure dependence was small and consistent with the outward migration of ions.

These results were substantiated by Cubicciotti (115) between 840 and 970°C but with a somewhat higher value of the activation energy (62 kcal/mole).

Gulbransen and Andrew applied transition state theory to their results for both the nitride and the oxide reactions, and found negative entropies for oxidation and positive entropies for nitridation. Thus, even though the activation energy for nitridation was much greater than for oxidation, the opposite sign of the entropy factor decreased the free energy of activation of the nitride reaction so that the two reactions occurred at about the same rate. Gulbransen stated that "positive values of ΔS^* indicate a surface reaction product with many possible paths for the metal to go to the activated state".

(b) Magnesium.

(1) Very thin films.

Rhodin (116) and Sack (117) have reported results on the early stages of oxidation using the Wagnerflow method (118). Rhodin noted that nucleation takes place on surface defects, followed by a logarithmic growth. Sack studied the early stages of the reaction up to a few layers, on evaporated polycrystalline surfaces and on (001) and (100) faces of single crystals. Electron micrographs showed that the evaporated magnesium films comprised overlapping hexagonal platelets of several thousand angstroms in diameter preferentially oriented with the basal plane parallel to the pyrex surface. The surface area was estimated to be a factor of 1.2-2 times greater than the apparent surface area.

Sticking probabilities at very low pressures (10^{-7} - 10^{-5} mm.Hg) increased slightly at first, then decreased sharply by several orders of magnitude, after several atomic layers of oxide had been formed. The rise was interpreted as being due to nuclei forming and spreading radially, as described by Bloomer (113) for barium, with very little vertical growth until a monolayer was formed. The rate in the falling portion of the sticking probability curve, could be interpreted equally well by the inverse log law of Mott and Cabrera or the direct log law of Landsberg. A dependence on pressure, of between the 0.8 and first

power was found, but no marked temperature dependence between -75° and $+130^{\circ}C$.

The results on single crystal faces studied using the vacuum microbalance technique at c.a. 400-450°C were complicated. Three distinct regions were detected. The first corresponded to a log or inverse log law. The two other regions were different for the two different faces. For the prismatic plane (100) a parabolic followed by a linear region occurs, whereas for the basal (001) plane a cubic, followed by a linear law was observed. The temperature dependence was slight, and varied for the different regions. Expressed as activation energies the values were less than 3 kcal/mole except for the parabolic region of the (100) plane, where the value was 8 kcal/mole.

From the small temperature dependence, it was decided that the migration of oxygen through cracks and pores was rate determining after the first logarithmic region.

The fact that oxidation was more rapid at first on the basal (001) plane, and then rapidly became more protective than on the prismatic (100) plane, was ascribed to better epitaxial matching between the (111) oxide plane parallel to the (001) Mg plane. It therefore grows more rapidly at first, but forms a continuous and adherent layer which is more protective than the other case, where matching is not so good.

Finch and Quarrell (119) produced evidence from electron

diffraction to show that thin films of MgO on Mg exhibited abnormal crystal habit. It could not be determined whether pseudo-morphism with the underlying layer occurred with thin films; however it did not occur after the oxide layer had grown to appreciable thicknesses.

(2) Thick films and scales at elevated temperatures.

At temperatures less than 450°C, and in the very early stages at somewhat higher temperatures, the thin film formed is protective (120, 121). Gulbransen (121) found the rate to obey a nearly parabolic law below 450°C, but above 475°C a linear law. The existence of a linear region has been confirmed frequently (122, 120, 123, 124, 125, 126) following the original work of Leontis and Rhines (122) on the high temperature oxidation of magnesium and magnesium alloys.

Leontis and Rhines studied the reaction between 412°C and 575°C. Below 450°C, a protective layer was formed; but above 475°C they obtained a non-protective one increasing at a linear rate. At the higher temperatures, a loose scale is produced, due to rupturing of the protective layer at a certain critical thickness. The activation energy was 50.5 kcal/mole and the action constant 6.2×10^{12} mg/cm^2/hr.; alloying increased the rate of oxidation whenever the melting point was significantly lowered by the alloying element. At still higher temperatures, approaching the melting point, combustion occurred producing a flame, burning at a distance

from the surface in the vapour phase. Only a small effect of pressure was found.

Applying transition state theory, and substituting an experimental rate and activation energy, they obtained good agreement between the number of active sites/cm^2 of surface, and the number of atoms in the close packed basal plane of magnesium, with a slight deviation indicating possibly more activated centres than actual atoms/cm^2. These were assumed to be caused by evaporation of magnesium on to the oxide surface, or due to some reaction occurring in the vapour phase.

A thin black uniform layer next to the metal was observed in most cases, which they ascribed to non-stoichiometry in the lattice in this region.

It was concluded that during the linear period of oxidation, cracks developing in the oxide layer allowed gaseous oxygen to diffuse to the surface of the metal and to react there forming a non-adherent layer.

Recently Gregg and Jepson (126) found an initial induction period (during which lateral growth of white oxide across the specimen surface was observed), followed by a linear process below 525°C. Above this temperature a second linear process occurred, having a much larger rate. The Arrhenius plot for the second region was not linear, but a good linear plot was obtained for the first process, giving an activation energy of 48.7 $\pm$ 1.1 kcal/mole, and a

value for the action constant of $(9.55 \pm 3.04) \times 10^{11}$ mg/cm^2/hr. These values compare well with those obtained by Leontis and Rhines. Gregg and Jepson questioned the conclusion of Leontis and Rhines, that cracks in the layer extended right down to the metal, allowing diffusion of gaseous oxygen to the metal interface, during the first process, on the grounds that this made it difficult to explain the second linear "breakaway". Instead they assumed that the first linear process represented a stationary state, where the rates of film growth and cracking were equal, whereas in the second process the cracks extended down to the metal itself, and reaction occurred in the vapour phase.

Presence of moisture lowered the temperature at which the oxide film ceased to be "protective", shortened the length of the induction period, increased the rate of the first linear process and inhibited the development of the second linear branch. The experimental activation energy decreased with increasing humidity.

At even higher temperatures, the rate of evaporation became large enough for combustion to occur in the vapour phase with a flame. According to Fassell, Gulbransen, Lewis and Hamilton (127) the ignition temperature of pure magnesium is $623^{\circ}C \pm 0.5$ at 1 atmosphere pressure of oxygen. The temperature varied with pressure in a complicated manner over the range 0.166 to 10 atmospheres and was

lowered by alloying.

Application of transition state theory gave reasonable agreement between calculated and experimental values but could not account for the effect of pressure.

(c) Calcium.

Pilling and Bedworth made the first systematic investigation, by measuring the decrease in resistance of calcium wires as the outer layers were converted to oxide (36).

At 300°C, the rate was linear but at 400°C and 500°C although initially linear, on reaching a certain thickness of oxide, a sharp increase occurred. This was attributed to the insulating effect of the oxide layer, which prevented the escape of heat generated by the reaction. At 550°C the wire ignited and burnt violently.

Cubicciotti (128), on the other hand, found that a parabolic rate law was obeyed between 330° and 435°C, while the linear relationship was only obtained above 435°C following an induction period.

More recently Gregg and Jepson (99) using purer material than that of Pilling and Bedworth, found the rate to be negligibly slow below 475°C consistent with the film having protective properties, but at 500°C and above, the rate became readily measurable, with an increasing rate up to a maximum, followed by a decreasing rate. At 550°C and above a "breakaway" reaction occurs, and a linear rate

of oxidation was observed only at one temperature, 500°C.

(d) Barium.

Wagener (129) found rapid uptake with negligible activation energy, of less than 0.05 kcal/mole, between 50°and 220°C, at low pressures of 10^{-7} to 10^{-6} mm.Hg. Arizumi and Kotani (130), working at considerably higher pressures, reported activation energies of 5-8 kcal/mole, presumably at higher coverages.

Exhaustive studies of barium oxidation in the thin film region have been carried out by Bloomer (25, 113) who found the process to conform closely to the Mott and Cabrera model of very thin film growth. He showed the existence of a critical temperature for the process, at approximately 40°C, above which a different rate law was obeyed and oxidation proceeded completely through the metal. The speed of pumping by the film was only 1/25 of the calculated theoretical speed, assuming a sticking probability of unity, and he concluded that the pumping speed was limited by the superficial density of interstitial barium in the oxide. The rate of uptake increased with temperature only above the critical temperature.

During the growth of the first monolayer or two, where Mott's theory does not apply, the rate increased with the square root of the time. This was attributed to nucleation which commenced at random defects on the surface and then spread laterally to form a monolayer; thereafter the process obeyed Mott's theory.

1.4.3. Nitridation of Lithium.

Lithium nitride (Li_3N), was first prepared by Ouvrard (96) by heating metallic lithium to a dull red heat in a stream of nitrogen. Guntz (97) obtained reaction with only slight heating and Dolandres (98) observed nitridation at room temperature. Guntz, Dafert and Miklauz (100) found that the best temperatures for its preparation were room temperature or 450°C. At room temperature the product was dull grey, hygroscopic and contained uncombined nitrogen whereas at 450°C it was more compact, crystalline, less hygroscopic and dark violet in colour. At the melting point (840°-845°C) the nitride attacks iron, nickel, copper, platinum, silicon and porcelain, and begins to react with iron at approximately 500°C (101).

Belyaev, Firsanova and Pomerantsev (102) have claimed that lithium nitride was produced in air when the relative humidity was less than 80% and that the rate of formation increased up to 35°C then decreased. Above 80% relative humidity, lithium hydroxide and lithium carbonate were produced. The rate increased with humidity and with the presence of sodium, potassium and aluminium impurities.

Besson and Müller (103) have stated that the thin black film, which is observed to form on freshly cut lithium surfaces, is the hydroxide and not the nitride, that dry nitrogen did not react with pure lithium at ordinary temperatures unless the metal was or had been, in contact

with moisture for a time sufficient to form an hydroxide film of a minimum thickness. Too thick an hydroxide layer retarded nitridation.

The first quantitative and systematic results on the reaction were those of Frankenberger (104), who evaporated lithium from an iron crucible in high vacuum on to glass rings, of calculable surface areas, and measured the uptake at constant pressure, over the temperature range of $-50^{\circ}C$ to $+50^{\circ}C$. A thin protective layer covering the surface uniformly was initially formed at rates too small for measurement. Then nuclei appeared in this layer; these spread laterally and hemispherically, down into the metal as determined by sectioning. An increasing autocatalytic rate curve was obtained before the whole surface became covered with a thick crust. This crust was a crystalline porous aggregate, which allowed easy diffusion of nitrogen to the metal surface through fine pores and cracks. In the autocatalytic period the rate law

$$-\frac{dp}{dt} = KM^{2/3}$$

was obeyed. Here M is the uptake of nitrogen at time t, and K the rate constant. K was temperature dependent and obeyed the Arrhenius equation giving an activation energy of 16.4 kcal/mole. Pure cylinder nitrogen, dried by passing it through various chemical drying agents and a liquid nitrogen trap, was used.

Soliman (105) studied the reaction of molten lithium with dry nitrogen in a constant volume system from ½ atmosphere pressure, and from 400° to 500°C. He obtained an activation energy of 47 kcal/mole, but did not characterize the form of the rate curve. No indication was given of the method used to maintain purity of the lithium samples during handling.

Longton (106) investigated the reaction at constant pressure over the range 50-750 mm.Hg between 300° and 450°C. The rate obeyed a parabolic law, and the activation energy was given as 16,980 ± 900 cals/mole, independent of pressure and temperature.

1.4.4. Nitridation of the Alkaline Earth Elements.

1.4.4.1. Nitridation at Elevated Temperatures with Formation of Thick Crusts.

(a) Calcium.

Sieverts and Brandt (107) found the rate of uptake of dry nitrogen was extremely rapid above the melting point of calcium, but slow with the solid. Below the melting point, the rate was more rapid when the surface of the metal was first covered with a layer of nitride.

Ruff and Hartmann (108) found, on the contrary, that pure nitrogen did not react appreciably below the melting point. A large number of alloys were examined comprising added alkali metals, a number of heavy metals and an alloy with calcium nitride. Metals which were more electro-positive than calcium stimulated reaction while less electro-positive metals had either no effect, or retarded it. Alloying with calcium nitride induced reaction, and they attributed Sieverts and Brandt's results to the presence of calcium nitride in their calcium samples. Ruff and Hartmann's studies were carried out at 520°C in a constant volume system; first the velocity increased slowly, then became almost constant and finally decreased as the pressure became very small. They observed that the nitride layer formed was permeable to nitrogen and cracked easily with changes of temperature.

Antropoff and Germann (109) using more rigorous

conditions in the purification of their specimens, reconciled these conflicting results; they showed that pure calcium surfaces were much less active than impure samples, nevertheless reaction eventually occurred with nitrogen. The presence of a preformed oxide layer had an inhibiting effect. Above 350°C the activity was enhanced by formation of a crust of nitride of a certain thickness. After an initial rapid reaction, a semi-permeable layer developed and the rate decreased rapidly. Thereafter a very slow rate continued, until the layer reached a thickness of approximately 1mm. The rate then became very rapid and constant and the nitride layer appeared to become a porous crystalline aggregate, permeable to nitrogen. It was found, by sectioning, that nuclei developed in the semi-permeable layer and grew in concentric shells in a manner resembling that described by Frankenberger for lithium nitride layers. Sodium, potassium and lithium, included as alloys or in contact with the surface, accelerated the reaction of calcium with nitrogen but calcium nitride in alloy form had no effect.

(b) Magnesium.

The kinetics of nitridation of magnesium have been investigated systematically by Sthapitanonda and Margrave (110) between 300° and 500°C at constant pressure. Reaction began at 300°C and the rate became appreciable above 415°C. Above 500°C the relatively high vapour pressure of

magnesium caused complications. Over the range studied a linear law was obeyed, the rate constant being expressed by

$$k\ (mg./cm.^2/hr.) = 2.2 \times 10^4 e^{-22,300/RT}$$

The rate was found to increase very slightly with pressure but no definite correlation could be found.

Investigation of the beryllium/nitrogen reaction kinetics have been carried out by Gulbransen and Andrew (114) with filed specimen surfaces, using the vacuum microbalance technique between 600° and 925°C for pressures of a few mm.s up to 7.6 cm.Hg. The uptake followed a parabolic law and a large activation energy was found, 75 kcal/mole. A very small increase in rate occurred with increasing pressure, consistent with outward diffusion of beryllium ions through the nitride scale, but no definite dependance could be determined.

1.4.4.2. Nitridation at Low Temperatures with Formation of Very Thin Films.

De Graff and Hamaker (111) reported the high reactivity of barium films, evaporated from barium redistilled in vacuo, towards both nitrogen and oxygen. Barium was evaporated both in vacuo and in atmospheres of various gases (argon and nitrogen in particular) and it was found that the uptake was greatly increased, even when the atmosphere consisted of nitrogen evolved from impurities in the evaporating pellet. This same effect has been noted in the present work when lithium was evaporated in an atmosphere of nitrogen evolved

at high temperatures from impurities in the lithium pellet. De Graff and Hamaker found that the activation energy for the nitride reaction varied, with increasing coverage, from 900 cal/mole to 9000 cal/mole.

Trapnell (112) has also reported activation energies, increasing from 1500-3800 cal/mole with increasing coverage, in the very thin film region, using evaporated calcium surfaces.

The only systematic investigation of the calcium/nitrogen reaction, in the thin film region, is that of Roberts and Tompkins (22). Using evaporated sintered calcium films they studied the kinetics of the reaction between 23° and 200°C, using a constant low pressure technique. The results were consistent with a modified Mott and Cabrera theory of very thin film formation. The rate was dependent on the first power of the pressure, suggesting a reversible adsorption to form a 'surface complex', N_2^-. A linear dependence of activation energy on the inverse thickness of the nitride layer was found as predicted by the theory and the value of the maximum activation energy at infinite thickness, obtained by extrapolation, was 22 kcal/mole. The theoretical value of the critical temperature was about 162°C. An estimation was also made of the total number of metal sites/unit area of interface from which the metal ion penetrates the nitride lattice. An initial short nucleation period was

observed with an increasing rate, during the formation of the first layer, similar to that found, for example, in the oxidation of barium (113). Then a period with a constant rate, and finally a rate diminishing rapidly with thickness, according to the inverse logarithmic behaviour.

2 EXPERIMENTAL

2.1. Oxidation of Evaporated Lithium Films.

2.1.1. Apparatus.

A pyrex high vacuum apparatus was constructed. The main pumping leads were of either 4 cm. or 3 cm. I.D. tubing, while for the remainder of the apparatus approximately 8 and 10 mm. I.D. tubing was used. In those portions of the apparatus where temperature gradients, large enough to necessitate thermal transpiration corrections, occurred over lengths of tubing the exact diameters were measured accurately by calipers before incorporation in the apparatus. Edwards "N" high vacuum grease and silicone high vacuum grease were employed as stopcock lubricants.

The apparatus is now considered in sections for purposes of detailed description.

2.1.1.1. Pumping Section. (Fig. 2.2.)

This consisted of a Klemperer single stage mercury diffusion pump P1 in series with a three-stage mercury diffusion pump P2, which in turn was backed by a Speedivac rotary oil pump No.1. This pumping system was used to evacuate the greaseless sections of the apparatus i.e. the absorption and gas dosage sections. It was known to be capable of attaining dynamic vacua of less than 10^{-7} mm. Hg., as measured by an Edwards I.G.2. ionization gauge. Two water-cooled traps of large contact area were built in series between the pumps and the absorption section to condense any mercury vapour.

2.1.1.2. Gas Storage and Preparation Section (fig. 2.1.).

This section, which could be isolated from the gas dosing section by the mercury cut off (1), was pumped out independ ntly of the main pumping section by means of the three-stage diffusion pump P3 and could be isolated from this pump by the stopcock 10.

(a) Hydrogen.

Bulb A was evacuated through stopcocks 1, 4 and 10, and filled with hydrogen from a cylinder through 1. It was evacuated and refilled a number of times to remove completely air from the connecting tubing. Hydrogen was then purified by diffusion through the palladium thimble B heated externally by a furnace to approximately 300°C.

(b) Oxygen.

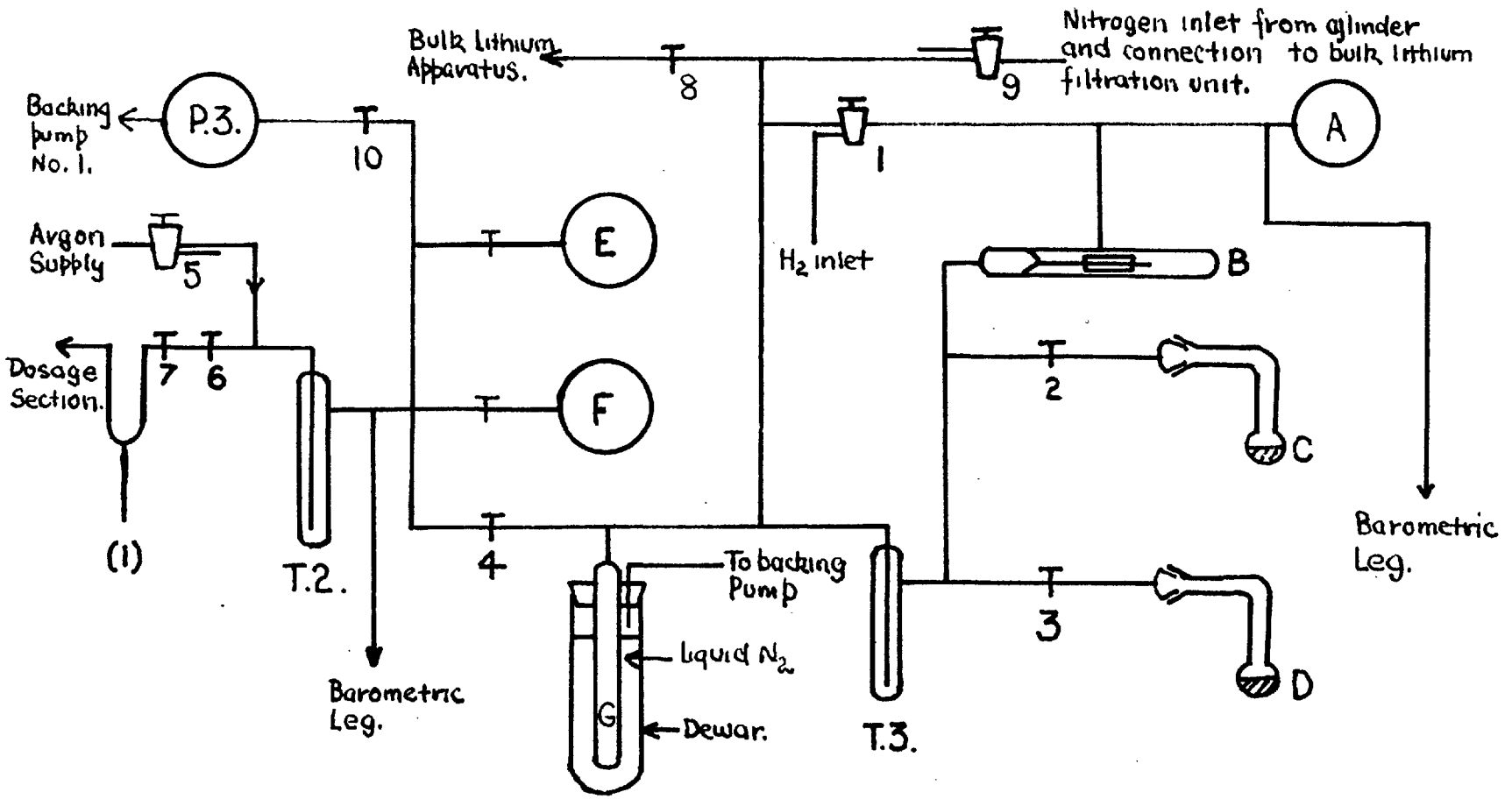
A.R. potassium permanganate after initial outgassing with partial decomposition in bulb D, was decomposed thermally at c.a. 300°C.

(c) Nitrogen.

Nitrogen was prepared by thermal decomposition of pure sodium azide at 310°C after lengthy outgassing at 200°C.

Gases so prepared were then passed through a liquid nitrogen trap T3 and stored in bulbs E and F until required. Whenever possible gases were prepared as required. While being used they were kept in contact with T2, which was submerged in liquid nitrogen, before admission to the dosage section.

FIG. 2.1. GAS PREPARATION AND STORAGE SECTION.



KEY. P.3. Hg PUMP. 1–10 STOPCOCKS T2, T3. TRAPS. (1) Hg CUT-OFF. A–G. SEE TEXT.

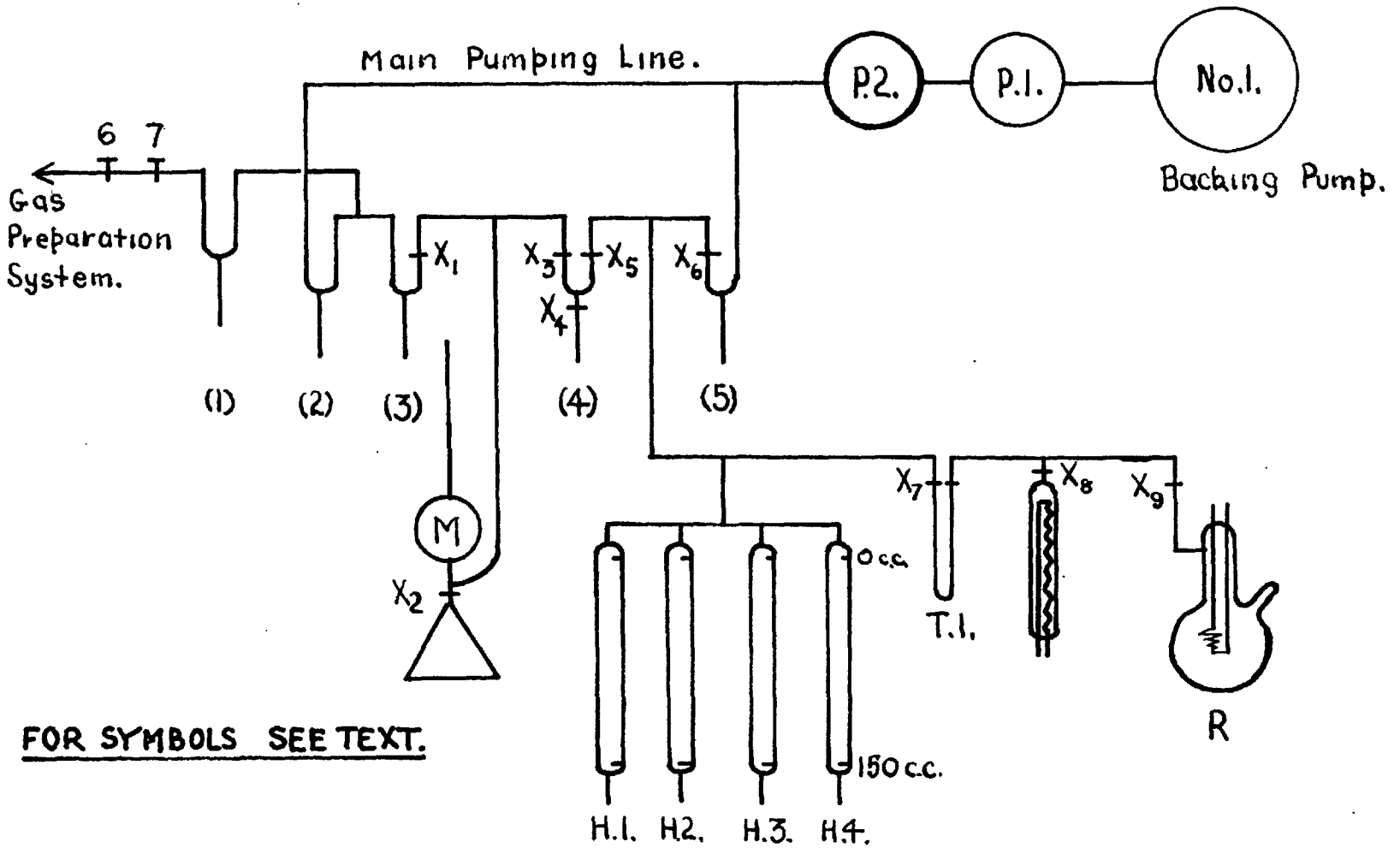
2.1.1.3. Gas Dosage Section. (fig. 2.2).

This section comprised stopcocks 6 and 7, cut offs (1), (2), (3) and (4) and McLeod gauge M. Quantities of gas could be transferred from the gas preparation section to the small volume between stopcocks 6 and 7 and expanded between 7 and cut off (1) in the raised position. With 7 closed it was further expanded between (1) and (3), with (2) raised to isolate the system from the main pumping line. From here it was transferred into the McLeod gauge M by raising (3) to X_1 and (4) to X_3. The volume enclosed between X_1, X_2 and X_3 was accurately known from gas calibrations using the known volume of the McLeod gauge as a standard. The pressure was then read off the McLeod which covered the range from 10^{-5}mm. Hg to 10^{-1}mm. Hg. This known quantity of gas was then added to the absorption section by raising (5) to X_6 isolating the absorption section from the pumps and lowering (4) to X_4. By means of this system, doses could be prepared while either reaction was proceeding between (4) and (5) in the raised position or while pumping in the absorption section with (4) raised and (5) lowered.

2.1.1.4. Gas Absorption Section (fig. 2.2).

This comprised the volume between (4) and (5) and the variable heights of the gas burettes H1,2,3,4 enclosing the trap T1, Pirani gauge J and the reaction vessel R. The fixed volume between X_5 and X_6 and the burettes, with mercury

FIG 2.2. GAS DOSAGE AND ABSORPTION SECTION.



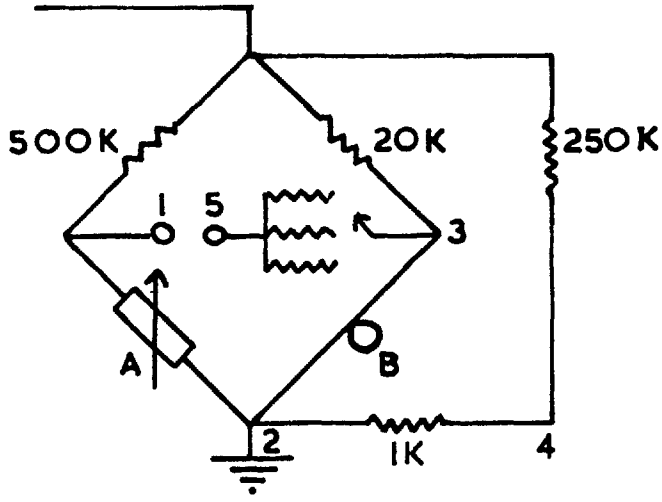
FOR SYMBOLS SEE TEXT.

raised to their highest calibration marking, was known from gas calibrations. The volumes of those portions of the apparatus immersed in fixed temperature baths, namely below X_7, X_8 and X_9 were also known from water calibrations, since these volumes were required for calculating the thermal transpiration corrections. The McLeod capillary was calibrated with a mercury pellet and the bulb with water in the usual way. The trap T1 was large so that it could be immersed to a sufficient depth in a large Dewar of liquid oxygen and left for long periods without danger of complete evaporation of liquid refrigerant. The gas burettes could be varied over a total volume of 600cc. and could be read accurately to 0.1cc. The levels of mercury could be raised steadily by means of a leak valve to atmosphere attached to a two way stopcock on the mercury resevoirs, or lowered by means of a secondary backing pump (No.2) through this two way stopcock.

2.1.1.5. Pirani Gauge (fig. 2.3).

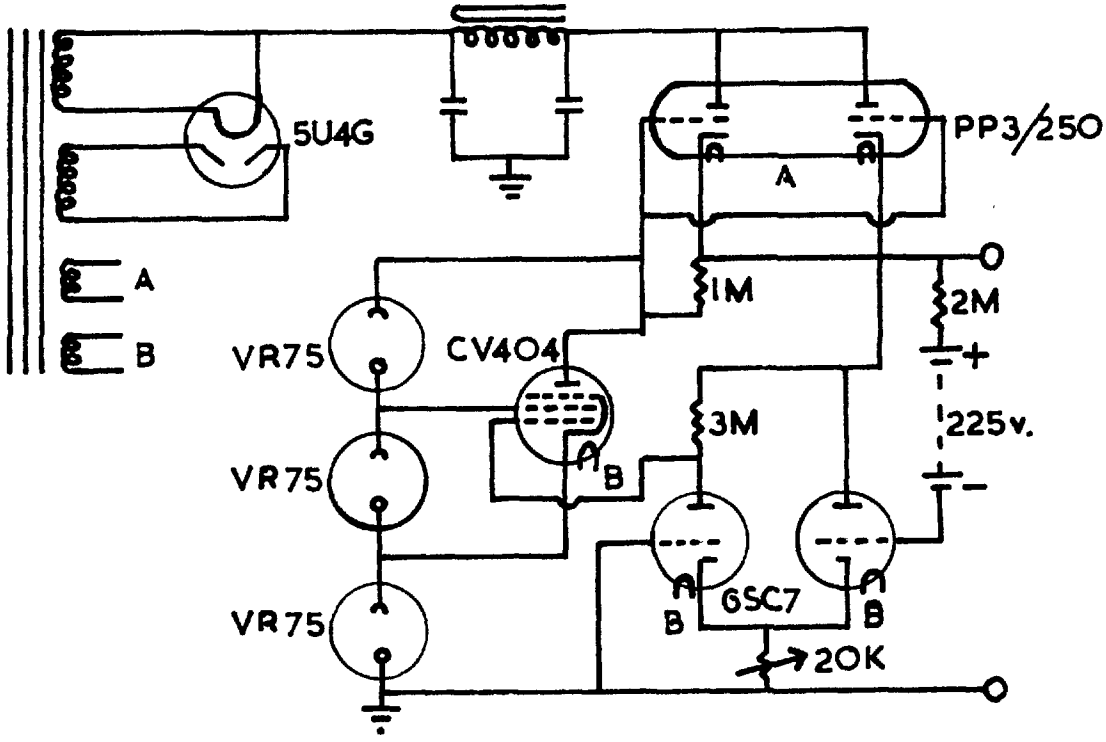
The Pirani gauge was of simple design; a tungsten filament (0.03 mm. diameter and approximately 150 ohms resistance) was stretched between and spotwelded to nickel clips approximately 15 cm. apart which in turn were spot-welded to the tungsten support rods (1.5 mm. diameter). The filament was stabilized electrically and mechanically before use by passing a current of 40 m.a. through it for 30 minutes, while the gauge head was being heated in vacuo

FIG 2.3. PIRANI CIRCUIT.



KEY A-DECADE BOX B-FILAMENT.

FIG 2.4. VOLTAGE STABILIZER CIRCUIT.



at 350°C in the outgassing furnace. Since the sensitivity of a Pirani gauge is dependent on the difference between the wall and wire temperatures, the Pirani was operated with the head immersed in liquid oxygen maintained at a fixed mark X_8 which was well above the top of the filament. If this were not carefully attended to, fluctuations were observed in the readings. The measuring circuit was simply a Wheatstone bridge (fig. 2.3). A high stabilized voltage (about 240 volts) was supplied across the bridge, which was stepped down by large resistors in two of the ratio arms, so that one had a constant voltage and virtually a constant current supply since the current drain through the Pirani (12 m.a.) was almost negligible. The constant voltage stabilizer was based on the design of Solomon (131) and the circuit is shown in fig. 2.4. The stability of the voltage, which was stepped down by a potential divider (250K to 1K), was investigated by measuring the voltage across the 1K resistor (2-4) with a potentiometer; short term fluctuations were of the order of 0.1%.

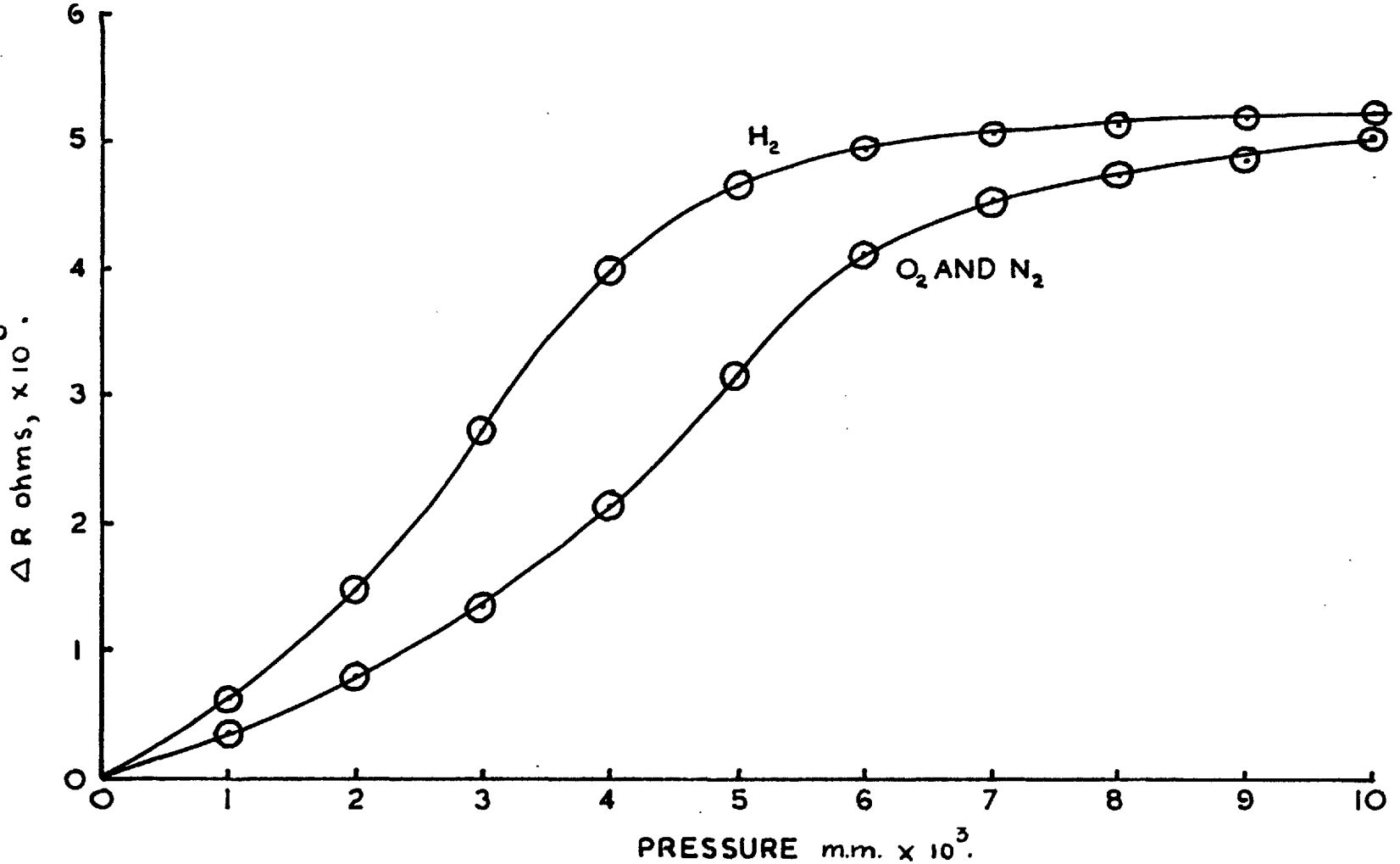
The ratio of the fixed arms of the bridge was 25 to 1 so that changes in the resistance of the Pirani filament (2-3) were magnified by this ratio before being balanced by the decade box (1-2). A Tinsley galvanometer type S.S.2. (sensitivity 22mm./μ amp.) (1-5) was found to be sufficiently sensitive for use in the measuring circuit.

The Pirani zero R_o i.e. the filament resistance in

vacuo was measured. After switching on the voltage stabilizer and putting up the liquid oxygen trap round the Pirani head, the instrument required about 30 minutes to equilibrate. Thereafter no fluctuations in the zero value either transitory or long term were noticed during operation. The Pirani was calibrated against the McLeod before use and such a set of calibrations with oxygen, nitrogen and hydrogen is shown in fig. 2.5, where the change in resistance ΔR (= $R_o - R_p$ resistance at pressure p), is plotted against pressure. The sensitivity of the gauge decreased rapidly above 10^{-2}mm., so that its use was restricted to below these values. For lower pressures the Pirani was exceptionally sensitive (1 ohm was equivalent to 10^{-6}mm.) so that since changes of 0.1 ohm could be determined readily, this corresponds to a sensitivity of 10^{-7}mm. over most of the pressure range used. Even well into the 10^{-2}mm. Hg region it could be used as a null point instrument with sufficient accuracy for practical purposes.

For rate measurements the Pirani was used as a null point instrument, the time being noted when the bridge was balanced at a specific resistance, the pressure being held constant by continually raising the gas burettes as the reaction proceeded. Readings could be taken every 15 seconds if necessary depending on experimental conditions. Unfortunately if pressures in the absorption section were increased suddenly, as was sometimes necessary there was a

FIG. 2.5. PIRANI CALIBRATION WITH O_2 N_2 AND H_2.



time lag of up to 150 seconds before equilibrium was attained.

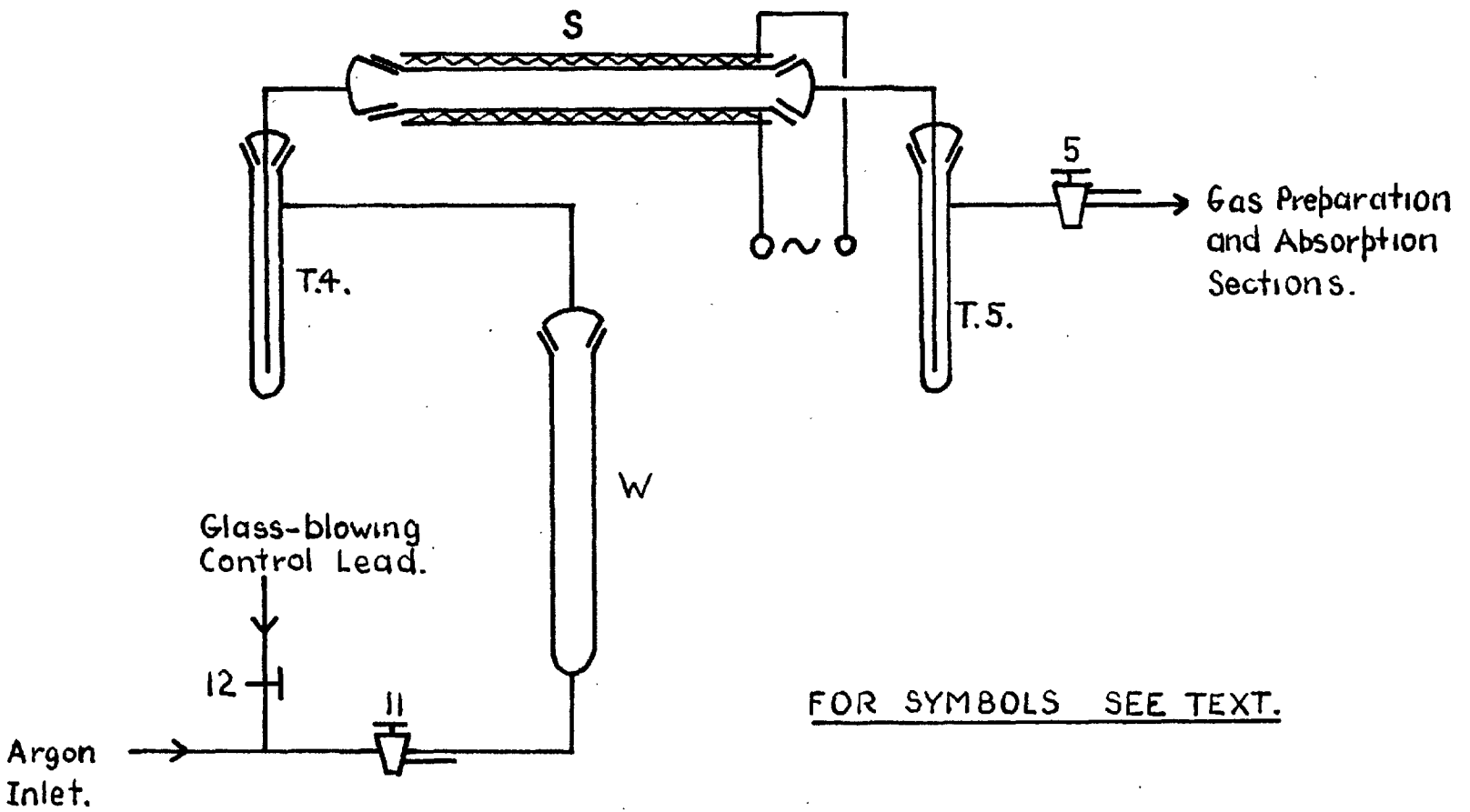
2.1.1.6. Preparation of Pure Inert Argon Atmosphere (fig.2.6).

Since an inert atmosphere was required for the handling, transfer and storage of lithium, cylinder argon 99.95% pure, as supplied by the British Oxygen Company was used. The analysis was given as follows:

oxygen	10 p.p.m.
carbon dioxide	1-2 p.p.m.
hydrogen	<1 p.p.m.
traces of other carbonaceous compounds	<5 p.p.m.
nitrogen	500 p.p.m.
water vapour	25 p.p.m. above 15 atmospheres pressure. Below this pressure a slight increase in content occurs.

Since water vapour represented the most reactive impurity as far as lithium was concerned, the argon was passed through a purifying train, comprising a column W, containing finely divided magnesium perchlorate, a trap T4 packed with glass wool immersed in a cardice-alcohol bath, a column S containing heated high purity calcium metal at 400-500°C to absorb any residual oxygen and nitrogen traces, and finally another cardice-alcohol trap. The pure gas could then be passed through stopcock 5 into the main apparatus or alternatively through the dry-box or desiccators as required. Spectroscopic analysis indicated no trace of water vapour, a reduction of oxygen impurities, but not much change in the nitrogen content. Nevertheless freshly cut lithium surfaces

FIG.2.6. ARGON PURIFICATION SECTION.



FOR SYMBOLS SEE TEXT.

stored under this atmosphere remained bright indefinitely without sign of contamination.

Taps 11 and 12 in fig. 26. were used for control of argon pressure during glass blowing as described later in section 2.1.2.3.

2.1.1.7. Storage and Handling of Lithium.

Lithium was used as supplied by two sources: (1) Johnson Mathey Ltd. who kindly provided, as a gift, a quantity of their highest purity lithium stored under argon. (2) The chemical engineering department of the A.E.A. at Aldermaston. It was supplied stored under high purity argon in sealed polythene screw top bottles contained in an argon atmosphere in a polythene envelope which was in an argon filled desiccator containing a desiccant. It was stored in this manner in the laboratory, and the original metallic lustre was maintained on undisturbed samples for up to at least 10 months. Two batches of prefiltered lithium from this source were used. The analysis of the lithium was given as:

(1) Lithium supplied by Johnson and Mathey Ltd.

sodium	0.120%
potassium	0.003%
iron	0.006%
calcium	0.019%
nitrogen	2.24%
6 other impurities	$<$0.001%

(2) Lithium supplied by the U.K.A.E.A.

sodium	0.3%
zinc	60 p.p.m.
cadmium	<10 p.p.m.
magnesium	<10 p.p.m.
manganese	<10 p.p.m.
boron	<20 p.p.m.
potassium	<200 p.p.m.
chloride	250 p.p.m.

The material from source (1) was used mainly for preliminary qualitative runs, while one batch from source (2) was used for the oxidation work and the second batch for the nitridation investigations.

For the cutting and handling of lithium a dry box was used, flushed with a stream of the purified argon and containing P_2O_5 as desiccant. Lithium was transferred to the apparatus from the dry box in two ways: either a small pellet was cut off and placed under argon in sealed polythene containers, or by means of a lithium pipette, made of nickel, stored in an argon-filled desiccator. (See fig. 2.7). The dry box had facilities for melting the lithium in a small electrically heated nickel crucible. A vacuum line was also attached to the dry box for drawing molten lithium into the heated pipette.

FIG.2.7. LITHIUM PIPETTE.

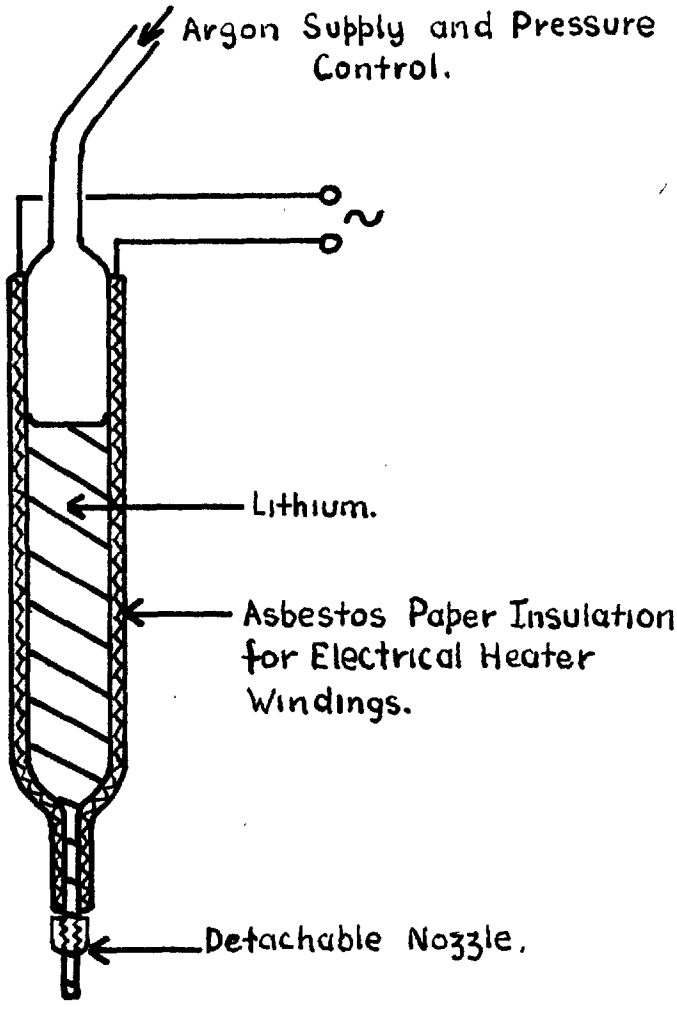
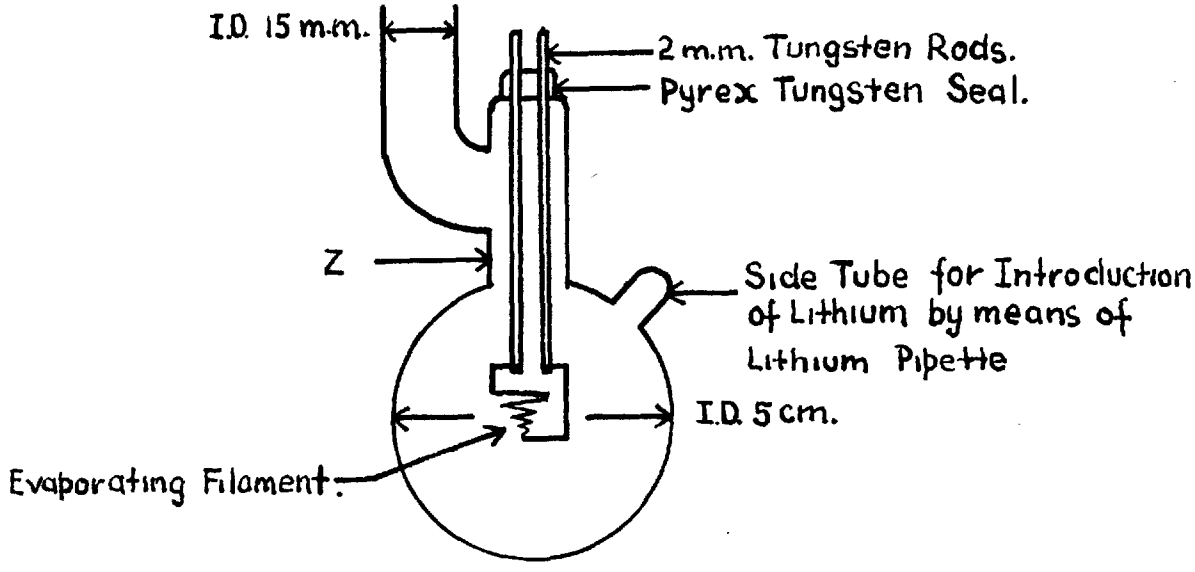


FIG. 2.8. REACTION VESSEL.



2.1.2. Experimental Procedure.

2.1.2.1. Preparation of Filament Basket (fig. 2.8).

The evaporating filament basket was constructed of 0.3 mm. molybdenum wire wound on a conical former and spot-welded to the tungsten terminals. Previous lithium films were removed with repeated boiling in distilled water and any surface oxide coating on the molybdenum filament was cleaned away by A.C. electrolysis in warm moderately concentrated A.R. caustic soda solution. After further rinsing with distilled water the reaction vessel was oven dried and sealed on to the vacuum system.

2.1.2.2. Preliminary Outgassing.

The apparatus was evacuated and the absorption cell was outgassed at 400°C with a furnace while the Pirani gauge, trap, burettes and cut offs were heated with electrothermal heating tapes. The remainder of the high vacuum system including the McLeod gauge was flamed out vigorously with a hand torch. During this period 1 cm. Hg of hydrogen was introduced and the evaporating basket was heated to a bright red colour. After about 30 minutes the molybdenum wire became silvery and then the hydrogen was pumped away. Further outgassing in vacuo with the filament glowing at approximately 1000-1200°C was continued overnight until the outgassing rate under these conditions was better than 10^{-4}mm. Hg per hour.

2.1.2.3. Introduction of Lithium to the Evaporating Basket.

The heaters were switched off and pure argon was introduced through stopcocks 5, 6 and 7. See figs. 2.6, 2.1, 2.2. Small quantities of argon were first flushed through, with the main Hg diffusion pumps P1 and P2, operating, so that any oil vapour in the connecting tubing between P1 and the backing pump was flushed out. Before the argon was completely pumped away the tap between P1 and the backing pump was closed. The mercury pumps P1 and P2 were then switched off and argon allowed to enter the entire system to pressure of 1 atmosphere, when stopcock 12 (fig. 2.6) was opened to atmosphere. Stopcock 12 was connected to a rubber lead, which could be constricted manually, producing increases of argon pressure above 1 atmosphere. A cardice-alcohol trap was now raised around T1. One of the two methods was now used for introducing lithium into the evaporating basket. The pipette heater was switched on, in order to melt the lithium, then the tip of the glass side tube on the reaction vessel bulb softened in a flame. By clamping the tube attached to stopcock 12 the pressure of argon blew a hole in the side tube (fig. 2.8). Stopcock 12 was then shut so that a stream of argon was emitted from the hole. The tip of the pipette was then introduced slowly through the side tube into the conical basket after first extruding and rejecting a small amount of contaminated lithium at the tip in a stream of argon. Control of the amount of lithium transferred was maintained by a pressure of argon in a similar way to the glass blowing procedure described above.

The pipette was then withdrawn and the side tube was sealed with a torch maintaining glass blowing control again by argon pressure through stopcock 12.

This method gave a very clean head of lithium, but trouble was sometimes experienced with the operation of the pipette, due to difficulty in handling and positioning when at a temperature above the melting point of lithium. The chief trouble was that, for a few seconds it was necessary to transfer the heated pipette through the atmosphere. This sometimes resulted in rapid formation of lithium nitride in the tip, blocking it completely, and necessitating cleaning out and refilling. Consequently a simpler method, which proved quite efficacious and reliable, was adopted. Small pieces of lithium were cut off in the dry box and transferred to the apparatus in an argon filled polythene screw-top container. A scratch was then made on the glass at the point Z (fig. 2.8) and the bulb cracked with a hot bead of molten glass at this point keeping the argon slightly above atmospheric pressure. The bulb was lowered to give access to the evaporating basket and the pellets inserted with tweezers. The bulb was then raised resealed under argon and evacuated. Since argon is heavier than air and because a large flow of gas was maintained downwards from the neck of the reaction vessel to envelop the filament only slight amounts of air were likely to enter the bulb during the short time for which it was separated. The whole operation took no more than 5-6 minutes.

Some contamination of the metal surface was observed during the annealing process but never more than the very thin black film which occurs before formation of a macroscopic nitride layer. In the best cases the metal surface retained its metallic lustre throughout.

2.1.2.4. Final Outgassing Procedure.

With all heaters on, except the reaction vessel furnace, the reaction vessel was thoroughly flamed out taking care that radiation did not produce a lithium film. The current through the evaporating filament was then raised until the lithium bead became molten. (M.P. 186°C (132)). Since the vapour pressure of lithium is small even considerably above the M.P. (133, 134), outgassing of the bead could be carried out for long periods without the production of a film. Outgassing was continued until the rate became immeasurable ($<10^{-6}$mm.Hg/hour). Sticking vacuums were obtained in the McLeod even after isolation from the pump for 30 minutes.

2.1.2.5. Evaporation of Film.

Liquid oxygen was raised to the fixed mark on the Pirani gauge and liquid nitrogen round the reaction vessel. Film evaporation was carried out slowly at as low a filament temperature as possible, the operation usually taking about 2 hours. During this time a negligible pressure increase was registered by the Pirani gauge even with cut offs (4) and (5) raised. However, if the temperature was too high

hydrogen evolution occurred. This was presumed to be due to decomposition of small amounts of lithium hydroxide impurities, unavoidably produced in the pellet during the glass blowing on the reaction vessel, viz:

$$2LiOH(s) \rightarrow Li_2O(s) + H_2O(g) \quad (1)$$
(in hottest region of pellet)

$$2H_2O(g) + 2Li(l) \rightarrow LiOH(s) + H_2(g) \quad (2)$$
(in colder regions of pellet)

These reactions constituted the main danger of contamination during film evaporation, since lithium nitride, oxide and carbonate are stable at far higher temperatures than lithium hydroxide (134, 135). The evolved gas was identified from the Pirani calibrations. However in most cases evaporation could be carried out at such a temperature that hydrogen evolution was negligible.

Very thin films of lithium are pink and blue, but become silvery when thicker. Thin films in vacuo at room temperature were observed to disappear in a short time indicating that reaction or absorption by the pyrex bulb had occurred. Somewhat thicker films at room temperature occasionally developed tiny pin holes, indicating that sintering or recrystallization processes had taken place. Finally if films were maintained at 100°C for a short time, they underwent colour changes ranging through gold to dark brown and finally black. This external appearance resulted, however, from changes in a thin layer next to the glass, since the surface remained silvery at the lithium/vacuum

interface. To reduce the possibility of these changes affecting the reaction surface of the lithium, relatively thick films, of the order of 10^{-3}mm. ere evaporated. Preceeding absorption measurements, the film was sintered at 50°C for 30 minutes. Due to the high sintering temperature relative to the melting point of lithium and the malleability of the metal it is assumed that the surface area of the film approximates to the geometric area of the reaction bulb. (Cp. calcium films evaporated similarly and sintered at a lower relative temperature, (22)). During sintering no alteration of the Pirani resistance R_o was normally observed.

2.1.2.6. Fixed Temperature Baths.

To permit rapid changes of temperature between 78°K and 320°K a number of fixed temperature baths were employed. These were:

Temperature Bath.	Published Temp. °K (136)	Observed Temp.
Boiling liquid nitrogen	77.3	Standard
Boiling liquid oxygen	90.0	standard
Melting isopentane (2 methyl butane)	113.5	113.95
Melting n-pentane	141.7-143.3	138.55
Melting methyl cyclo hexane	146.6	147.54
Ether	160.0	160.0
Melting toluene	177.8	180.88
Cardice in alcohol	195.0	standard
Chloroform	210.0	210.91
Melting diethyl malonate	223.2	221.43
Melting carbon tetrachloride	250.3	250.94
Melting methyl benzoate	260.66	260.68
Ice-water	273.2	standard
Running tap water	289-294	
Various oil baths normally controlled		

Temperatures were measured by means of a copper constantan thermocouple with one ice cooled junction and calibrated for use in the low temperature region using the standard temperatures above and the method described in International Critical Tables (135).

2.1.2./. Measurements of Reaction Rate.

With the reaction vessel immersed to the point X_9 at the lowest temperature (liquid nitrogen), the Pirani immersed to X_8 in liquid oxygen, the trap to X_7 in liquid oxygen, the gas burettes set at their lowest calibrated mark, cut off (6) raised to X_6, a dose of oxygen was prepared in the volume space V_{o+1} (between marks X_1, X_3 and the McLeod open at X_2). The pressure was measured with the McLeod and then the McLeod was reset at X_2. The volume of the McLeod bulb alone (i.e. the volume with McLeod just closed at X_2) will be denoted V_o. The volume between X_1 and X_3 with the McLeod just closed at X_2 is denoted V_1. The cut off (4) was then lowered to X_4 and the time zero taken. With a clean film the initial rates were too rapid to maintain constant pressure so that it was usually necessary to add another dose or two, until the rate became slow enough to be followed at some constant pressure. After sufficiently characterizing the rate curve, the next higher temperature bath was quickly raised around the reaction vessel and at the same time the burette levels were altered so as to keep the pressure constant. The new rate was then characterized

and the next temperature bath was raised. This was continued until the highest temperature was reached. A period of 2-3 minutes was usually required to change the temperature and reach thermal equilibrium. In this way the temperature dependence with increasing oxide thickness could be studied.

Alternatively the effect of pressure on the rate was studied at a fixed temperature by characterizing the rate at one pressure and then either pumping away a fraction of the gas or quickly adding an extra quantity of gas at a higher pressure and characterizing the new rate.

2.2. Nitridation of Bulk Lithium.

2.2.1. Apparatus (fig.2.9).

The apparatus was constructed partly of pyrex with main pumping leads as in section 2.1.1. while the remainder of the connecting tubing was approximately 8 mm. I.D. The two manometers were constructed of 5 mm. I.D. pyrex tubing and the reaction vessel and filter unit were of Austenitic stainles steel. The connection between the glass apparatus and the metal reaction vessel was by means of a machined and hand ground ball joint held by a spring clip. Silicone high vacuum grease was used as the lubricant for stopcocks and ball and socket joints.

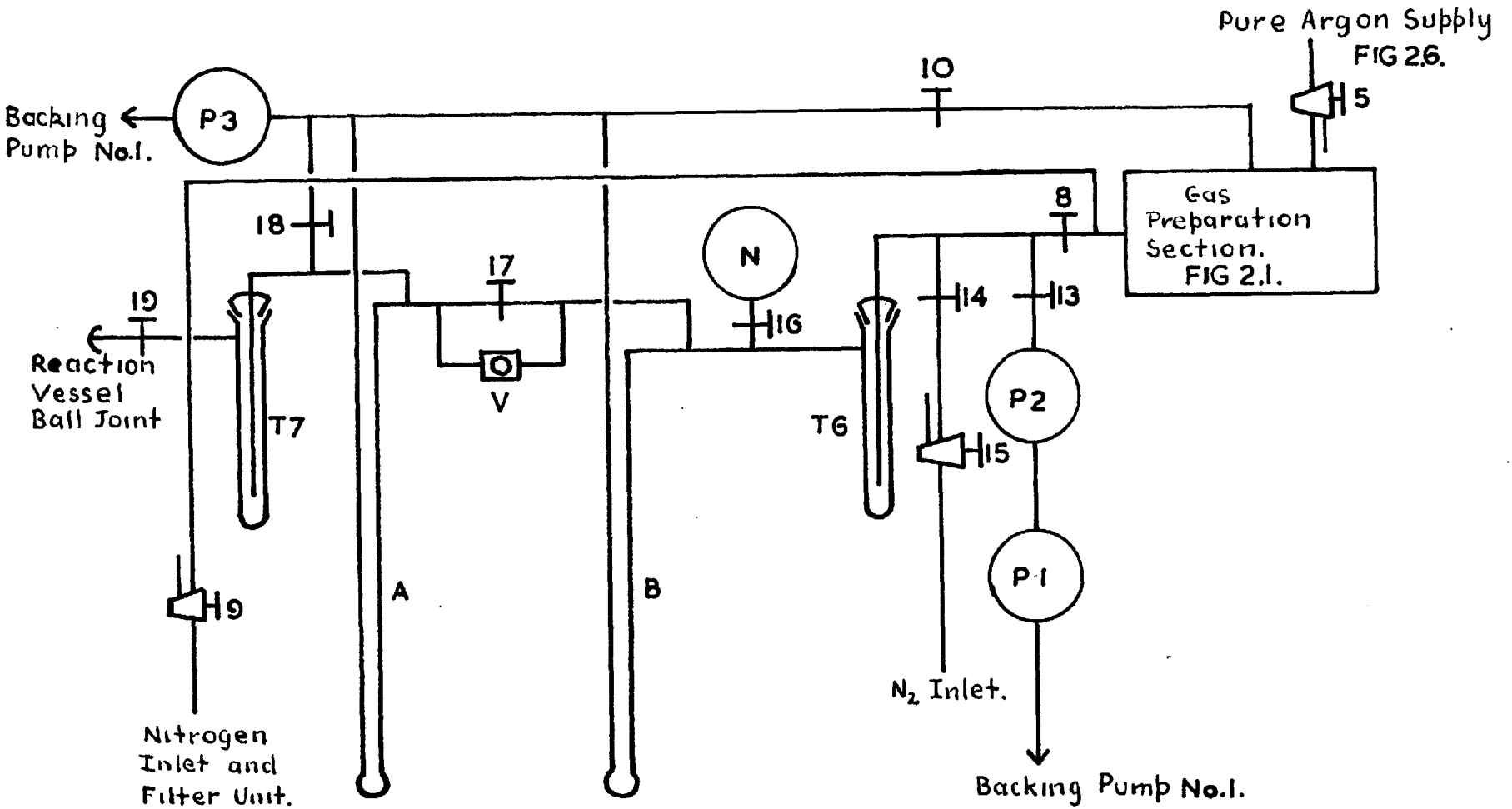
2.2.1.1. Pumping Section.

This was the same as described in section 2.1.1.1. and connected as shown in fig. 2.9.

2.2.1.2. Gas Preparation and Storage.

The nitrogen used was high purity cylinder nitrogen as supplied by the British Oxygen Company. Since the main impurity was water vapour this was removed using the nitrogen liquefaction apparatus marked G in fig. 2.1. This consisted of a Dewar flask containing liquid nitrogen with a vacuum tight rubber bung surrounding the glass finger G. and having a pumping lead through the rubber bung attached to a rough backing pump. Nitrogen was admitted through stopcock 9 at approximately 1 atmosphere pressure and

FIG 2.9. APPARATUS FOR NITRIDATION OF BULK LITHIUM.



FOR SYMBOLS SEE TEXT.

condensed to the liquid in G. This was brought about by pumping in the liquid nitrogen in the Dewar surrounding G causing a considerable cooling below 77°K. When sufficient nitrogen had condensed inside tube G stopcock 9 was closed and taps 4 and 10 were opened to vacuum. This produced further cooling and white crystalline solid nitrogen was formed rapidly. Pumping was continued until all the uncondensed nitrogen gas and any water vapour or uncondensed impurities were removed. The Dewar was removed after closing stopcock 10 and replaced with another Dewar containing liquid nitrogen at its normal boiling point. The nitrogen was stored as liquid at 1 atmosphere pressure. The nitrogen level in the Dewar was never allowed to drop below that at which the solid nitrogen was originally formed, so that any water vapour condensed remained as solid at 78°K thereby contributing negligible v.p. as contaminant.

2.2.1.3. Gas Dosage and Absorption Section.

Gas dosages and rate measurements were carried out by means of two mercury manometers A and B the nitrogen flow valve V and the nitrogen reservoir N. The volume V_N of bulb N was known from water calibrations and was used as the standard for calibrating other relevant volumes of the apparatus by gas expansions. Due allowance in subsequent calculations was made for variations in Volume V_B between

taps 8, 13, 14, 16, 17 and V, caused by fluctuations in the height of mercury in the manometer B. Valve V was of brass construction welded to two copper glass seals and operated by screw pressure on a P.T.F.E. diaphragm with a return spring.

2.2.1.4. Reaction Vessel (fig.2.10) and Lithium Filter (fig. 2.11).

The reaction vessel and detachable filter unit were constructed entirely of welded Austentic stainless steel components. Metal vacuum seals were made via softened copper gaskets in bolted flanges so that three line seals were produced on each gasket. Details are given in fig. 2.10. Since rates were high and operating pressures large, outgassing rates less than 10^{-2}mm. Hg/hour were negligible. Thus one hundred hours would have been required to reach a pressure of 1 mm, a value still small compared to operating pressures. The reaction vessel itself consisted merely of a cylindrical pot sealed with a blank end-plate to flange A when in use, which could be replaced by the filter unit when required. A side arm with a stainles steel socket which was machined and hand ground to fit a standard pyrex ball joint with a spring clip attachment connected the metal apparatus to the remainder of the absorption section. A stainless steel apparatus is necessary when working with molten lithium since lithium at elevated temperatures reacts rapidly with glass.

The filter unit (fig. 2.10) consisted of a cylindrical

FIG. 2.10. REACTION VESSEL.

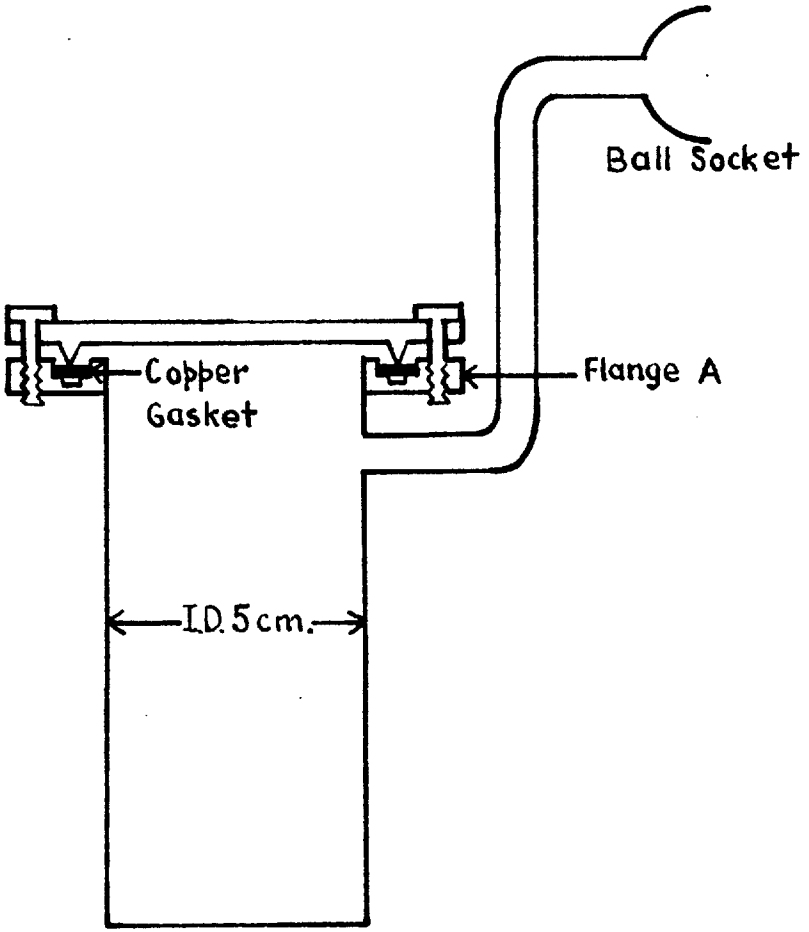
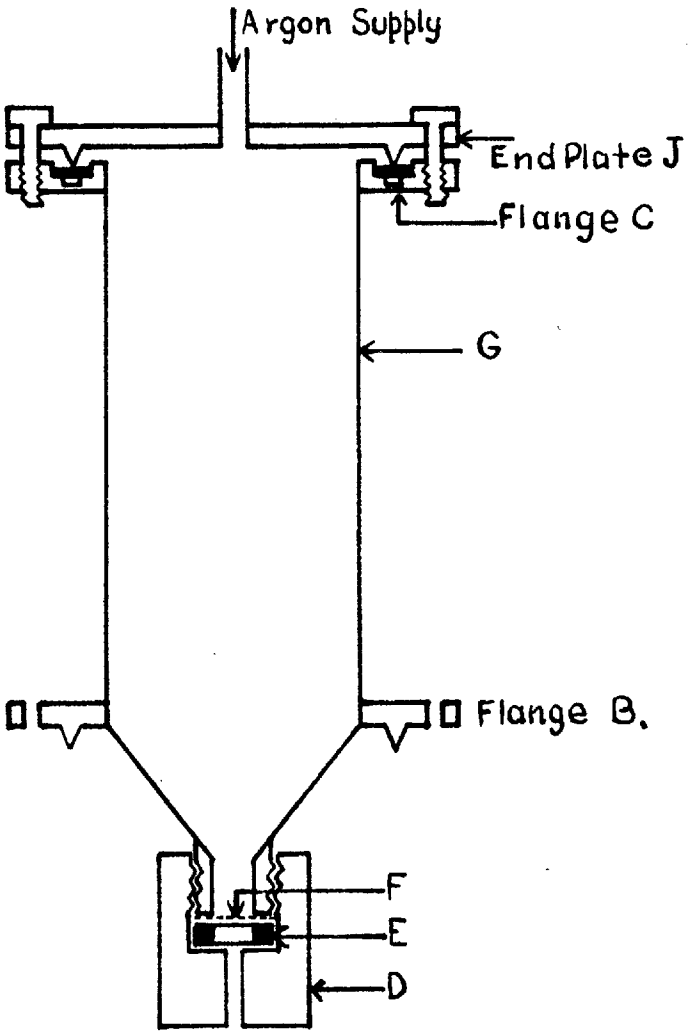


FIG. 2.11. FILTER UNIT.



tube G (containing the pieces of cut lithium) which could be attached to the reaction vessel pot by flange B. A detachable end plate J with an inlet tube from the argon supply was bolted to tube G via flange C. Tube G tapered into the detachable nozzle D containing the positioning ring E for holding the stainless steel fine wire mesh filters F in place. D was of large mass to insure a high heat capacity so that molten lithium was unlikely to solidify and block the nozzle.

2.2.2. Experimental Procedure.

2.2.2.1. Outgassing and Filtration of Lithium.

The reaction vessel with the filter unit attached was mounted evacuated and torched out and the liquid oxygen trap raised around T7 in order to remove adsorbed water and any mercury vapour from the adsorption section. When a good vacuum had been produced, pure argon was introduced at 1 atmosphere pressure. End plate J was removed and sufficient lithium was transferred rapidly into tube G under the argon stream. End plate J was replaced and again evacuated; a furnace was raised around the reaction vessel and filter unit and the lithium melted and outgassed at 300°C, tapping from time to time on the filter unit with a hammer to settle the lithium into the filter funnel. After several hours the lithium was filtered under a pressure of 10-15 cm. of argon. The furnace was removed and the apparatus cooled. Argon at 1 atmosphere pressure was again admitted and the filter unit replaced by the blank end plate H and evacuated once more. When a good vacuum was obtained further outgassing at 300°C was continued for several hours.

2.2.2.2. Fixed Temperature Baths.

Some of the freezing baths described in section 2.1.2.6. were used, but as most of the work was done above room temperature liquid paraffin baths, either manually controlled, when rapid temperature changes were needed, or by means of a

sunvic controller with switching relay when long periods at a fixed temperature were required. For work above the melting point of lithium an electrical furnace was used, thermostatically controlled by means of a tungsten resistance thermometer.

Temperatures above the melting point of lithium were measured by a chromel-alumel thermocouple strapped in contact with the outside of the reaction vessel. The air temperature inside the furnace could be controlled to $\pm$ 0.1°C by the resistance thermometer, but there was a lag in the control of the reaction vessel due to its high heat capacity. Other factors which made temperature control difficult were the high cooling rate due to thermal conduction along the metal portions of the apparatus, particularly at high temperatures, and self heating when the reaction proceeded at very fast rates. This necessitated some manual manipulation of the thermostat settings until steady states were obtained at the various temperatures, but once obtained control could be maintained at c.a. $\pm$0.5°C for sufficient periods of time to characterize the rate curves.

2.2.2.3. Absorption Measurements.

Rate measurements were made at constant pressure by allowing nitrogen to leak through valve V, keeping manometer A at a constant value.

Uptake was measured by following the decrease of pressure in the small volume V_B (189.1 cc) using manometer

B, for slow rates, adding fresh increments of gas to V_B from the nitrogen resevoir (V_N = 2950 cc.), when necessary. Alternatively, for very rapid uptake, or when using high pressures, tap 1.6 was left open, and the pressure decrease with time was followed in the large volume $V_N + V_B$. The ratio $\frac{V_N + V_B}{V_B} \sim 18$, thus a large range of rates could be determined with reasonable accuracy. Manometers could be read to $\pm$ 0.2 mm. and manometer A could be held at a constant pressure (from 20-600 mm.Hg) with an accuracy of approximately $\pm$ 0.5%. Trap 7 was at liquid oxygen temperature during runs.

Rates were measured using solid lithium from 0°C to the m.p. of lithium and on the molten lithium from the m.p. up to approximately 350°C.

3 RESULTS AND DISCUSSION

3.1. Oxidation of Evaporated Lithium Films.

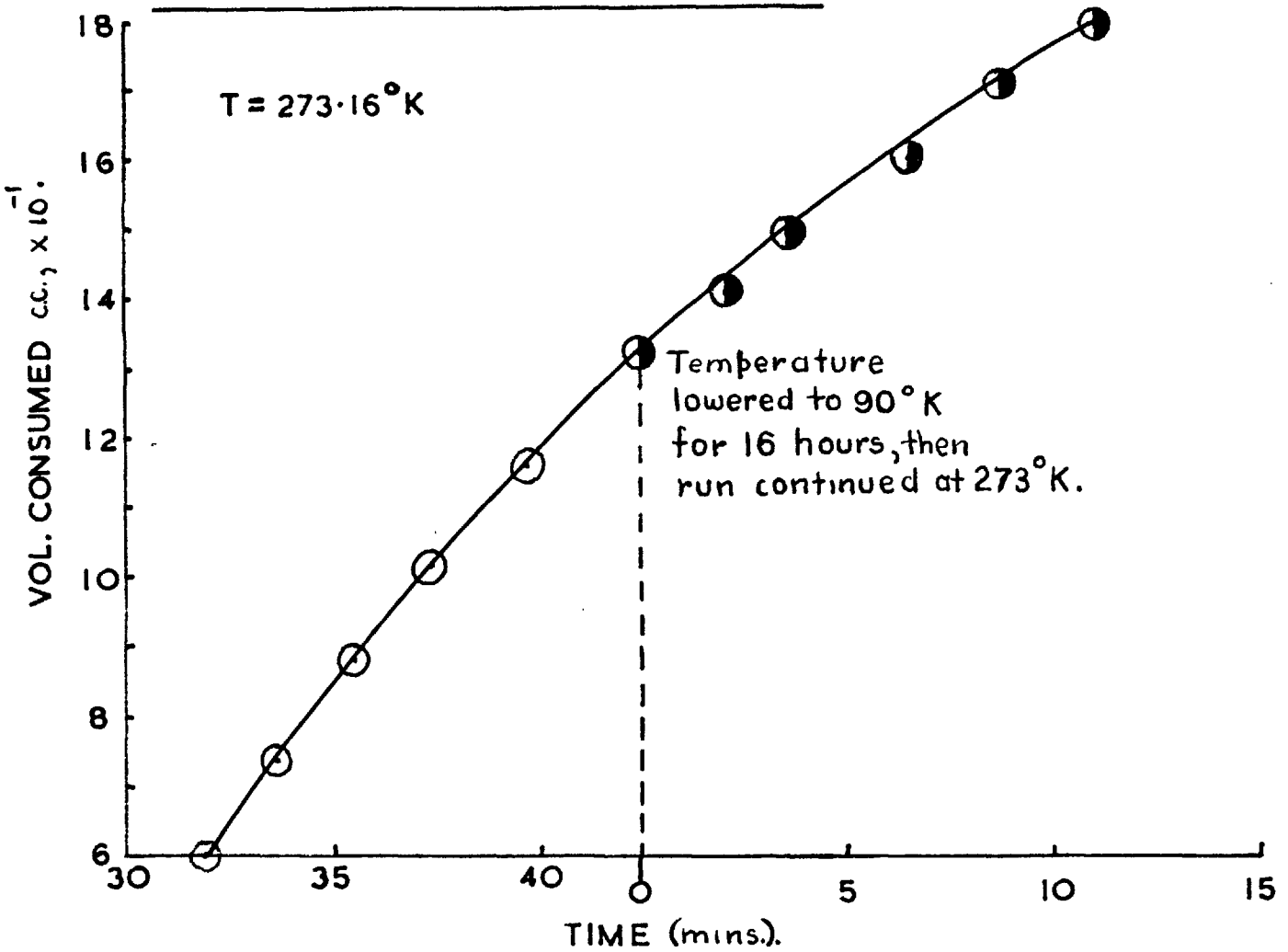
3.1.1. Qualitative Observations.

When oxygen was added at 78°K to a clean sintered evaporated film, a rapid initial absorption occurred, corresponding to about 9 or 10 atomic layers of oxide, at a rate too rapid to be followed either at constant volume or constant pressure. After this the rate become slow enough to be measured at constant pressure and progressively decreased to a low value; by increasing the temperature at this stage the rate was initially increased but then again decreased rapidly. This sequence was repeated with each temperature increase up to 300°C when the rate rapidly accelerated to a much larger value despite the increasing thickness of the oxide layer; at this stage successive doses of oxygen were taken up within 1-2 minutes of contacting the film. A typical series of results is shown in Figs. 3.4., 3.5., 3.6., 3.7., 3.8., 3.9., 3.10.

If the rate was characterized at some temperature T_1, before 300°K had been reached and then suddenly the temperature was considerably reduced to T_2, reaction ceased, resuming again at an identical rate on returning to the higher temperature T_1, even after a lapse of many hours, Fig. 3.1.

Once the temperature had been raised above 300°K, however, reaction did not cease on lowering the temperature,

FIG. 3.1. RATE RECOVERY (RUN 17).



but proceeded as though for a clean film once more. This phenomenon is referred to henceforth as breakaway.

3.1.2. Kinetics of Sorption.

At 78°K it was necessary to add as many as three doses (the maximum value of a dose in the present apparatus being about 1.5 micromoles) before measurable rates were obtained; consequently due to the time lapse necessitated by dose preparation, the time zero in any kinetic run was arbitrary, and was chosen as the instant of commencing a run at constant pressure. From the burette readings and the constant pressure maintained in the apparatus the oxygen uptake, w, micromoles of oxygen was obtained. Direct plots of w against time gave a curve indicating a highly protective layer. Plots of w, and $1/w$, against log $(t+t_o)$ however, could be linearized using particular values of t_o obtained graphically by trial and error. (See Figs. 3.2., and 3.3.). These were always greater than 10 minutes, although they were usually smaller for the inverse log. plots than for the direct log plots. Clearly the plots were somewhat insensitive to the particular functional form, although they could not be fitted to a parabolic law.

Linearity of both types of log plot, was obtained at all temperatures used throughout the experimental work. Thus it can be reasonably concluded that the kinetics of sorption is constant and independent of temperature.

To differentiate between the two log forms it is noted that the theory of Mott and Cabrera for the growth of oxide layers, up to approximately 50 Å thickness, (see section

1.3.2.1.(a)(ii)), predicts the inverse log form, and that furthermore, it predicts that the activation energy is dependent on film thickness and should decrease linearly with the reciprocal of the film thickness (see section 3.1.6.).

FIG. 3.2. LINEARIZATION OF ω/LOG t PLOT (RUN 8)

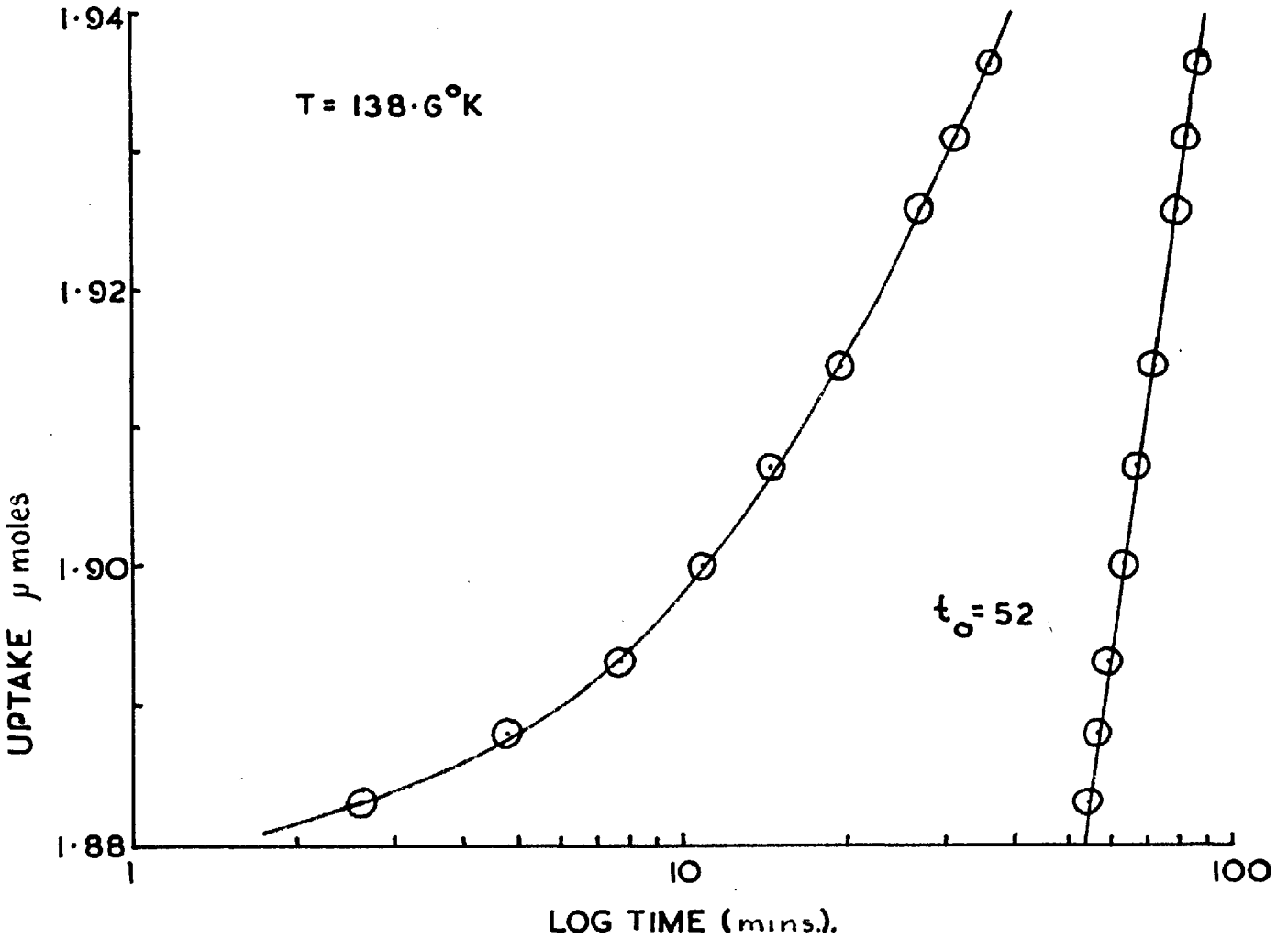
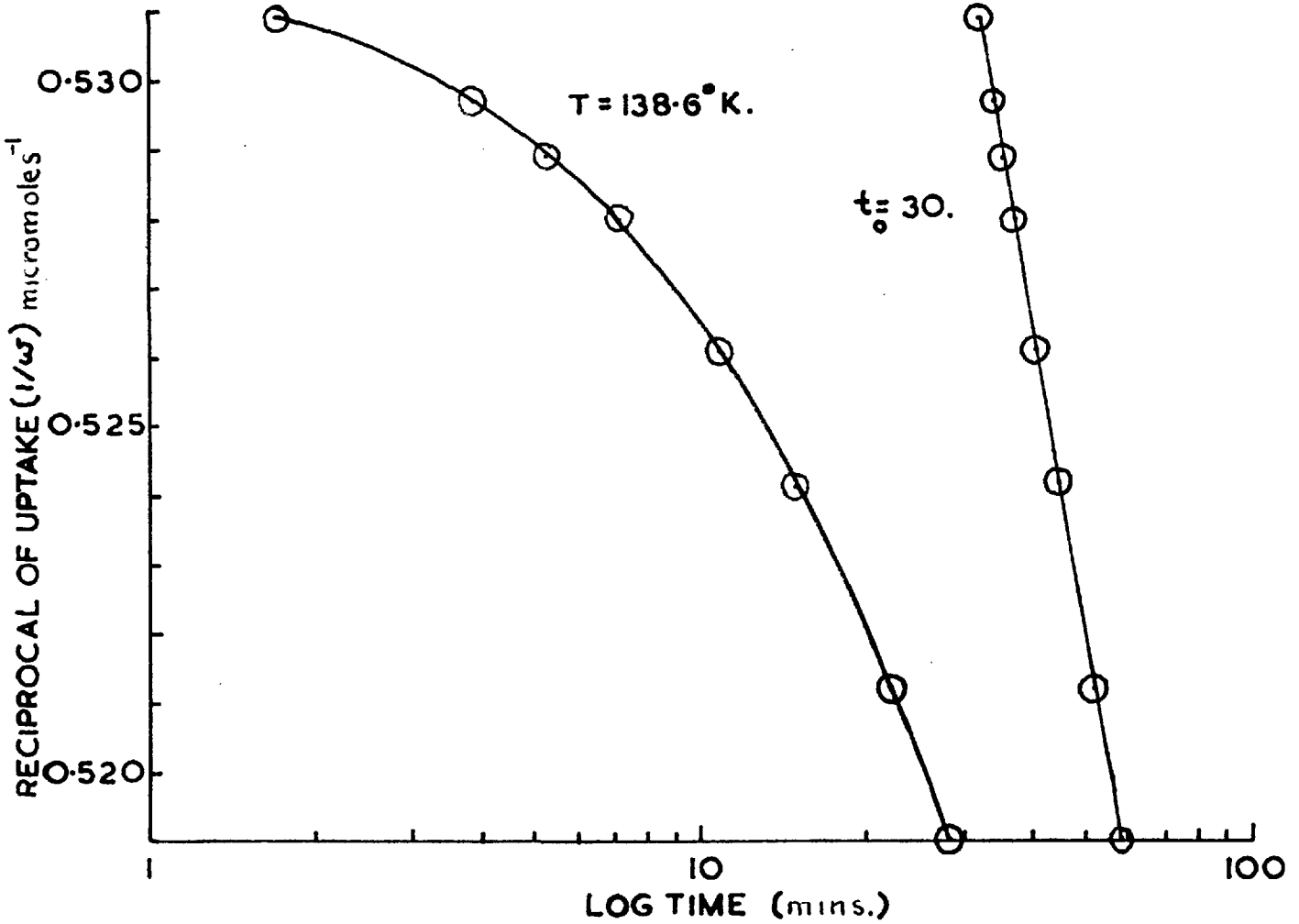


FIG.3.3. LINEARIZATION OF $1/\omega$/ LOG t PLOT. (RUN 8).



3.1.3. Dependence of the Rate on Temperature.

3.1.3.1. Procedure.

In order to determine activation energies at constant film thickness, the rate was characterized at the lowest temperature for a sufficient time, then as quickly as possible the temperature bath was changed to effect a 10-20°K rise in temperature and the new rate characterized maintaining the pressure constant throughout. The time required for the change and the attainment of steady state conditions was 3 to 4 minutes. This procedure was then repeated with successive pairs of temperature baths until the highest temperature or breakaway was reached. The time zero for each activation energy determination was taken as the instant each constant pressure run was commenced and quantities of both gas added or pumped out of the system were measured at all times. It was thus possible to calculate, at any stage, the amount of gas absorbed by the film, and hence the oxide thickness, or the amount present in the gas phase in any section of the apparatus.

Since, as pointed out in the preceeding section, the t_o values required to linearize the log plots were greater than 10 minutes, these plots were insensitive as far as the degree of linearity was concerned, and thus could not be used, with accuracy, for interpretive purposes. It was therefore necessary to extrapolate the empirical (w/t) curves to the instant of intersection at the moment of changing the

temperature bath. This represented constant thickness and the activation energy was determined graphically by drawing tangents to the two curves at the point of intersection.

By this means it was possible to evaluate activation energies at constant calculable film thickness, with increasing film thicknesses but it must be pointed out that the activation energies were determined at varying temperatures. It is assumed in the following, therefore, that the values of activation energy are independent of temperature over the range studied. This is a reasonable assumption, however, because as indicated in the preceeding section, the kinetics of sorption showed no variation with temperature over the experimental range.

3.1.3.2. Calculation of Results.

Since experiments were carried out at low pressures, of the order of 10^{-4}-10^{-2} mm. Hg, with the temperature of the pressure measuring instrument different to that of the absorbent, it was necessary to apply thermal transpiration correctionsto the pressure when calculating quantities of gas in the gas phase, in order to determine the uptake by the film at any stage. For this purpose a series of graphs were drawn using the Bennett and Tompkins (137) modification of Liang's equation covering the range of pressures used, the diameter of pyrex tubing and all the constant temperature baths. By this means it was possible to calculate the actual steady state pressure over the film and the quantities

of gas in any section of the apparatus at a given instant.

The ratio of the rates (r_1/r_2), at the moment of intersection of the (w/t) curves was obtained graphically from the tangents, and activation energies were calculated from the Arrhenius equation in the usual way.

Thus $$E = 2.303 \times R \log_{10}\left(\frac{r_1}{r_2}\right) \times \frac{T_2 \times T_1}{T_2 - T_1} \text{ cal.mole}^{-1}.$$

A complete tabulation of the empirical data, and apparatus constants for a typical run for the determination of activation energies, on an initially clean film (Run 19(a)) is given below, (Table 3.1.), with graphs of the (w/t) curves, (Figs. 3.4., 3.5., 3.6., 3.7., 3.8., 3.9., 3.10.); a calculation of the uptakes, with thermal transpiration corrections, at various stages during the run, has also been set out, (Table 3.2.).

Table 3.1. Empirical Data. Run 19(a).
Film sintered at 323°K.

Dose	Press. mm.Hg	Operation
		Raised liquid N_2 bath round (R.V.) reaction vessel.
1	6.373×10^{-2}	Pressure decreased to Pirani zero R_o in 1½ minutes.
2	5.365×10^{-2}	Pressure decreased to 6.77×10^{-3} after 3 mins. (rate measurable). Raised cut off (4) [C.O.(4)] with all burettes H,1,2,3,4, at 150 cc. (max. burette calibration). Raised H.1. to 100 cc. Room temperature (R.T.) ~ 302°K throughout run. Commenced run at constant pressure ($P_c = 6.03 \times 10^{-3}$). Factor for converting c.c. of gas to micromoles = f.

Dose Press. mm.Hg Operation

time mins. secs.		Vol. c.c.	time mins. secs.	Vol. c.c.	time mins. secs.	Vol. c.c.
($f=3.223\times10^{-4}$)						
0:0	H.1.	100.0	27:28	82.1	64:47	76.4
0:53		89.3	33:54	72.8	66:30	67.2
2:03		80.2	37:27	63.4	68:19	61.0
3:33		69.3	39:02	58.7	69:33	55.0
4:42		59.6	41:07	51.8	71:42	48.4
6:14		49.5	42:52	46.2	73:12	42.3
7:42		40.1	45:02	40.0	75:12	36.4
9:14		29.8	48:22	33.0	77:03	30.5
10:52		19.7	51:00	26.4	79:03	23.5
12:38		9.7	53:50	21.4	81:53	11.7
14:08		0.0	55:52	16.5	85:22	5.3
16:05	H.2.	139.4	raise liquid O_2		87:55	0.0
17:37		130.8	lower H.2.		raise liquid N_2	
19:50		120.0	59:20	106.9	bath while	
21:50		110.7	60:20	100.2	preparing new	
24:11		100.2	61:43	92.3	run.	
25:51		91.1	63:26	83.4		

Lowered H2,3,4, to 150c.c. and H1 to 100.0 c.c.
Raised isopentane slurry.
$P_c = 5.22 \times 10^{-3}$ at t = 0

time		vol.	time	vol.	time		vol.
($f=2.794\times10^{-4}$)							
0:0	H.1.	100.0	21:45	45.6	34:28		0.0
3:10		89.5	26:10	38.4	36:09	H.2.	138.3
6:12		84.0	raise n-pentane		37:48		125.3
8:46		74.9	bath, lower H.1.		40:22		110.2
11:57		68.3	28:35	53.0	42:45		97.2
14:52		61.6	30:18	33.8	44:38		86.2
17:53		52.2	32:13	16.7	47:31		73.7
					50:28		60.4

Dose	Press. mm.Hg	Operation
		Left under liquid O_2 overnight. Lowered H2,3,4, to 150 cc. and H.1. to 100 cc. Raised cyclohexane bath. $P_c = 3.74 \times 10^{-3}$ at t = 0.

time	vol.	time	vol.	time	vol.
($f=1.991\times10^{-4}$)					
0:0 H.1.	100.0	21:31	17.4	39:02	78.3
1:20	92.7	23:50	9.9	40:43	67.7
3:26	84.3	26:34	2.5	42:56	56.3
5:28	76.5	raise ether bath		44:54	45.5
7:22	69.5	28:25	0.0	47:10	33.4
9:26	62.7	29:22 H.2.	141.7	49:50	21.4
12:31	48.8	32:40	120.0	raise liquid O_2 around reaction vessel.	
14:47	41.2	34:05	109.3		
16:59	32.4	35:25	99.6		
19:31	25.0	37:10	89.3		

3	1.923×10^{-2}	Raised toluene slurry and added dose 3. Raised C.O.(4) at 5.50×10^{-3} with H2, 3,4, at 150 c.c. and H1 at 100 c.c. $P_c=5.04 \times 10^{-3}$ at t = 0.

time	vol.	time	vol.	time	vol.
($f=2.684\times10^{-4}$)					
0:0 H.1.	100.0	21:16	31.5	35:48	99.7
2:11	90.2	23:10	26.2	37:28	89.1
3:57	82.7	raise cardice bath		39:10	78.4
6:40	74.3	26:33	11.5	40:48	68.4
8:38	67.5	28:02	0.0	42:35	56.4
11:00	60.3	29:28 H.2.	140.9	45:00	44.7
13:25	52.3	30:58	130.2	46:55	33.5
16:07	44.2	32:24	120.4	49:06	22.3
19:43	37.0	33:32	110.0		

4	3.497×10^{-2}	Left under cardice bath overnight. Most of the residual pressure was used up overnight. Added dose with reaction vessel under cardice and all burettes at 150 c.c.

Dose	Press. mm.Hg	Operation
		C.O.(4) at 7.49×10^{-3} mm.Hg. Raised $CHCl_3$ bath. $P_c = 6.93 \times 10^{-3}$ at t = 0.

time		vol.	time		vol.	time		vol.
($f=3.689\times10^{-4}$)								
0:0	H.1.	150.0	26:55		113.4	43:58		96.5
3:45		143.7	29:21		110.4	46:38		91.7
6:36		139.7	32:50		106.9	50:40		86.8
8:40		136.1	raise diethyl			53:42		82.0
12:10		129.9	malonate bath			59:15		77.0
16:05		125.3	35:15		110.4	63:06		72.9
19:10		121.4	37:50		105.6	67:22		69.5
21:40		117.6	40:13		101.5			

Raised liquid O_2 bath round reaction vessel while preparing new slurry. Raised CCl_4 slurry. $P_c = 5.61 \times 10^{-3}$ at t = 0, with H2,3, 4 at 150 c.c. and H1 at 100.0 c.c.

time		vol.	time		vol.	time		vol.
($f=2.967\times10^{-4}$)								
0:0	H.1.	100.0	19:44	H.2.	140.1	34:33		47.3
1:07		90.0	22:25		129.5	36:06		35.0
3:06		79.8	25:01		118.5	37:52		22.5
4:59		68.5	raise methyl			39:32		10.2
6:41		58.3	benzoate slurry			40:52		0.0
9:08		45.9	26:43		112.7	43:00	H.3.	136.0
11:40		32.7	27:49		100.2	45:35		120.8
14:29		20.1	29:41		87.8	47:31		107.0
15:33		10.1	31:15		73.1	49:13		96.4
18:21		0.0	32:55		60.1			

5	2.573×10^{-2}	Left under liquid O_2 overnight. Raised ice bath. Lowered all burettes to 150.0 c.c. Added dose; C.O.(4) at 6.90×10^{-3} mm.Hg. $P_c = 6.40 \times 10^{-3}$ at t = 0.

Dose	Press. mm.Hg.	Operation

Time		vol.	time		vol.	time		vol.
(f=3.396x10^{-4})								
0:0	H.1.	150.0	26:08		27.7	40:44		89.7
1:27		139.1	raise tapwater			42:09		70.6
3:10		130.1	bath at 21.2°C			43:42		47.5
5:15		120.3	29:03	H.2.	141.7	45:20		26.3
7:22		110.0	30:09		121.2	46:53		5.0
9:10		100.2	32:13		82.4	48:32	H.4.	132.4
11:25		90.3	33:06		65.5	50:05		111.4
13:22		81.3	33:55		49.7	51:55		89.3
15:08		72.3	34:47		34.3	53:48		67.5
17:18		63.3	35:44		18.3	56:37		46.0
19:44		54.0	36:45		0.0	57:46		25.4
21:57		45.1	38:13	H.3.	130.0	59:35		6.3
24:08		36.1	39:37		108.1			

Reaction was allowed to proceed at constant volume with all burettes at 150.0 c.c., at the above temperature. After 1 hour C.O.(4) at residual pressure of $1.1\text{x}10^{-4}$ mm.Hg.

6	$2.798\text{x}10^{-2}$	After 2 mins. C.O.(4) at $1.2\text{x}10^{-4}$.
7	$5.434\text{x}10^{-2}$	After 2 mins. C.O.(4) at $1.1\text{x}10^{-4}$.
8	$5.722\text{x}10^{-2}$	After 2 mins. C.O.(4) at $1.3\text{x}10^{-4}$.
9	$6.164\text{x}10^{-2}$	After 2 mins. C.O.(4) at $1.7\text{x}10^{-4}$.
		Raised reaction vessel temperature to room temperature and found all residual gas absorbed.
10	$5.795\text{x}10^{-2}$	After 2 mins. (at 30°C) C.O.(4) at $1.6\text{x}10^{-4}$. All gas absorbed before new run commenced.

FIG. 3.4. (RUN 19(a))

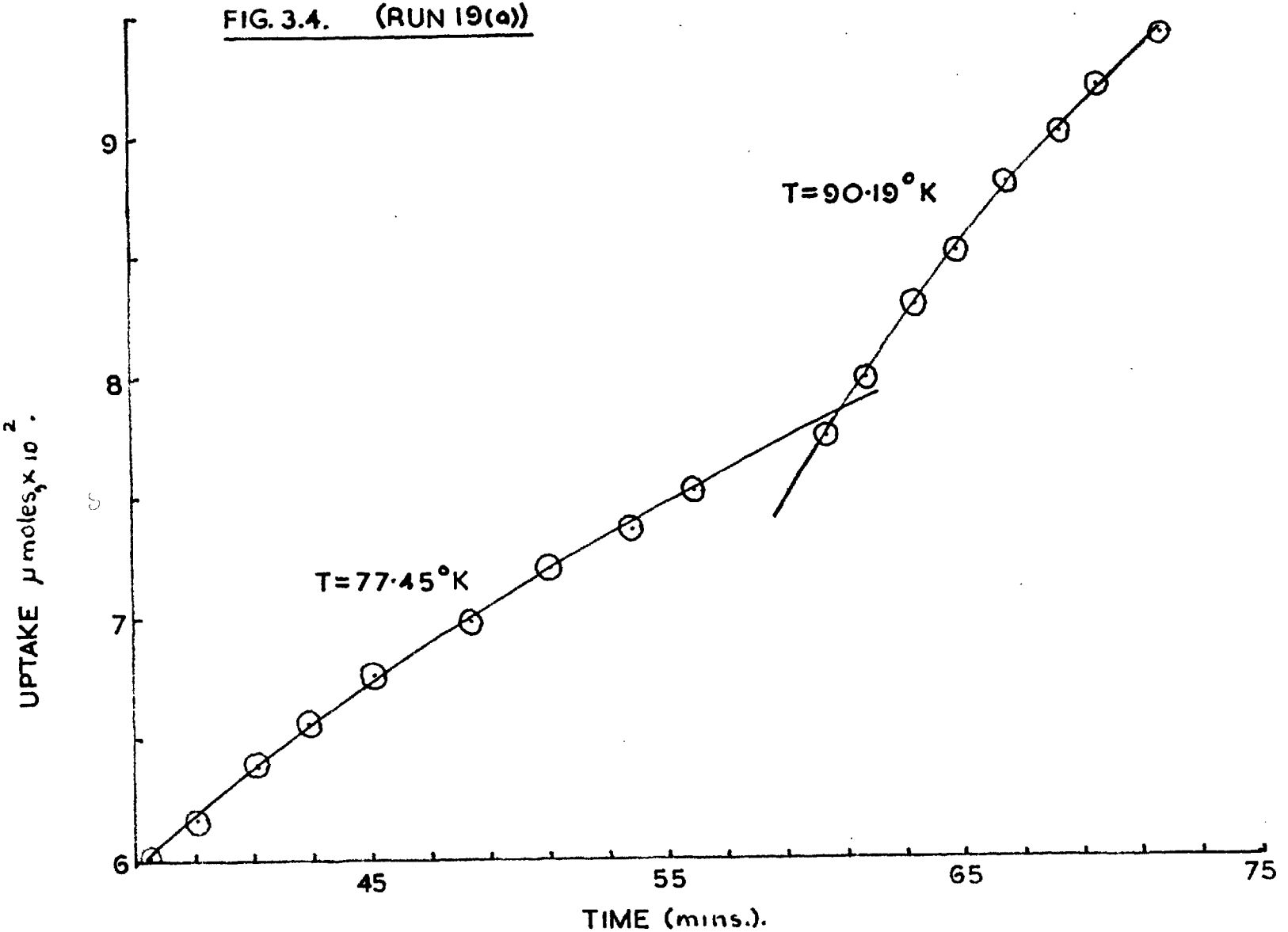


FIG. 3.5. (RUN 19(a)).

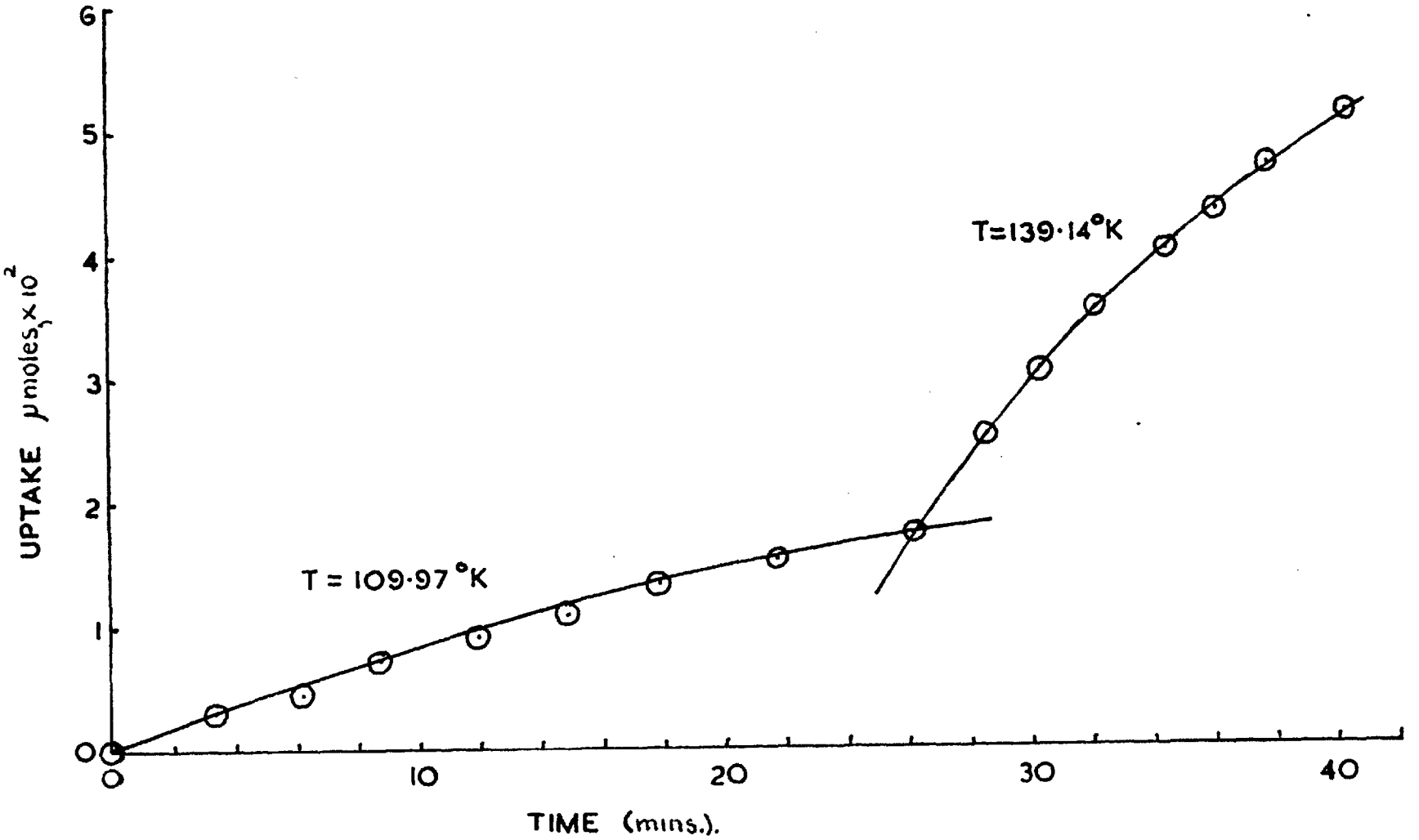


FIG.3.6. (RUN 19(a)).

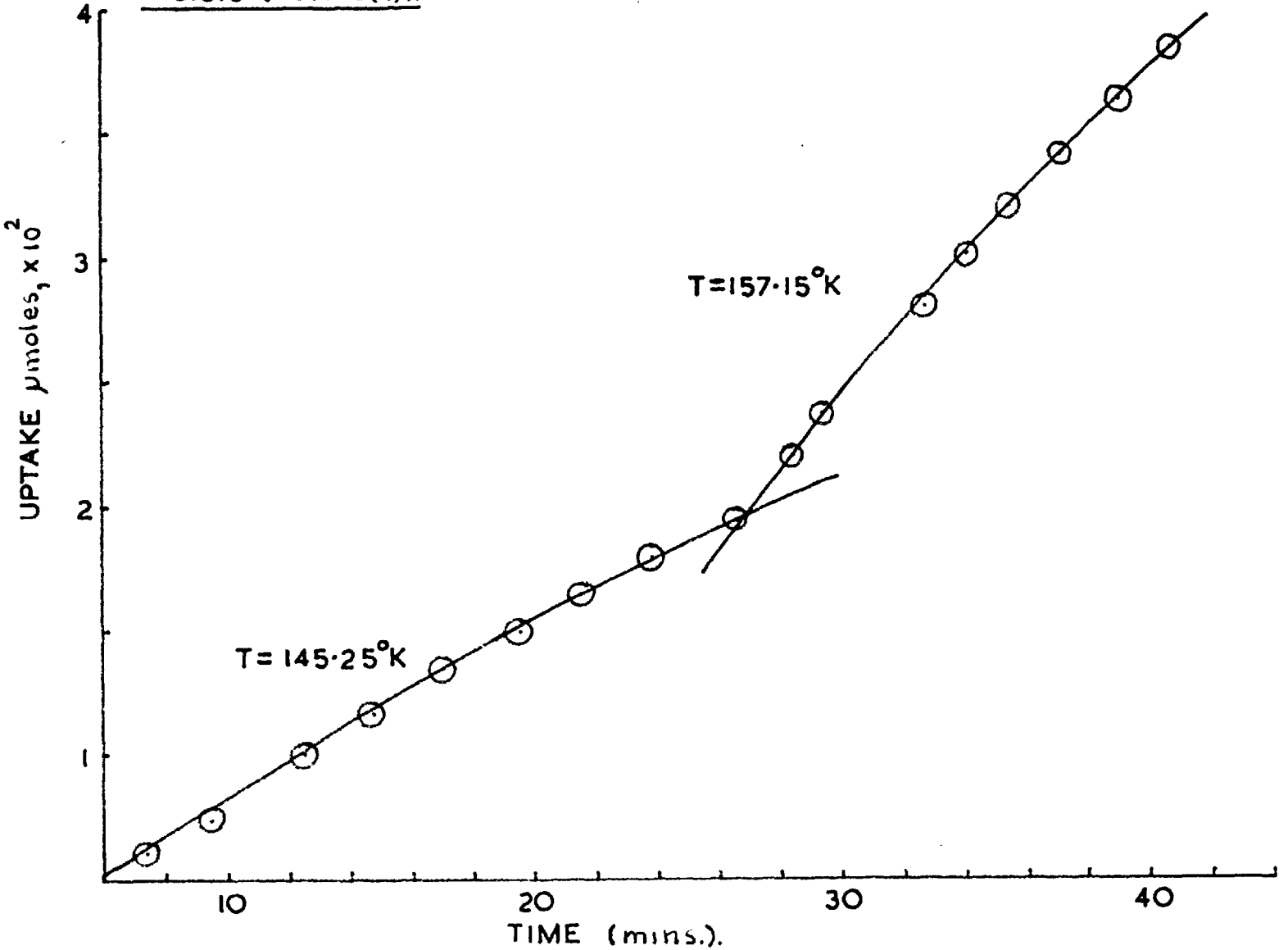


FIG. 3.7. (RUN 19(a)).

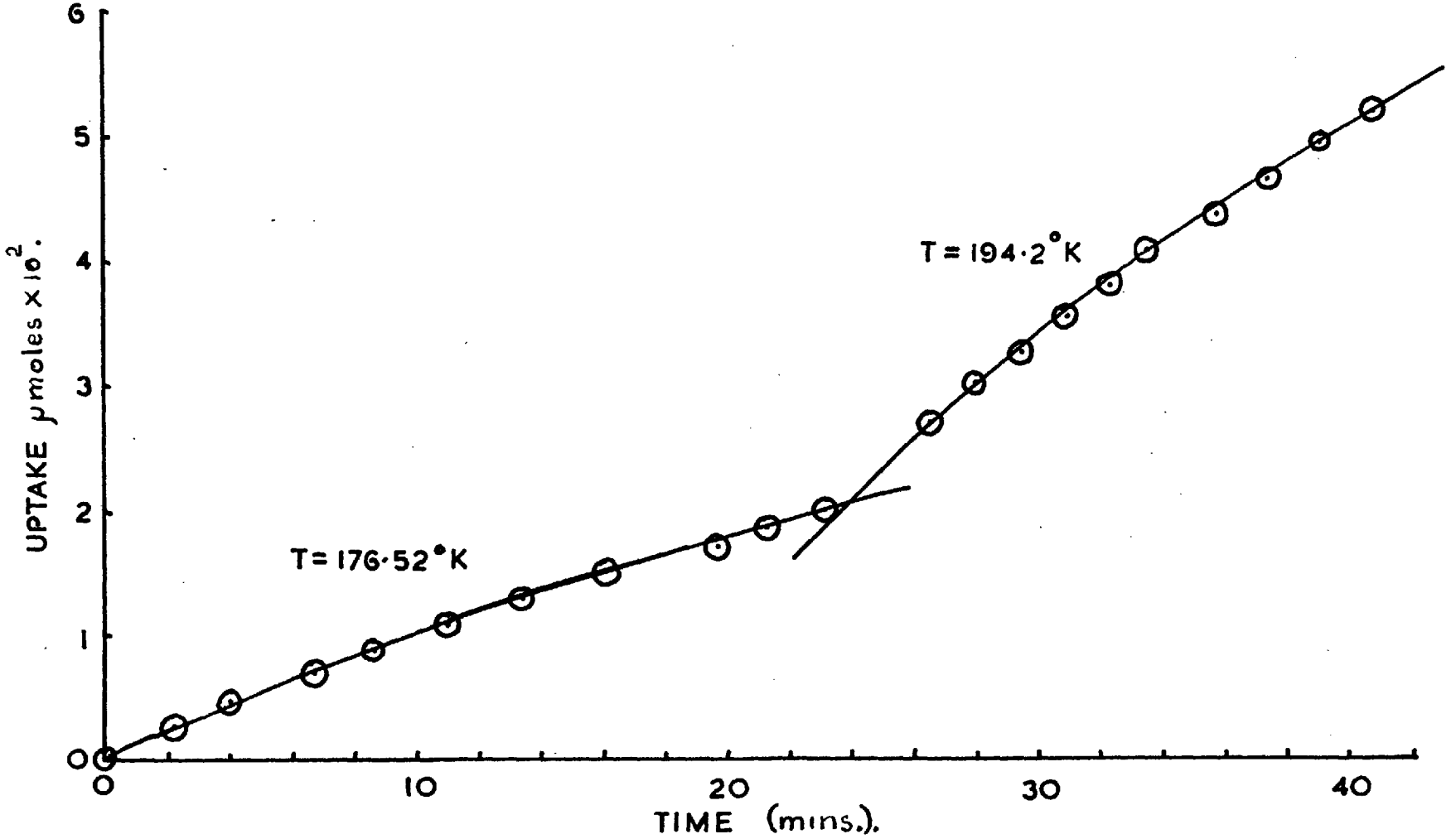


FIG. 3.8. (RUN 19(a)).

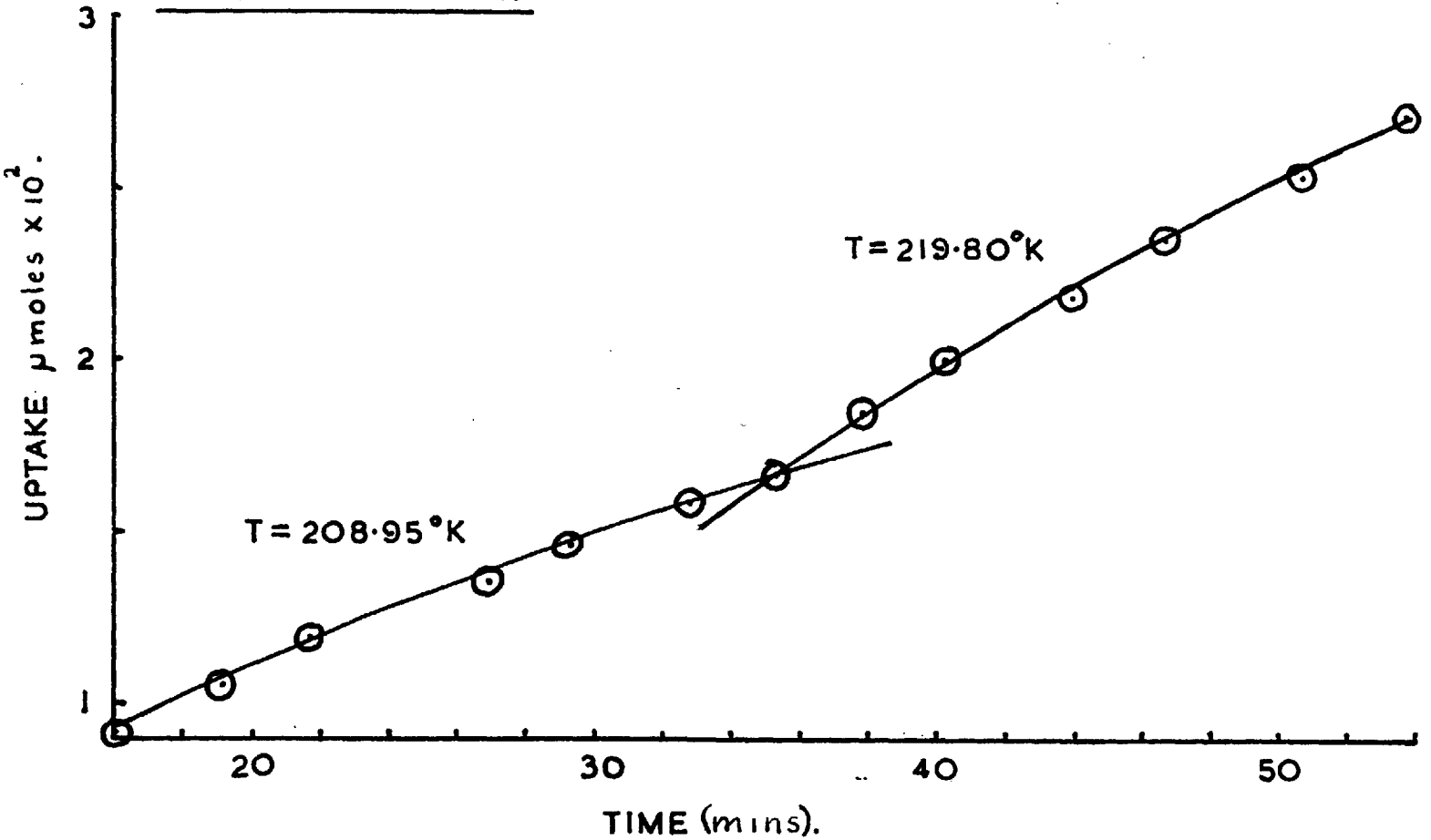


FIG. 3. 9. (RUN 19(a)).

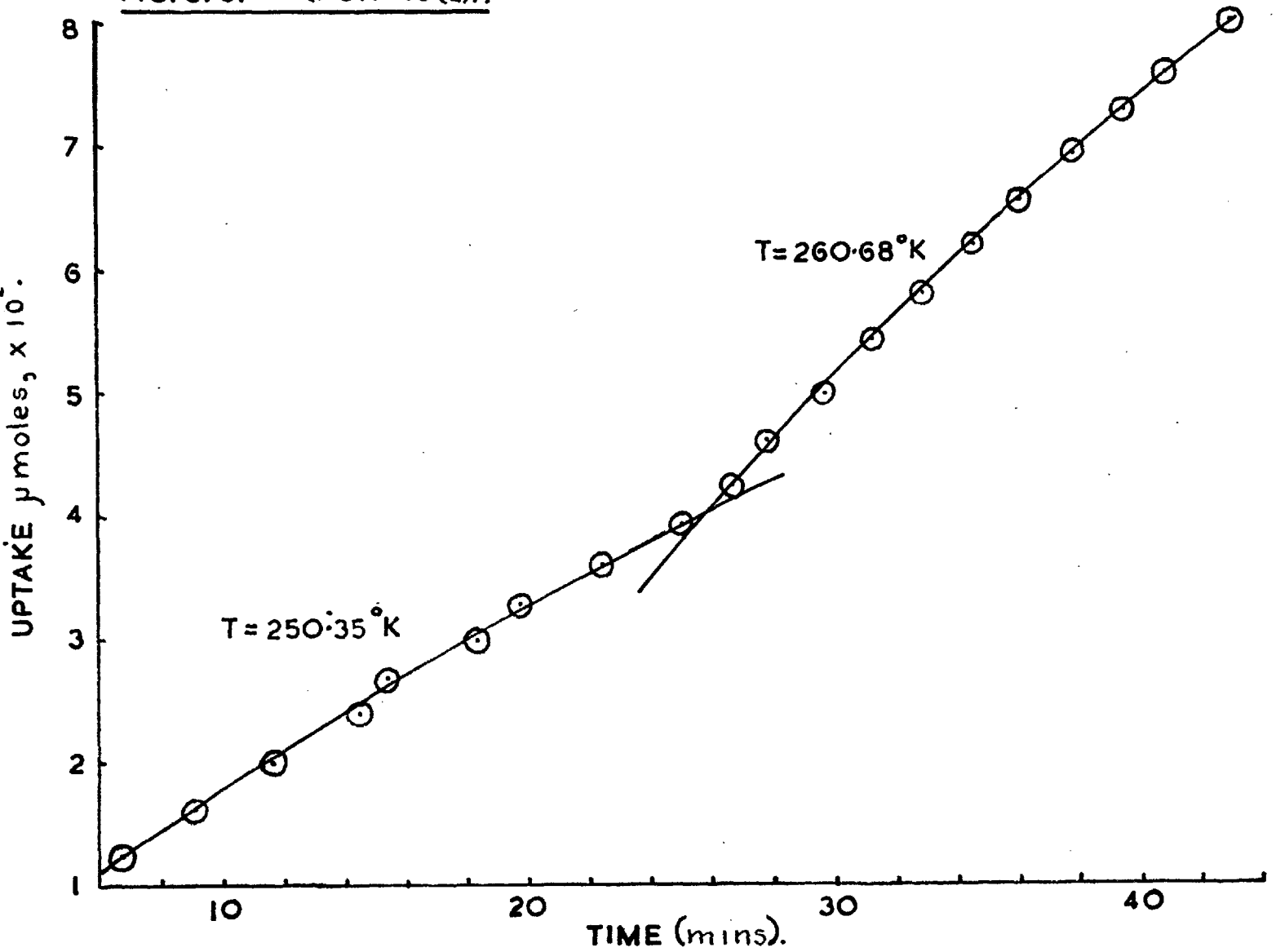


FIG. 3.10. (RUN 19(a)).

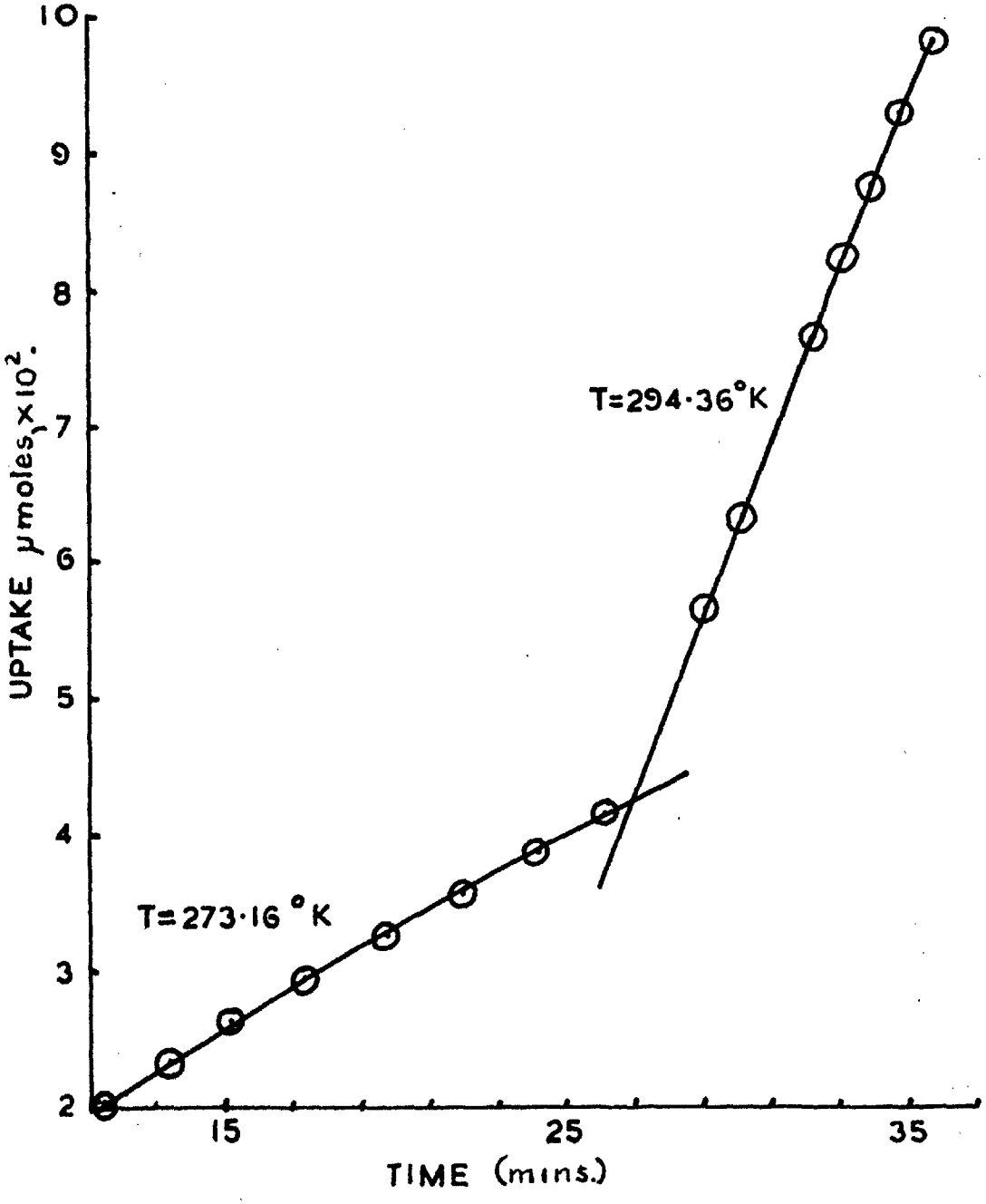


Table 3.2.

Table 3.2. Calculation of uptake (w micromoles) applying Run 19(a).

Dose	Stage	P_D	n_D f=18.38	$P_{c_{R.T.}}$ $x10^{-3}$	$n_{R.T.}$	$P_{c_{Tr.}}$ $x10^{-3}$
1	liquid N_2 bath	$3.673x10^{-2}$	.675			
2	" " "	$5.365x10^{-2}$	.986			
	C.O.(4)	$6.77\ x10^{-3}$	.124			
	at start P_c run (N_2 - O_2)			6.03	f=44.17 .266	4.896
	at start P_c run (iso-n-pentane)			5.22	f=44.17 .231	4.14
	at start P_c run (cyclohexane-ether)			3.74	.165	2.80
3	toluene bath	$1.923x10^{-2}$	.353			
	C.O.(4)	$5.50\ x10^{-3}$	.101			
	at start P_c run (toluene-cardice)			5.04	f=44.17 .223	3.98
4	$ChCl_3$ bath	$3.497x10^{-2}$	.643			
	C.O.(4)	$7.49\ x10^{-3}$	.138			
	at start P_c run ($ChCl_3$-diethyl malonate)			6.93	f=46.84 .325	5.77
	at start P_c run (CCl_4-methyl benzoate)			5.61	f=44.17 .248	4.50
5	ice bath	$2.573x10^{-2}$	.473			
	C.O.(4)	$6.90\ x10^{-3}$	.127			
	at start P_c run (ice-tapwater)			6.40	f=46.84 .300	5.25
6		$2.798x10^{-2}$	.514			
	C.O.(4)	$1.2\ x\ 10^{-4}$	.002			
7		$5.434x10^{-2}$	.999			
	C.O.(4)	$1.1\ x\ 10^{-4}$	.002			
8		$5.722x10^{-2}$	1.052			
	C.O.(4)	$1.3\ x\ 10^{-4}$	.002			
9		$6.164x10^{-2}$	1.133			
	C.O.(4)	$1.7\ x\ 10^{-4}$	.003			
10		$5.795x10^{-2}$	1.065			

thermal transpiration corrections.

$n_{Tr.}$ f=14.66	$P_{c_{Pi.}}$ $x10^{-3}$	$n_{Pi.}$ f=3.100	$P_{c_{R.V.}}$ $x10^{-3}$	$n_{R.V.}$	increments in μ moles	w progressive total μmoles absorbed.
				f=21.15		
.072	4.896	.0152	4.86	.103		
					.075	1.156
				f=14.89		
.061	3.99	.012	4.23	.063		
					.017	1.187
				f=11.28		
.041	2.71	.008	3.03	.034		
					.021	1.309
				f=9.279		
.058	3.83	.012	4.34	.040		
					.021	1.477
				f=7.839		
.085	5.56	.017	6.29	.049		
					.017	1.835
				f=6.543		
.066	4.34	.014	5.26	.034		
					.040	1.973
				f=5.966		
.077	5.07	.016	6.40	.038		
					.043	2.252
						7.394

Meaning of abbreviations used in Table 3.2.

P_D - pressure in the dosage space.

n_D - number of micromoles in the dosage space.

$P_{c_{R.T.}}$ - constant pressure in those sections of the apparatus at room temperature (R.T.) after C.O.(4) had been raised.

$P_{c_{Tr.}}$ - constant pressure, corrected for thermal transpiration, in the volume of traps immersed in liquid oxygen.

$P_{c_{Pi}}$ - constant pressure, corrected for thermal transpiration, in the volume of the Pirani immersed in liquid oxygen.

$P_{c_{R.V.}}$ - constant pressure, corrected for thermal transpiration, in the volmue of the reaction vessel immersed in the various constant temperature baths.

f - various factors for converting pressures to micromoles of oxygen in the various sections of the apparatus.

Apparatus constants during Run 19(a).

Volume of reaction vessel up to immersion level = 102.1 c.c.

Volume of McLeod (in dosage space) = 218.1 c.c.

Volume of remainder of dosage space (i.e. between C.O.(3) and C.O.(4) with McLeod just cut off at the bulb) = 128.0 c.c.

Volume of traps below the immersion level = 82.26 c.c.

Volume of Pirani below the immersion level = 17.4 c.c.

Volume of burettes when all at 150 c.c. = 600 c.c.

Constant volume at room temperature between C.O.(4) and C.O.(5) = 282.1 c.c.

Internal Diameters of glass tubing over which temperature gradients are operative.

Traps - 15 mm. Pirani - 12 mm. Reaction vessel 15 mm.

Temperatures of baths employed in Run 19(a).

Bath	T^oK
Boiling liquid N_2	77.45
Boiling liquid O_2	90.19
Melting isopentane	109.97

Bath	$T^{o}K$
Melting n-pentane	139.14
Melting cyclohexane	145.25
Melting ether	157.15
Melting toluene	176.52
Cardice	194.20
Melting $CHCl_3$	208.95
Melting diethyl malonate	219.80
Melting CCl_4	250.35
Melting methyl benzoate	260.68
Melting ice	273.16
Running tap water	294.36

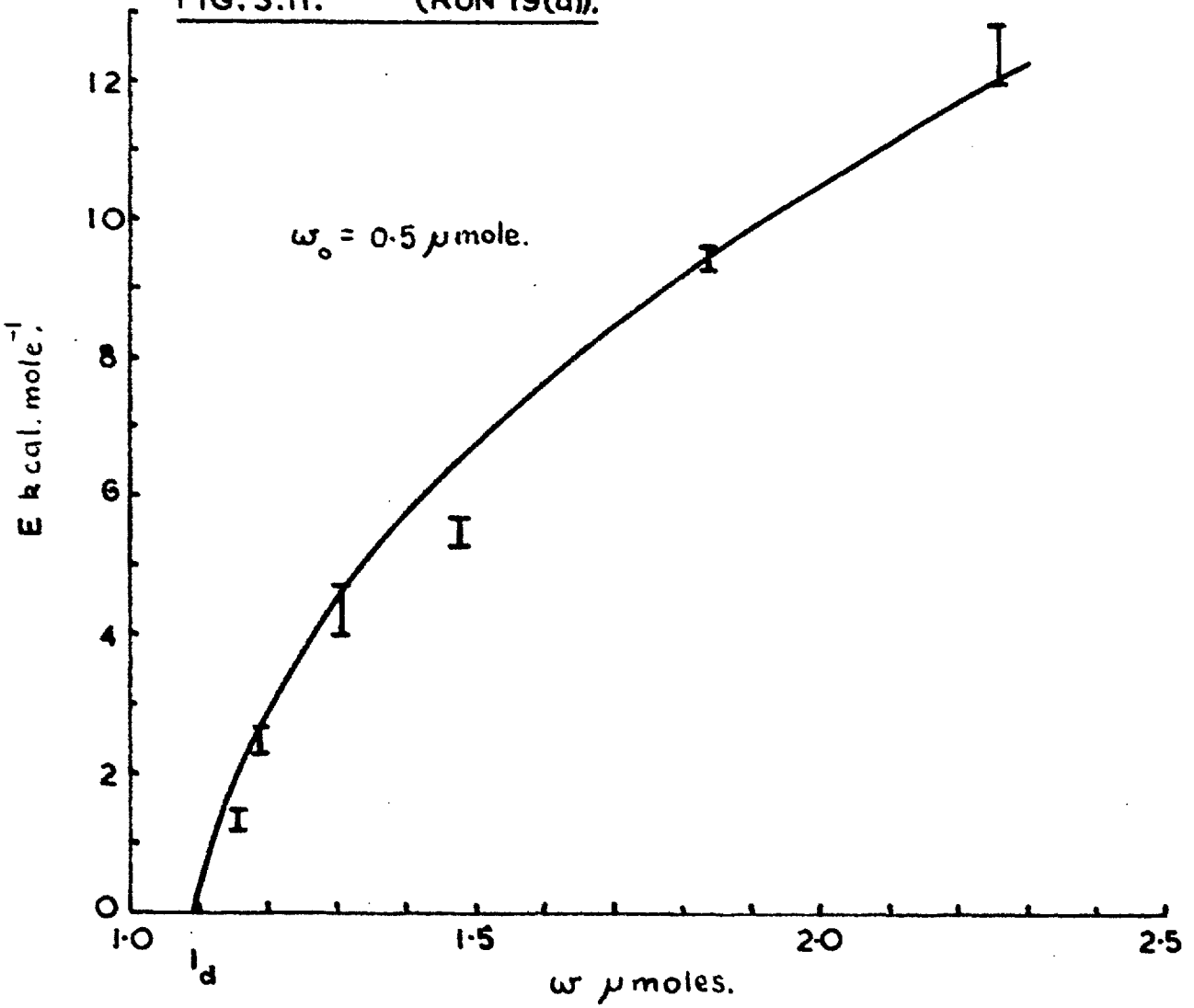
3.1.3.3. Results.

Activation energies were found to increase with increasing film thickness (e.g. fig. 3.11., run 19(a)) varying from approximately 1 kcal.mole^{-1} at thicknesses of about 8-12 atomic layers on initially clean metal surfaces (runs 8, 9, 19(a)) up to approximately 11 kcal.mole^{-1} at thickness around 15-18 atomic layers (see tables 3.3., 3.4., 3.6.).

Furthermore when the temperature and oxide thickness reached certain critical values, breakaway occurred, giving an enormously increased rate of uptake. However, on lowering the temperature, and repeating the activation energy determinations, results identical to those on initinally clean films were obtained.

In runs 18(a) and 18(b), a clean film was deposited, a layer of oxide of thickness greater than that corresponding to the breakaway point was allowed to form and then activation energies were determined as for a clean film (18(a)).

FIG. 3.11. (RUN 19(a)).



When the breakaway point was again reached, and further oxide had formed above it the results were repeated 18(b).

After run 19(a) on the clean metal surface, two further runs 19(b) and 19(c) were carried out above the first and second breakaway points respectively; a further breakaway was observed following run 19(c). (See Tables 3.5, 3.6.).

Because the apparent areas of films oxidized above the breakaway point are not known with the same degree of accuracy as those of the clean metal surfaces, results will be given as plots of either, E in kcal.mole^{-1} against uptake in micromoles or the reciprocal of uptake, rather than against thickness or the reciprocal of thickness. The uptake is of course related to the thickness, by a proportionality factor involving the area of the surface.

In order to calculate the proportionality factor it was assumed that the major lattice plane (100), was oriented parallel to the metal surface and that the roughness factor was unity. These arbitrary assumptions were made merely to fix a standard of reference for average film thickness for comparative purposes, where the surface area was known with reasonable accuracy.

Since the number of oxygen atoms in the (100) plane of the Li_2O lattice is 1.89 x 10^{16} cm^{-2} and the distance between planes is 2.301 Å, (138),

$$x = \frac{1468 \times w}{A} \qquad (1)$$

where x is in Å, w in micromoles and A is the apparent

surface area of film in cm^2.

Since some variation in the graphical determination of tangents to the point of intersection of the w/t plots was unavoidable, the maximum spread of error in the activation energies due to this has been shown in the graphs and tables.

Reasonably good linear plots were obtained when E was graphed against $1/(w-w_o)$, where w_o is an empirical constant, both on initially clean metal surfaces and on surfaces which had been subsequently oxidized above the breakaway point. On extrapolation of the curve to $1/(w-w_o) = 0$, there was good agreement between the values of the intercept W. (See E/$1/(w-w_o)$ plots, Figs. 3.12., 3.13., for runs 19(a) and (c) being a typical clean film and oxidized film respectively.)

Table 3.3. Variation of experimental activation energy with uptake, reciprocal of uptake, and oxide thickness.

Run 8.

Apparent area of metal surface = 91.1 cm^2.

T_1 °K	T_2 °K	E kcal.mole^{-1}	w	$\frac{1}{w-w_o}$ w_o=1.13	x	number of atomic oxide layers.
77.45	90.19	0.98±0.07	1.778	1.543	28.64	12.46
90.19	109.97	1.55±0.15	1.867	1.357	30.08	13.08
138.6	177.0	3.85±0.35	1.948	1.222	31.38	13.65
177.0	194.0	7.20±0.50	2.245	0.897	36.17	15.73
221.0	250.9	9.85±0.35	2.697	0.638	43.45	18.90

w is the uptake in micromoles and x is the thickness of the oxide layer in Å.

FIG.3.12. (RUN 19(a)).

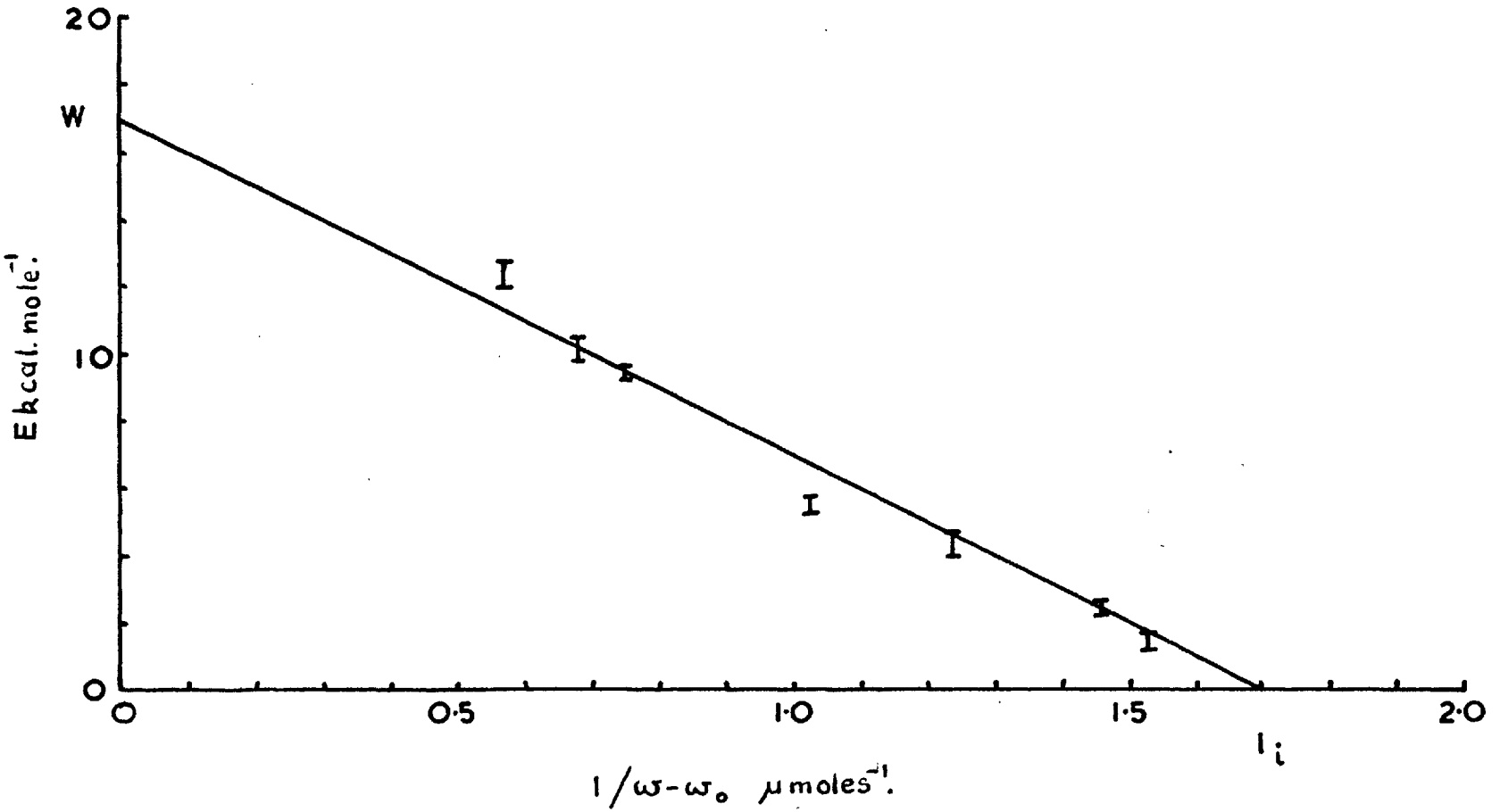


FIG. 3.13. (RUN 19 (c)).

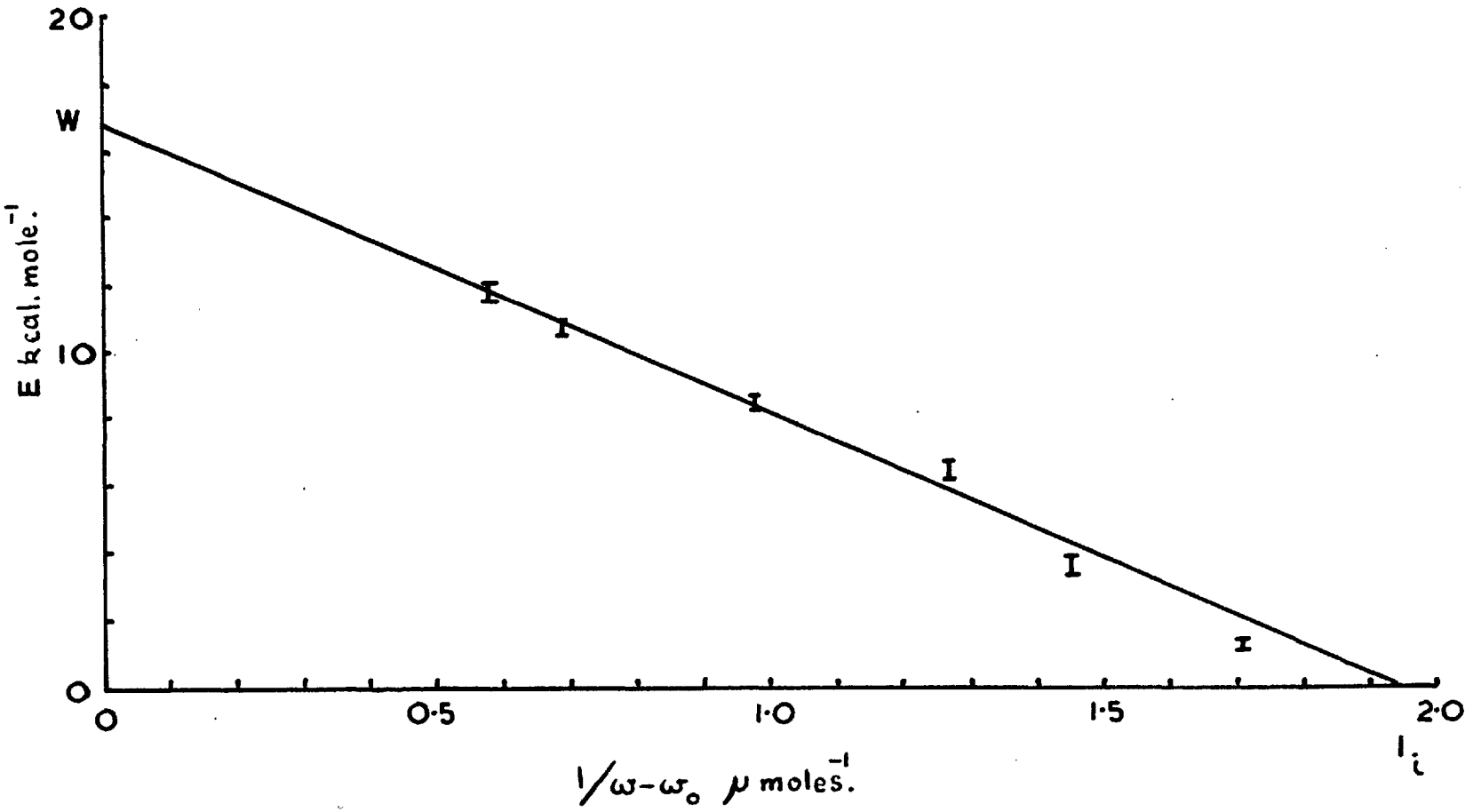


Table 3.4.

Run 9.

Apparent area of metal surface = 101.6 cm^2.

T_1 °K	T_2 °K	E kcal.mole^{-1}	w	$\frac{1}{w-w_o}$ w_o=0.6	x	number of atomic oxide layers
90.19	109.97	1.45±0.15	1.509	1.101	21.81	9.49
138.6	146.6	3.85±0.35	1.674	0.931	24.19	10.52
146.6	177.8	4.50±0.30	1.740	0.877	25.14	10.94
177.8	194.0	5.75±0.45	1.866	0.790	26.96	11.73
194.0	221.0	6.45±0.35	2.030	0.699	29.33	12.76
221.0	250.9	9.00±0.50	2.182	0.632	31.53	13.72

w is the uptake in micromoles and x is the thickness of the oxide layer in Å.

Table 3.5.

Rune 18(a).

Apparent area of film in run 18(a) and 18(b) oxidized above breakaway = 78.4cm^2 (approx.)

T_1 °K	T_2 °K	E kcal.mole^{-1}	w	$\frac{1}{w-w_o}$ w_o=5.4	x	number of atomic oxide layers.
77.45	90.19	0.86±0.04	5.844	2.255	109.40	47.59
109.97	139.14	2.05±0.25	5.870	2.130	109.89	47.80
145.25	157.22	3.60±0.20	5.918	1.931	110.78	48.19
176.52	194.20	5.35±0.25	5.981	1.722	111.96	48.70
208.95	219.28	8.90±0.40	6.264	1.157	117.26	51.01
248.20	260.90	10.75±0.15	6.514	0.898	121.94	53.04
273.16	289.0	11.60±0.30	6.704	0.767	125.50	54.59

Table 3.5. continued.

Run 18(b).

T_1 °K	T_2 °K	E kcal.mole^{-1}	w	$\frac{1}{w-w_o}$ w_o=11.2	x	number of atomic oxide layers.
77.45	90.19	1.25±0.05	11.753	1.808	220.02	95.71
145.25	157.22	5.00±0.20	11.856	1.525	221.94	96.54
176.52	194.20	5.25±0.25	11.951	1.332	223.72	97.32
208.95	219.68	8.35±0.55	12.396	0.836	232.05	100.94
248.20	260.90	11.15±0.55	12.636	0.696	236.55	102.90
273.16	289.80	11.85±0.35	12.809	0.622	239.78	104.30

w is the uptake in micromoles and x is the thickness of the oxide layer in Å.

Table 3.6.

Run 19(a).

Apparent area of metal surface = 90.3 cm.^{2}

(See Tables 3.1., 3.2. and Figs. 3.4.,3.5.,3.6.,3.7.,3.8., 3.9.,3.10., 3.11.,3.12.)

T_1 °K	T_2 °K	E kcal.mole^{-1}	w	$\frac{1}{w-w_o}$ w_o=0.5	x	number of atomic oxide layers.
77.45	90.19	1.30±0.10	1.156	1.524	18.80	8.18
109.97	139.14	2.45±0.15	1.187	1.455	19.30	8.40
145.25	157.15	4.35±0.35	1.309	1.236	21.28	9.26
176.52	194.20	5.50±0.20	1.477	1.024	24.02	10.45
208.95	219.80	9.45±0.15	1.835	0.749	29.84	12.98
250.35	260.68	10.15±0.35	1.973	0.679	32.08	13.95
273.16	294.36	12.40±0.40	2.252	0.571	36.62	15.93

Table 3.6. Continued.

Run 19(b). Apparent area of surface oxidized above breakaway = 78.4 cm.^{2} (approx.)

T_1 °K	T_2 °K	E kcal.mole^{-1}	w	$\frac{1}{w-w_o}$ w_o=7.08	x	Number of atomic oxide layers.
77.45	90.19	2.00±0.20	7.718	1.569	144.48	62.85
145.25	157.22	5.50±0.20	7.784	1.420	145.72	63.39
177.05	192.13	6.50±0.20	7.889	1.237	147.68	64.24
208.95	219.28	8.10±0.40	8.207	0.888	153.64	66.83
249.80	259.67	10.85±0.45	8.487	0.711	158.88	69.11
273.16	294.66	10.65±0.35	8.759	0.596	163.78	71.24

Run 19(c). Apparent area of surface oxidized above breakaway = 78.4 cm.^{2} (approx)

T_1 °K	T_2 °K	E kcal.mole^{-1}	w	$\frac{1}{w-w_o}$ w_o=15.5	x	Number of atomic oxide layers.
77.45	90.19	1.25±0.15	16.086	1.705	301.13	130.99
145.57	157.25	3.70±0.20	16.190	1.449	303.08	131.84
177.09	191.60	6.45±0.25	16.289	1.267	304.93	132.64
208.95	219.68	8.50±0.20	16.524	0.977	309.33	134.56
250.04	259.86	10.70±0.20	16.956	0.687	317.42	138.08
273.16	294.36	11.75±0.25	17.231	0.578	322.56	140.31

w is the uptake in micromoles and x is the thickness of the oxide layer in Å.

Various parameters of theoretical interest obtained from the E/$1/(w-w_o)$ plots, have been collected in Table 3.7. They are the slope, S, of the linear plot, $\frac{dE}{d(1/w-w_o)}$, the

intercept on the E axis, W, which is the activation energy after extrapolation to $1/(w-w_o) = 0$, the values of $1/(w-w_o)$ when E = 0 i.e. the intercept on the $1/(w-w_o)$ axis, I_i, and values of $(\frac{1}{I_i} + w_o) = I_d$, the point of direct uptake above which E first assumes a positive value.

Table 3.7. Values of parameters obtained from E/$1/(w-w_o)$ plots.

Run	W kcal. $mole^{-1}$	S kcal, $x10^{-6}$	I_i $mole^{-1}$ $x10^6$	w_o $moles^{-1}$ $x10^6$	I_d moles $x10^{-6}$
8	17.07	10.84	1.58	1.13	1.762
9	17.10	14.02	1.20	0.60	1.433
18(a)	17.00	7.00	2.43	5.40	5.812
18(b)	17.04	8.48	2.01	11.20	11.698
19(a)	17.00	10.00	1.70	0.50	1.090
19(b)	16.80	8.70	1.93	7.08	7.593
19(c)	16.85	8.71	1.95	15.5	16.013
Average	16.98				

3.1.4. Dependence of Rate on Pressure.

The effect of pressure on the rate at constant thickness was studied in a similar manner to the determination of activation energies. The rate curve was characterized at a constant low pressure in the 10^{-4} to 10^{-3} m.m. range at a fixed temperature, then as rapidly as possible the pressure was raised, by adding a large dose, into the 10^{-2} mm. region and the rate curve characterized at this new constant pressure. A period of 2-3 minutes was necessary for temperature equilibration of the new dose and the attainment of steady state conditions. The w/t curves were then extrapolated to the instant of pressure change, to obtain comparison at constant thickness of oxide, and the rates determined graphically. It was assumed that any variation in physical adsorption was negligible.

The pressures measured experimentally, in the two regions, p'_l and p'_h, were the values of pressure within the system at room temperature, while the effective pressures, for calculating the rate dependence, were the pressures of gas, in contact with the oxide film, at the temperature of the film, p_l and p_h, being the lower pressure and higher pressure respectively. p_l and p_h were calculated from p'_l and p'_h by means of the usual thermal transpiration method since quite large corrections were necessary at the lower temperatures and pressures.

If at any temperature the functional variations of p

and w, on the rate are independent variables, i.e.

$$r = f(p) \times f(w)$$

Then at the same w, $$\frac{r_h}{r_l} = \frac{f(p_h)}{f(p_l)}$$

The simplest assumption which can be made about the form of the pressure dependence is that it is a simple power law, i.e.

$$f(p) = p^n$$

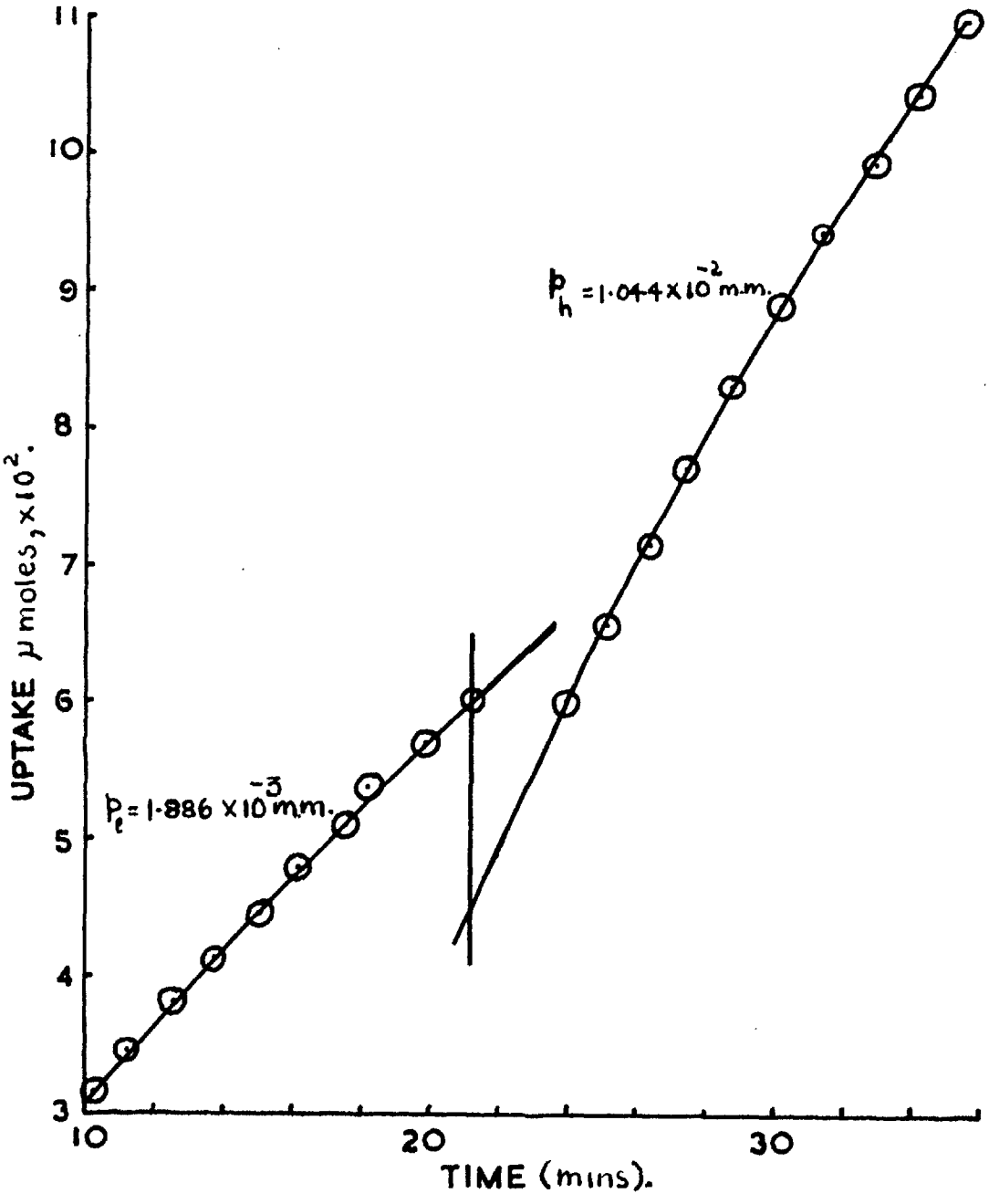
$$\frac{r_h}{r_l} = \left(\frac{p_h}{p_l}\right)^n$$

or $$n = \frac{\log\left(\frac{r_h}{r_l}\right)}{\log\left(\frac{p_h}{p_l}\right)}$$

The pressure dependence, n, was examined at 77.45, 90.19, 109.97, 176.52, 194.20, 223.0°K on initially clean metal surfaces rune 15 and 16 sumilar to run 19(a) with pressure changes varying over approximately an order of magnitude in the range 10^{-4}-10^{-2} mm.Hg. An average value of 0.52 was found, which was independent of temperature and oxide thickness over a wide range, indicating that the rate was proportional to the square root of the oxygen pressure. The thicknesses of oxide varied during the determination from approximately 8 to 16 atomic layers. A typical example of a determination has been shown in Fig. 3.14.

The results, listed in Table 3.8. were obtained by pressure increase, since it was found that attainment of steady state conditions was more rapid than when the pressure

FIG. 3.14. PRESSURE DEPENDENCE (RUN 16).



was decreased, when the time lag was large enough to make the positioning of the tangents at the point of intersection difficult. Nevertheless, the results indicated a rough qualitative agreement with those obtained by pressure increase.

Table 3.8. Approximate values of n.

Run	$T^{\circ}K$	p_l mm.	p_h mm.	r_l moles x 10^{-9} $min.^{-1}$	r_h moles x 10^{-9} $min.^{-1}$	n
15	77.45	1.346×10^{-3}	4.362×10^{-3}	0.512	0.926	0.50
	90.19	1.850×10^{-3}	6.332×10^{-3}	0.595	1.173	0.55
	109.97	9.743×10^{-4}	6.712×10^{-3}	0.241	0.926	0.70
	176.52	1.115×10^{-3}	8.073×10^{-3}	1.511	3.876	0.48
	194.20	1.676×10^{-3}	8.408×10^{-3}	1.314	3.003	0.51
	219.8	1.168×10^{-3}	7.385×10^{-3}	2.045	4.902	0.47
16	77.45	1.644×10^{-3}	1.060×10^{-2}	2.865	6.726	0.46
	109.97	1.934×10^{-3}	8.146×10^{-3}	0.802	1.606	0.48
	176.52	1.602×10^{-3}	7.687×10^{-3}	2.193	5.207	0.55
	194.20	1.886×10^{-3}	1.044×10^{-2}	2.388	5.792	0.52

Average value of n = 0.52.

3.1.5. The Point of Breakaway.

In run 19(b), on changing the temperature from 21.5°C to 33.4°C, the onset of breakaway was observed, i.e. the usual protective curve changed to an accelerating non-protective curve. (Fig. 3.15.). Thereafter, at constant volume the pressure decreased rapidly to the Pirani zero. With further large additions of oxygen, uptake was rapid, the pressure falling to zero within 2 minutes.

Breakaway phenomena were observed after run 19(a), 19(b) and 19(c), before and after run 18(a) and after run 18(b). The temperatures at which breakaway occurred, the approximate thicknesses and the amounts of oxygen added to the film above breakaway for these runs have been set out in Table 3.9.

Further analysis of the data in Tables 3.7., 3.8., and 3.9. is given in the discussion.

FIG. 3.15. BREAKAWAY (RUN 19(b)).

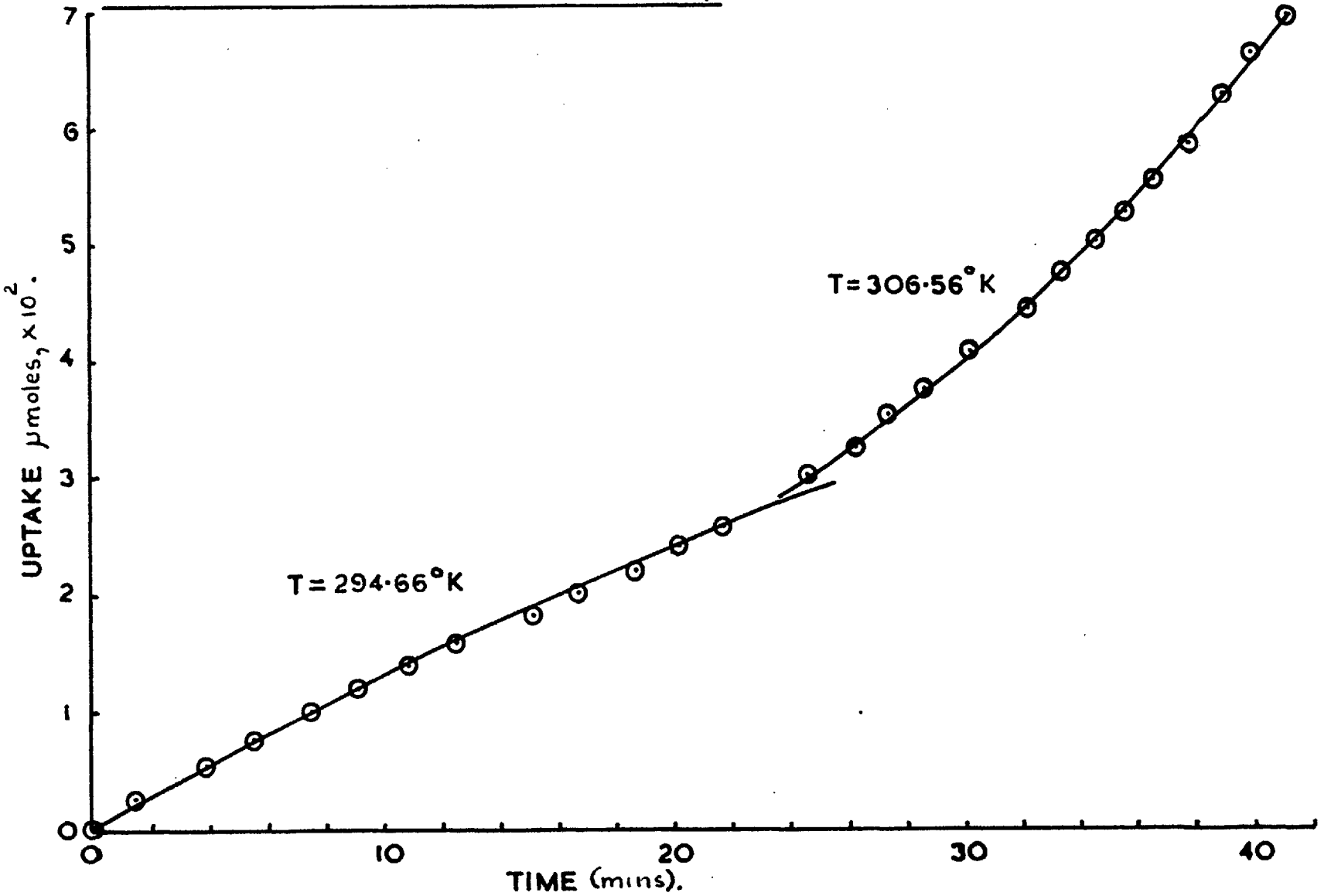


Table 3.9. Thickness and temperature of oxide film at breakaway point and amounts absorbed above breakaway.

Run	Stage	Thickness at Breakaway			Breakaway temp.	Amounts added above breakaway		
		w	$\overset{o}{xA}$	No. of layers	T_B °K	w	$\overset{o}{xA}$	No. of layers
18	Before commencing run 18(a)	not observed			299.5	5.578	104.42	45.42
	Before run 18(b)	6.761	126.57	55.06	296.2	4.738	88.70	38.58
	After run 18(b)	12.866	240.85	104.77	296.6	3.593	67.26	29.26
19	After run 19(a)	2.363	38.42	16.71	294.4	5.030	94.16	40.96
	After run 19(b)	9.181	171.87	74.76	306.6	6.428	120.33	52.34
	After run 19(c)	17.329	324.40	141.11	294.0	2.762	51.70	22.49
	Average				297.9			

3.1.6. Discussion.

The linear relationship between the reciprocal of uptake and activation energy ($E \propto 1/(w-w_o)$ plots) and the fact that the kinetics obeyed the inverse logarithmic form, (see section 1.3.2.1.1.(a)(ii)) provided strong evidence that Mott's theory of the formation of very thin films (<40-50 Å) was applicable, i.e. that the rate of reaction is governed by the rate at which metal ions are released from the metal and move through the oxide lattice under the influence of the electric field, F, arising from the constant potential difference V set up between the metal oxide interface and a chemisorbed layer on the outer oxide surface.

According to this theory, the rate of increase in thickness of the oxide layer is,

$$\frac{dx}{dt} = N'\nu\Omega \exp\left(\frac{qa'F - W}{RT}\right) \qquad (2)$$

where N' = the number of special sites/unit area ($cm.^{-2}$) from which a metal ion moves into the oxide layer.

$W = W_i + U$ where W_i is the heat of solution of a Li ion in the oxide, and U the activation energy for its diffusion within the oxide lattice, both in kcal./mole. W, therefore, is the energy barrier which must be surmounted by the metal ion in moving from the special site into the oxide.

a' = the distance between the special metal site and the top of the barrier, (Å).

q = the charge carried by the mobile lithium ion in the oxide, in kcals.(volt equiv.)$^{-1}$

$F = V/x$ the field in units of V $cm.^{-1}$

Ω = the volume of the oxide layer per metal ion ($cm.^{-3}$).

ν = the frequency of vibration of the metal ion at the temperature T°K and is assumed to be the same on either side of the barrier W.

$qa'F$ is therefore the decrease in energy of the barrier in the direction of the field.

From equation (2) the activation energy is given by

$$E = W - qa'V/x \qquad (3)$$

Applying equation (1),

then $$E = W - \frac{qa'VA}{1468w} \qquad (4)$$

In the present work with the introduction of the empirical constant w_o equation (4) becomes

$$E = W - \frac{qa'VA}{1468(w-w_o)} \qquad (5)$$

giving linear plots of $E/1/(w-w_o)$

3.1.6.1. Interpretation of the $E/\frac{1}{(w-w_o)}$ plots.

From equation (4) it can be seen that there exists a certain point of uptake above which the activation energy becomes greater than zero. This point is given by the intercept of the $E/\frac{1}{(w-w_o)}$ plots on the $\frac{1}{(w-w_o)}$ axis, (see figs. 3.12., 3.13.) defined as I_i in table 3.7. The reciprocal of I_i values plus w_o, therefore, gives the value of direct uptake in micromoles, I_d, (Table 3.7.) which is required before the activation energy becomes greater than zero;

below the value of I_d, uptake is therefore non-activated, as can be seen in Fig. 3.11. showing the direct uptake (E/w) plot for the clean film used in run 19(a).

Furthermore, for Mott's theory to be valid, the potential V on the growing oxide layers must be constant. During the growth of the first few layers on a clean film this is unlikely to be so, consequently w_o is the uptake at which the conditions at the surface have become sufficiently constant for V to have a constant value. For the three runs on clean surfaces, 8, 9 and 19(a), the number of oxide layers equivalent to w_o are 7.9, 3.8 and 3.5 respectively.

While the values for run 9 and 19(a) are in reasonable agreement, that for run 8 is not, and can probably be ascribed to inherent irreproducibility of evaporated surfaces due to the following causes:

(i) lack of accurate control of the temperature of evaporation with consequent variation of the radiation factor, and hence temperature of deposition,

(ii) variation of the rates of evaporation and deposition producing differences in the structure of the deposit and hence different behaviour during sintering,

(iii) variation in structure of substrate surface.

Furthermore oxidative sintering, a phenomenon which has been well established in recent investigations (139), is known to be important during the growth of the first few layers.

For that non-activated portion of the uptake, after V becomes constant, represented by $(I_d - w_o)$ or $1/I_i$ (see Fig. 3.11.), Mott's theory can provide no interpretation and it is probable that a different process is operative such that the rate of electron tunnelling is the controlling factor.

The theory described by equation (2) is based on the assumption that the rate controlling process is the rate at which ions are released from the metal interface under the action of the field. However, as discussed in section 1.3.2.1.1.(a)(i), when the film is only a few layers thick, the field produced by the constant potential, V, acting across it is so enormous that the rate of electron tunnelling becomes the limiting process, i.e. more of the readily available ions can cross the barrier per unit area per unit time than electrons can tunnel through per unit area per unit time.

Since the quantum mechanical tunnel effect is temperature independent this process is non-activated giving added support to the speculation. At some film thickness the fields will decrease to a value at which the rate of ion release becomes rate controlling and the activation energy becomes greater than zero i.e. at point I_d.

Extrapolation of the E / $\frac{1}{(w-w_o)}$ plots to $\frac{1}{(w-w_o)} = 0$, (or $(w-w_o) = \infty$), gives the value of W. These values listed in table 3.7. give an average result of 17 kcal.mole^{-1}. Roberts and Tompkins in a similar investigation of the

nitridation of calcium found W to be 22 kcal.mole^{-1} (22).

From Mott's theory, values of S/A = qa'V/1468, (where S is the slope of the E/$\left(\frac{1}{wcw_o}\right)$ plot), should be constant for all films. However, since the assumption that real area is equal to apparent area is arbitrary, (roughness factors may in fact vary as much as 200% or more) values of S/A may be taken as an indication of the reproducibility of real areas, (Table 3.10).

Table 3.10.

Run	S/A = qa'V/1468
8	0.119
9	0.138
18(a)	0.089
18(b)	0.108
19(a)	0.111
19(b)	0.111
19(c)	0.111
Average	0.112

Maximum variation = 0.1135 $\pm$ 0.0245 or $\pm$ 21.6%

The maximum variation of $\pm$21.6% is well within the limits of uncertainty of the roughness factor. Run 9 although carried out on a pure metal surface was evaporated onto the surface of the previously oxidized film produced by run 8 and hence may be expected to behave differently during sintering and to have a considerably different real surface area. The good agreement in run 19(a), (b) and (c) shows clearly that despite the very large quantities of oxide formed above

the points of breakaway (listed in table 3.9.) no change in surface area occurred. In runs 18(a) and (b), agreement is reasonable, a small increase of real area being possible after the second oxidation above breakaway. It is therefore concluded that films oxidized above the breakaway point, behave substantially as clean metal surfaces when the temperature is lowered once more and the activation energies redetermined.

For films oxidized above breakaway w_o includes, therefore, the amounts of oxide formed above the breakaway point.

It is not possible to evaluate the separate terms in $qa'V/1468$ without making further assumptions, nor to evaluate W_i and U respectively, from the value of W.

3.1.6.2. The Limiting Thickness and its Variation with Temperature.

An important corollary of equation (2) is that - provided the solubility of Li in the oxide is very small and V is substantially independent of temperature - at any temperature below a certain critical temperature, growth proceeds until a limiting thickness x_L of the nitride layer is attained. Experimentally, x_L, is defined as the thickness at which the rate of oxidation equals some arbitrarily chosen, very small, value (see table 3.11). If equation (2) is re-arranged after substituting $x_L = x$, then

$$x_L = \frac{Va'q/W}{1 - CT} \qquad (6)$$

where

$$C = -\frac{R}{W} \ln\left(\frac{dx_L}{dt} \frac{1}{N\Omega\nu}\right) \qquad (7)$$

Hence on plotting x_L against $x_L T$ a linear plot of slope C and intercept $Va'q/W$ should be obtained. In the present work plots have been expressed in terms of uptake, and include the values of w_o determined for each film;

i.e. $$x_L = \frac{1468 \times (w-w_o)_L}{A}$$

therefore $$(w-w_o)_L = \frac{Va'qA/1468W}{1 - CT} \qquad (8)$$

and $$C = -\frac{R}{W} \ln\left(\frac{d(w-w_o)_L}{dt} \frac{1468}{N'A\Omega z}\right) \qquad (9)$$

Hence on plotting $(w-w_o)_L/(w-w_o)_L T$, the slope = C, and the intercept = $Va'qA/1468W$.

The values of the uptake $(w-w_o)_L$, corresponding to the arbitrarily chosen very small limiting rate, $\frac{d(w-w_o)_L}{dt}$, were obtained graphically from the empirical w/t plots, (e.g. Figs. 3.4.,3.5.,3.6.,3.7.,3.8.,3.9.,3.10.), by drawing tangents, of slope $\frac{d(w-w_o)_L}{dt}$, to the curves at the various experimental temperatures. The results obtained are set out in Table 3.11.

Table 3.11.

Run	T^oK	limiting rate $\frac{d(w-w_o)_L}{dt}$ micromoles $x\ 10^{-3}$ $min.^{-1}$	w	$(w-w_o)_L$	$(w-w_o)_L xT$
18(a)	194.2	2.06	6.060	0.660	128.23
	210.0		6.258	0.858	180.18
	223.0		6.318	0.918	204.71
	250.0		6.479	1.079	269.65
	260.86		6.549	1.149	299.83
	288.80		6.737	1.337	386.01

Table 3.11 continued.

Run	$T^{o}K$	limiting rate $\frac{d(w-w_o)_L}{dt}$ micromoles $\times 10^{-3}$ $min.^{-1}$	w	$(w-w_o)_L$	$(w-w_o)_L xT$
18(b)	195.0	2.06	12.026	0.826	161.07
	210.0		12.367	1.167	245.13
	223.2		12.418	1.218	271.81
	250.0		12.608	1.408	350.62
	261.0		12.687	1.487	388.13
	273.2		12.778	1.578	431.05
	289.6		12.863	1.663	481.60
19(a)	77.45	1.77	1.116	0.616	47.71
	90.19		1.160	0.660	59.55
	139.14		1.217	0.717	99.75
	157.15		1.309	0.809	127.10
	194.20		1.495	0.995	193.21
	250.35		1.935	1.435	359.30
	260.68		2.024	1.524	397.15
	273.16		2.222	1.722	470.25
19(b)	157.22	1.16	7.791	0.711	111.70
	177.05		7.869	0.789	139.62
	208.95		8.202	1.122	234.44
	273.16		8.732	1.652	451.26
	294.66		9.166	2.086	614.69

Experimental verification of the validity of the

relationship expressed by equation (8) is shown in Fig. 3.16. Values of the limiting rate used, C, the intercept I_t, and I_t W/A (= qa'V/1468), as well as the values of S/A (= qa'V/1468) from table 3.10. (obtained from the $E \not\propto \frac{1}{(W-W_o)}$ plots) have been collected in Table 3.12. for comparison.

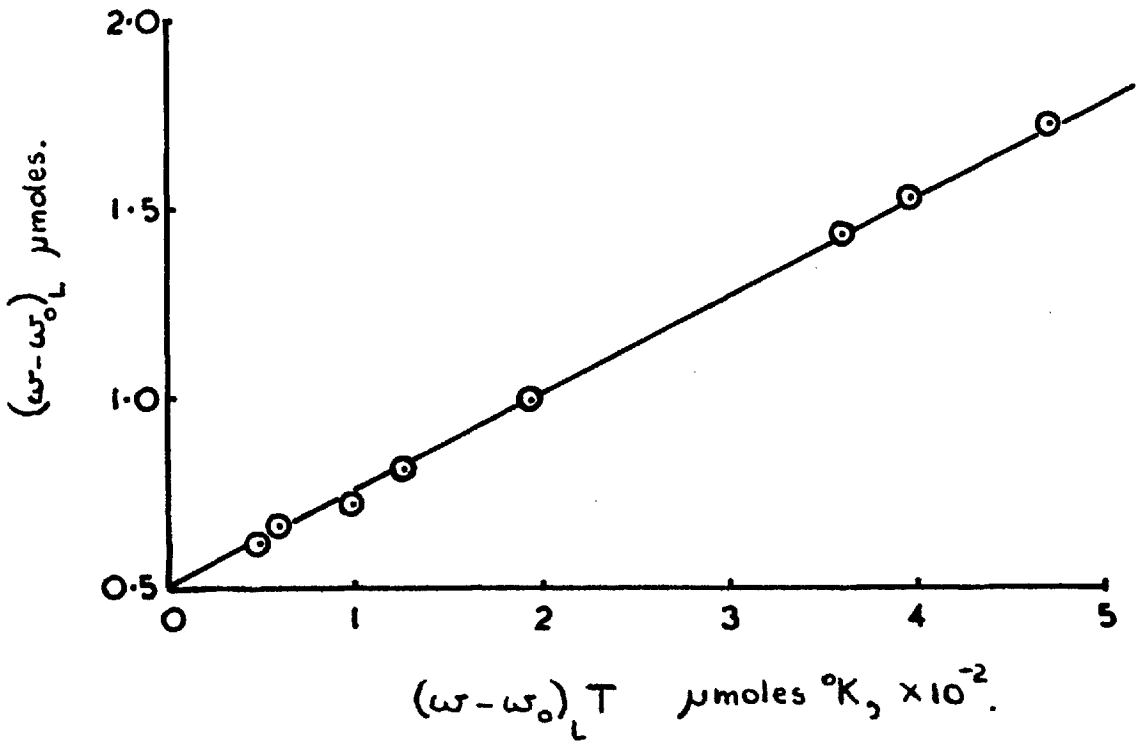
Table 3.12.

Run	limiting rate micromoles $x\ 10^{-3} min.^{-1}$	C T^oK^{-1}	I_t	$I_t W/A$	S/A
8					0.119
9					0.138
18(a)	2.06	2.53×10^{-3}	0.39	0.185	0.089
18(b)	2.06	2.43×10^{-3}	0.55	0.119	0.108
19(a)	1.77	2.55×10^{-3}	0.51	0.096	0.111
19(b)	1.16	2.54×10^{-3}	0.50	0.107	0.111
19(c)					0.111
Average				0.102	0.112

Examination of the last two columns in Table 3.12., shows agreement for the value of qa'V/1468 by these two independent methods to within 10%, thus giving further strong support to the applicability of the Mott theory, both on clean films, and films oxidized above the breakaway point.

For a roughness factor arbitrarily taken as 2, and assuming that the distance from a special metal site to the top of the potential barrier, a' is 2 Å, with q = e,

FIG.3.16. (RUN 19(a)).



(assuming that the Li^+ ion is the mobile species), then for $\frac{qa'V}{1468}$ = 0.109 kcal.x10^{-6}cm.$^{-2}$, (the average of all values from both methods) V = 1.2V. Cabrera and Mott (21) have suggested that a very rough estimate of V may be obtained from the equation

$$eV = E + W_A - \phi, \qquad (10)$$

where ϕ is the electronic work function of the metal, E is the electron affinity of the gas (O_2) and W_A is the adsorption energy of the oxygen molecule at the oxide surface. A value of about 1V can be expected.

3.1.6.3. The Critical Temperature.

According to the theory of Mott and Cabrera there is a temperature, T_c, above which (due to the metal ions becoming interstitially soluble in the oxide lattice) the growth of the oxide layer is no longer dependent on the field produced across the oxide film by the adsorbed oxygen. Thus above this temperature reaction proceeds until all the metal has reacted with a consequent change in kinetics. On the other hand, below this temperature, since the ions are not thermally very soluble, growth is dependent on the field pulling metal ions through the lattice. As the thickness increases for a given temperature, the field decreases until it is no longer large enough to cause growth and hence critical thicknesses exist for given temperatures.

From equation (7), $T_c = \frac{1}{C}$, as $(w-w_o)_L$ tends to

infinity, where C is the slope of the $(w-w_o)_L/(w-w_o)_T$ plots (see Fig. 3.16 and Table 3.12.). The average value is 398°K or 125°C.

3.1.6.4. Concentration of Special Sites at the Metal/Oxide Interface.

From equation (9),

$$C = -\frac{R}{W} \ln\left(\frac{d(w-w_o)_L}{dt} \frac{1468}{N'A\Omega\nu}\right)$$

and has a value (for run 19(a)) of $2.55 \times 10^{-3}(°K)^{-1}$. The limiting rate is 1.77×10^{-3} micromoles $min.^{-1}$, and $A = 90.3$ $cm.^2$ Substitution of these values in equation (8) together with the following

$\nu = 10^{12} \times 60$ $min.^{-1}$, $\Omega = 12.183$ $Å^3$

$W = 17.00$ $kcal.mole^{-1}$, $R = 1.986 \times 10^{-3}$ $kcal.mole^{-1}$

and multiplying the resulting value for N' per $Å^2$ by 10^{16} gives the number of special metal sites per $cm.^2 = 1.19 \times 10^9$. From a knowledge of the crystallographic constants for the b.c.c. Li_2O lattice (138), the total number N, of metal sites per $cm.^2$ of metal surface in the (100) plane is calculated to be 8.163×10^{14} per $cm.^2$, cp. with 1.19×10^9 for N'.

The ratio N'/N, which gives the fraction of total metal sites from which Li ions move into the oxide layer, is $\sim 10^{-6}$ compared with corresponding values of $10^{-3} - 10^{-4}$ for the nitridation of Ca (22) and approximately 10^{-2} found in the oxidation of Cu (21).

The value of N'/N found for lithium is considerably

lower than for calcium and copper, but the sequence of results for these three metals is as expected. Thus due to the relatively high sintering temperature of the lithium films, compared to the melting point, and due to the softness and malleability of the metal in general, surface disorder would be considerably lower than for a harder metal such as Ca which would be in turn lower than for Cu.

3.1.6.5. The Point of Breakaway.

It is first necessary to distinguish the phenomenon of breakaway from that predicted by the Mott theory above the critical temperature, T_c. The theoretical critical temperature, T_c, predicted by the Mott equation is about 398°K whereas the breakaway temperature, T_b, is in the region of 298°K.

Furthermore when growth was allowed to proceed to a thickness well above 50 Å at T_b, and then the temperature was lowered to liquid nitrogen temperature, growth should be stopped completely if T_b were the theoretical critical temperature since this thickness is very much greater than the critical thickness predicted by the Mott theory for 78°K.

In actual fact, even with thicknesses of 200 Å, (run 18(b)), and 700 Å (run 19(c)), (see table 3.9.), on returning to lower temperatures rates similar to those for a clean film were obtained.

This new phenomenon therefore bears no relation to the

critical phenomenon which was not observed due to the intervention of breakaway.

To compare, approximately, the number of layers of oxide formed at lower temperatures up to the temperature of breakaway, the quantity $(n_b - n_o)$ was used, where

n_b = the approximate number of layers at the onset of breakaway after a run at lower temperatures and

n_o = the number of layers corresponding to the uptake w_o, for the particular run.

Values of this parameter, $(n_b - n_o)$, thus defined as the breakaway thickness, and values of the corresponding breakaway temperatures, T_b, from table 3.9 have been collected in Table 3.13 below.

Table 3.13. Critical Temperature and Thickness at Breakaway.

Run	(n_b-n_o)	T_b °K
18(a)	11.08	296.2
18(b)	13.57	296.6
19(a)	13.18	294.4
19(b)	17.11	306.6
19(c)	14.89	294.0
Average	13.97	297.6

From these results it would appear that a critical film thickness and a critical temperature should be simultaneously attained for the process to occur. The spread in the values of the critical thickness would result from the difficulty of producing and maintaining a

constant real area; furthermore, the past history of the film, e.g., whether produced quickly at higher temperatures or more slowly at lower temperatures, will undoubtedly affect both the mechanical strength of the film and its coherence to the substrate in turn affecting the thickness at which stress build-up becomes too great to be sustained.

The main difficulty of interpretation of the breakaway phenomena is to explain the complete regeneration of the original surface area of the metal covered by only 2-3 layers of oxide, after large additions of oxide have been made above the breakaway point, and also the corollary, that the original highly protective oxide layer, after breakaway, offers little or no resistance to the penetration of oxygen to this regenerated surface.

In the past, the Pilling and Bedworth principle has usually been invoked. Many metals, however, provide exceptions to this rule (140) and its usefulness has been questioned (141, 142, 48). Some authors (142, 48) consider that the oxide/metal volume ratio is unimportant when oxidation takes place by cationic diffusion and therefore at the outer oxide surface unconstrained by the substrate. These authors conclude that it need only be considered for anionic diffusion, but even in this case, Vermilyea has doubts of its validity.

A theoretical discussion of epitaxial overgrowths has been given by Frank and van der Merwe (143), and van der

Merwe (144). The authors considered the effect of the substrate on the epitaxial lattice parameter, using a one dimensional model where the oxide layer was concieved as a row of spheres coupled by elastic forces, in the periodic potential field of the substrate. They define a term "the critical misfit" between the substrate and epitaxial lattice parameter, below which the epitaxial lattice is constrained to fit exactly the substrate parameter, by either compression or extension, giving an oriented pseudomorphic uniform epitaxial layer, and above which dislocations occur, relieving the strains, and giving a randomly oriented discontinuous layer. Mott and Cabrera (21) point out that as the oxide grows, (initially constrained to fit the substrate parameter) at some film thickness, breakaway must occur with the film achieving its equilibrium lattice parameter, since bulk material exhibits a much lower compressive strength than thin films. Thus a process of recrystallization will occur.

Some of the concepts involved in this treatment, particularly that of a critical misfit in terms of resultant epitaxial orientation, and the concept of basal plane pseudomorphism, have been criticized on theoretical grounds by Blackman and Smollett (145), and on experimental results by Pashley (146). Nevertheless, the influence of the lattice parameter of the substrate on the structure of at least the first few layers of the oxide will be large. Thus epitaxial strains are undoubtedly set up, whether or

not pseudomorphism occurs, in the initial layers of the oxide film. Consequently as the oxide layer thickens, and as the temperature is increased, a point will be reached where recrystallization processes will occur with the possibility of cracking and porosity developing in the oxide layer.

Since it is likely that the predominantly mobile species in the growth of the uniform layer is the lithium ion, (on account of its small ionic radius (0.6 Å) (1), and the consequent close packing and small interstitial sites in the oxide lattice), metal vacancies will be generated at the metal/oxide interface. These vacancies may be partially filled by a counter flow of anions from the first few layers of oxide, under the action of the field, leaving anion vacancies in the oxide. As the temperature is raised, the number of defects in the oxide lattice near the metal/oxide interface will tend to increase leading to a weakening of the adhesive forces near the substrate interface. Furthermore, since a widely differing thermal coefficient of expansion is to be expected between the lithium metal and lithium oxide, stresses already present will be enhanced as the temperature approaches the breakaway point.

Thus, on attainment of a certain critical thickness and temperature, strains present in the metastable epitaxial layer cannot be sustained and a process of "recrystallization" to the equilibrium lattice condition occurs. Due to the

weakening of the adhesive forces in the layers near to the metal/oxide interface by the generation of vacancies the oxide will tend to strip away from the metal surface regenerating the "original" surface as porosity develops throughout the bulk of the oxide and allowing oxygen gas to penetrate once more close to the metal surface. New growth at lower temperatures will then be possible once more, with formation of another protective layer at the base of the porous crust, pushing the porous layer up as it grows until the breakaway point is again reached, whereupon the whole process can be renewed.

3.1.6.6. Dependence of Rate on Pressure.

A major problem in the present system is the explanation of the observed pressure dependence.

It is clear that once a three dimensional oxide growth has been established i.e. after the formation of the first 2-3 layers which occurs during the rapid non-activated uptake at the beginning, then all subsequent oxidation must be preceeded by an initial chemisorption of oxygen on the outer surface of the oxide layer. The behaviour of the oxide towards chemisorption will undoubtedly be modified by the close proximity of the underlying metal substrate as compared to that of a bulk oxide. Thus chemisorption at the outer surface will be taking place in a reducing environment.

That the rate of oxygen uptake varies as the square

root of the pressure is in agreement with the general view that oxygen is dissociatively adsorbed. For an immobile randomly adsorbed layer in which the adsorbed species remains on adjacent sites the act of chemisorption cannot be rate determining. The rate determining process involves therefore passage of ions or adatoms into a state of lower free energy than can be attained directly by molecules from the gas phase.

Furthermore in order to explain the rapid adjustment of rates with pressure changesit is necessary that chemisorption be pressure reversible. If coverage is low ($\theta \ll 1$), then the reaction is taking place in the Henry law region of, say, the Langmuir isotherm which under these conditions reduces to $p = k\theta$. This is consistent with the experimental conditions of low pressures - 10^{-4}-10^{-2} mm.Hg.

For convenience, the adsorbed species will be written as O_2^- to denote a localized electron concentration in the vicinity of the adsorbed O_2 molecules. This type of incomplete charge transfer is consistent with a weak reversibly adsorbed species, which unless stabilized during its lifetime by accepting another electron or by dissociation, will be desorbed.

It might be noted that the sites for adsorption must be unique localities on the oxide surface such as kink sites or terraces (terminations in the surface, of spiral dislocations where there is an abnormal electron density), and

where ion movement, necessary for incorporation, is sterically and energetically easier.

A possible mechanism could be envisaged thus:

$$O_2(gas) + e \underset{}{\overset{K_1}{\rightleftharpoons}} O_2^-(ads.) \qquad (a)$$

$$O_2^-(ads.) + e \underset{}{\overset{K_2}{\rightleftharpoons}} 2O^-(ads.) \qquad (b)$$

$$O^-(ads.) + e \underset{}{\overset{k}{\rightleftharpoons}} O^{2-}(incorp.) \qquad (c)$$

The reaction $O_2(gas) + 2e \longrightarrow 2O^-$ would be energetically improbable and must go through the intermediate step. The molecule-ion is weakly chemisorbed until it accepts another electron.

In order to maintain the $p^{\frac{1}{2}}$ relationship, it is necessary that the O_2^- (ads.) and O^-(ads.) species be weakly held although the absorptive bond in (b) is stronger than that in (a). Both equilibria are thus well over to the left and the adsorption is within the Henry law range ($\theta \ll 1$). Incorporation and rearrangement into the lattice (c) is slow consequently $[O^-(ads.)]$ is determined by (a) and (b) and the rate of uptake is therefore

$$r = k[e]^2(K_1K_2p_{gas})^{\frac{1}{2}}$$

$[e]$ represents the concentration of electrons in the oxide at the outer surface resulting from tunnelling and is constant since the changes in rate with pressure change were compared at constant uptake w.

Fig. 3.17. Diagram of the Mechanism.

1.



2.



(Li^+) = interstitial lithium ion drawn through the oxide under the action of the field.

The number of chemisorbed species "n" per unit area determines the field strength in the Mott and Cabrera rate equation;

$$\frac{dx}{dt} = \text{const. } \exp(qa'F/RT) \qquad (2)$$

where F is the field averaged over the whole surface.

It is therefore evident that since the value of "n" varies exponentially with temperature, i.e. "n" is some function of $\exp.(-\Delta H/RT)$, where $-\Delta H$ is the heat of chemisorption. V and therefore F if regarded as averaged over the entire surface, will not be temperature independent as required in the derivation of equation (2).

In order to explain this difficulty and also the pressure dependence, it is concluded that due to the sorbed species being widely separated on the surface, the field induced is confined to narrow tubes isolated from one another and representing isolated active patches on the oxide surface.

The field F induced is thus independent of temperature and independent of the amount of adsorption, although the number of tubes active in the rate process at a constant temperature id dependent on the square root of the pressure. This is so, since a tube exists, as far as the rate of reaction is concerned, only when the adsorbed species is the O^-(ads.) ion as in the above mechanism - the formation of this species being dependent on the square root of the oxygen pressure.

The potential V is therefore independent of temperature but the number of tubes depend exponentially on the temperature. This will not invalidate the relationship $E \propto 1/x$, but E, the experimental activation energy, now contains an energy term which corresponds to the dependence of "n" with temperature. If the number of sites is independent of temperature, i.e. if they represent positions where dislocations terminate at the surface, then the energy term corresponds to the heat of chemisorption and the true value of W is $(15 + \Delta H)$ kcal.mole^{-1} where $-\Delta H$ is the heat of chemisorption.

Clearly the number of special sites at any temperature must be statistically constant with time, i.e. they are self-generating as oxidation proceeds and this suggests that growth of the oxide layer proceeds from where spiral dislocations are originally present and that the growth of these is the fundamental process. This provides a

mechanism whereby growth may spread over the surface but the number of isolated special sites throughout remains statistically constant.

3.2. Nitridation of Bulk Solid Lithium.

Lithium exists in the solid state up to 186°C; the reaction with nitrogen was first studied from 0°C to about 160°C, over approximately 20 mm. to 600 mm.Hg.

3.2.1. Nucleation Period.

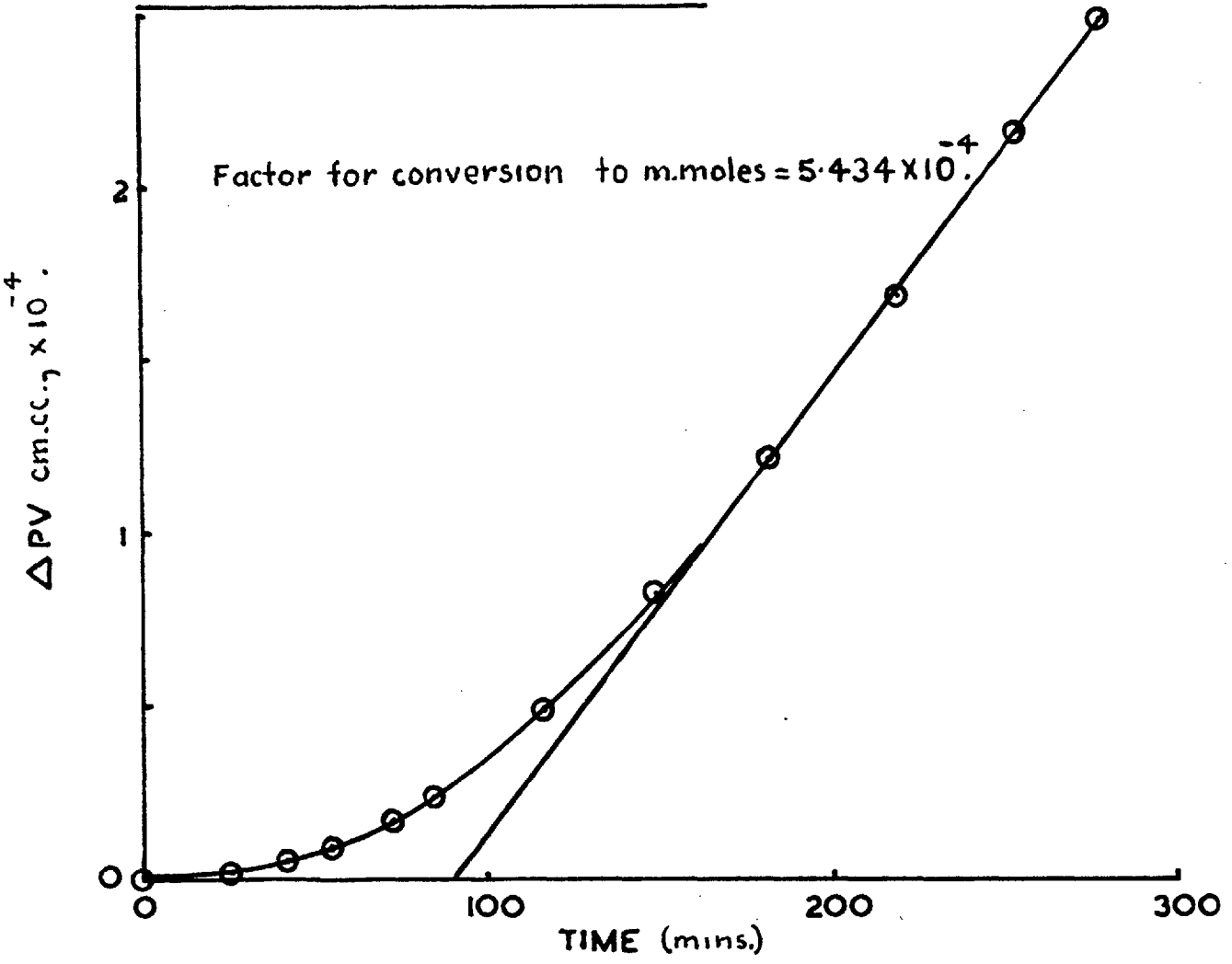
After filtering, outgassing, and cooling the lithium to the constant reaction temperature, nitrogen was admitted, at constant pressure, to the reaction vessel. In most cases a curve of the form shown in Fig. 3.18. was obtained with an initial accelerating period OA followed by a linear period of uptake. The uptake at point A for run 14 was 79 millimoles N_2 which was equivalent to a thickness of $\sim$1 mm. of nitride assuming that bulk lithium nitride has the same density as the crystallographic density of the unit cell, and that the area of the reacting surface equals the cross sectional area of the reaction vessel (138).

Since this behaviour is, in general, indicative of nucleation, with the nuclei growing either three dimensionally into the bulk or spreading laterally over the surface, (2-dimensional growth), a power law is to be expected of the form

$$w \propto t^n$$

where w is the uptake (in millimoles of gas in the present work), t is the time (in minutes) and the value of the exponent is 3 for three dimensional growth or 2 for two dimensional growth.

FIG.3.18. NUCLEATION (RUN 10).



This was tested by plotting the portion of the w/t curve, OA, on log log paper. (See Figs. 3.19, 3.20., 3.21.). To simplify calculation, plots have in some cases been expressed in units of PV (cm.cc.). Where this has been done a factor has been given for conversion to millimoles of nitrogen uptake. A value of 2 for the exponent was obtained in runs 14 and 10; in run 14 a slightly higher value was initially found, and in run 6 the value was 3 for about the first 7-8 minutes decreasing to 2 and finally the uptake was linear.

Frankenberger (104), in an investigation of the nitridation of lithium films over a comparable temperature range, reported a similar acceleratory period up to a thickness of approximately 1 mm. of nitride and observed on sectioning that the lithium nitride grew from nuclei at the surface in concentric hemispherical shells, giving a power law with an exponent of 3. (See section 1.4.3.).

The present results suggest three dimensional growth of nuclei up to some limiting size, whereafter, due to breakaway, caused by stresses set up by incongruence of lattice parameters, further growth proceeds by lateral spreading until the surface is covered. Alternatively, penetration into the bulk of the lithium may occur two dimensionally, along dislocations and grain boundaries; this would also lead to an exponent of 2.

FIG. 3.19. NUCLEATION (RUN 14).

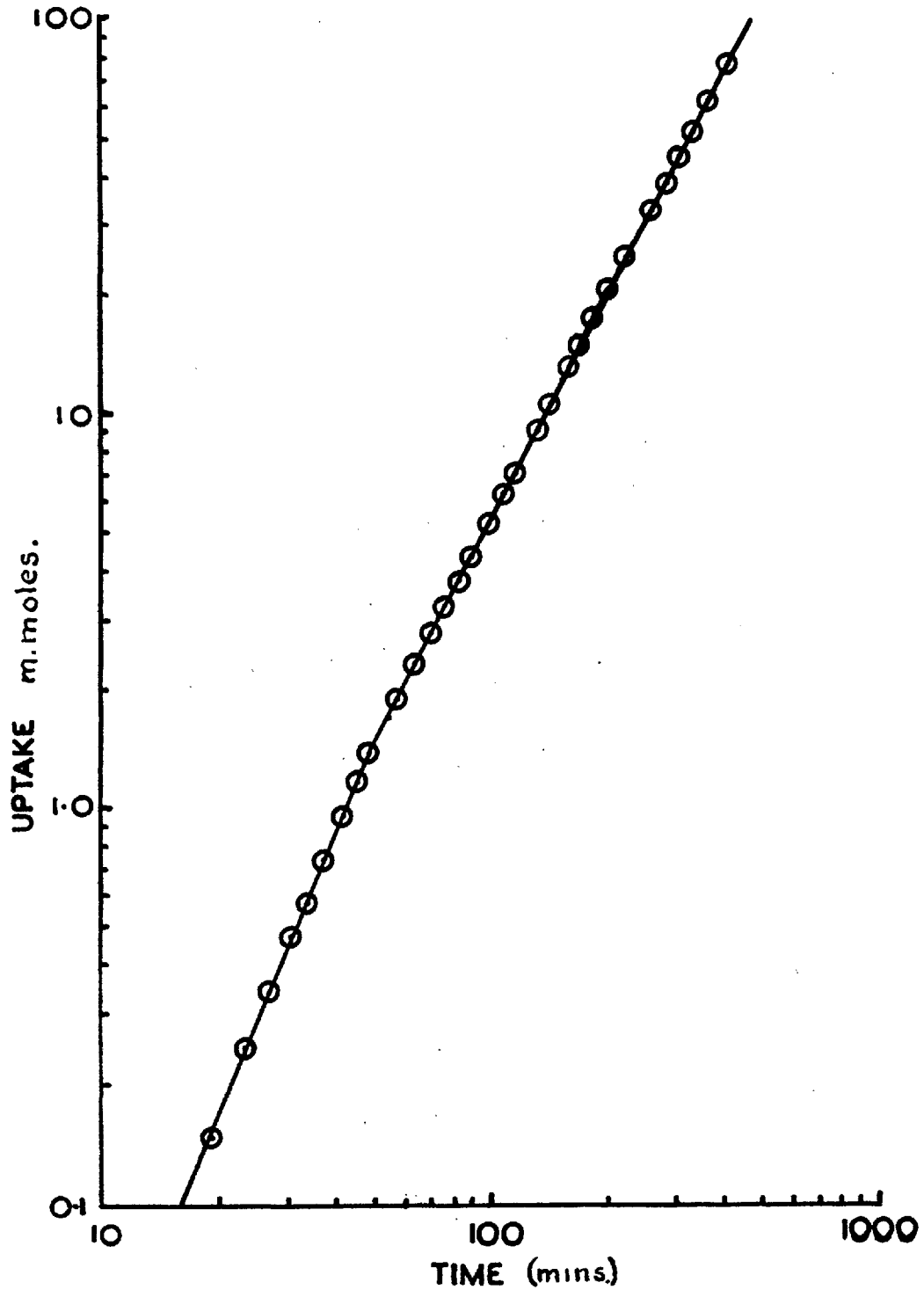


FIG. 3.20. NUCLEATION (RUN 10.)

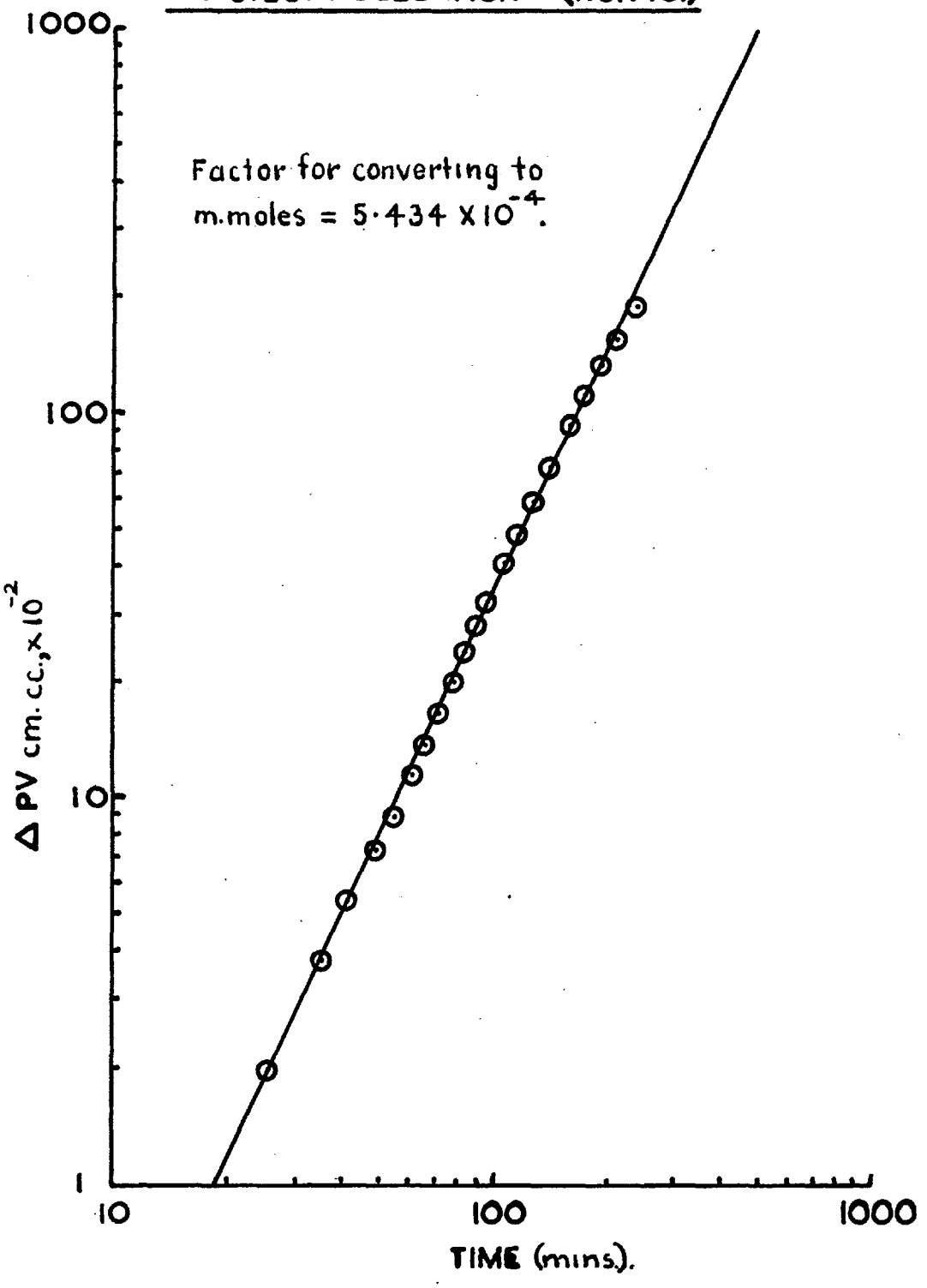
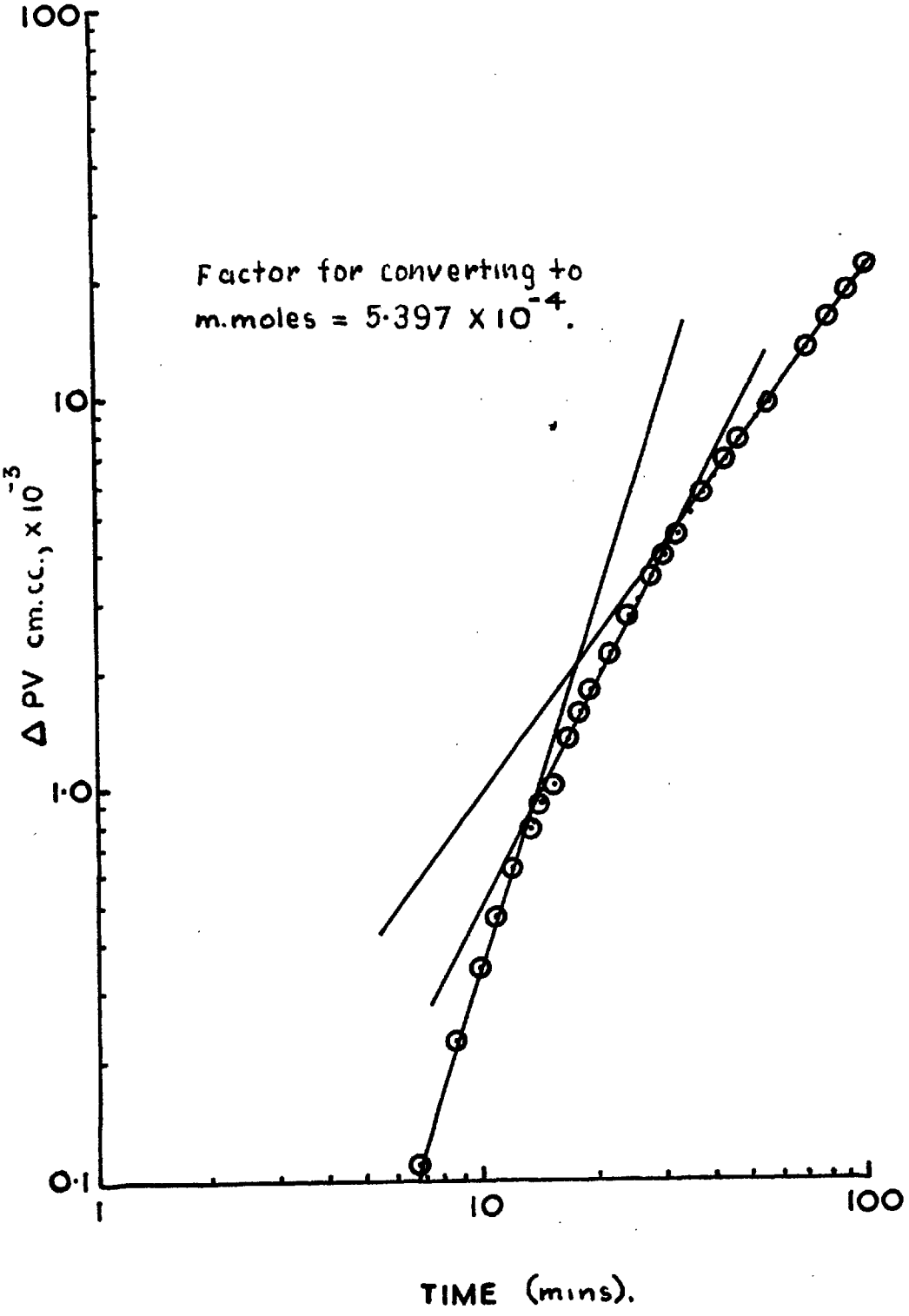


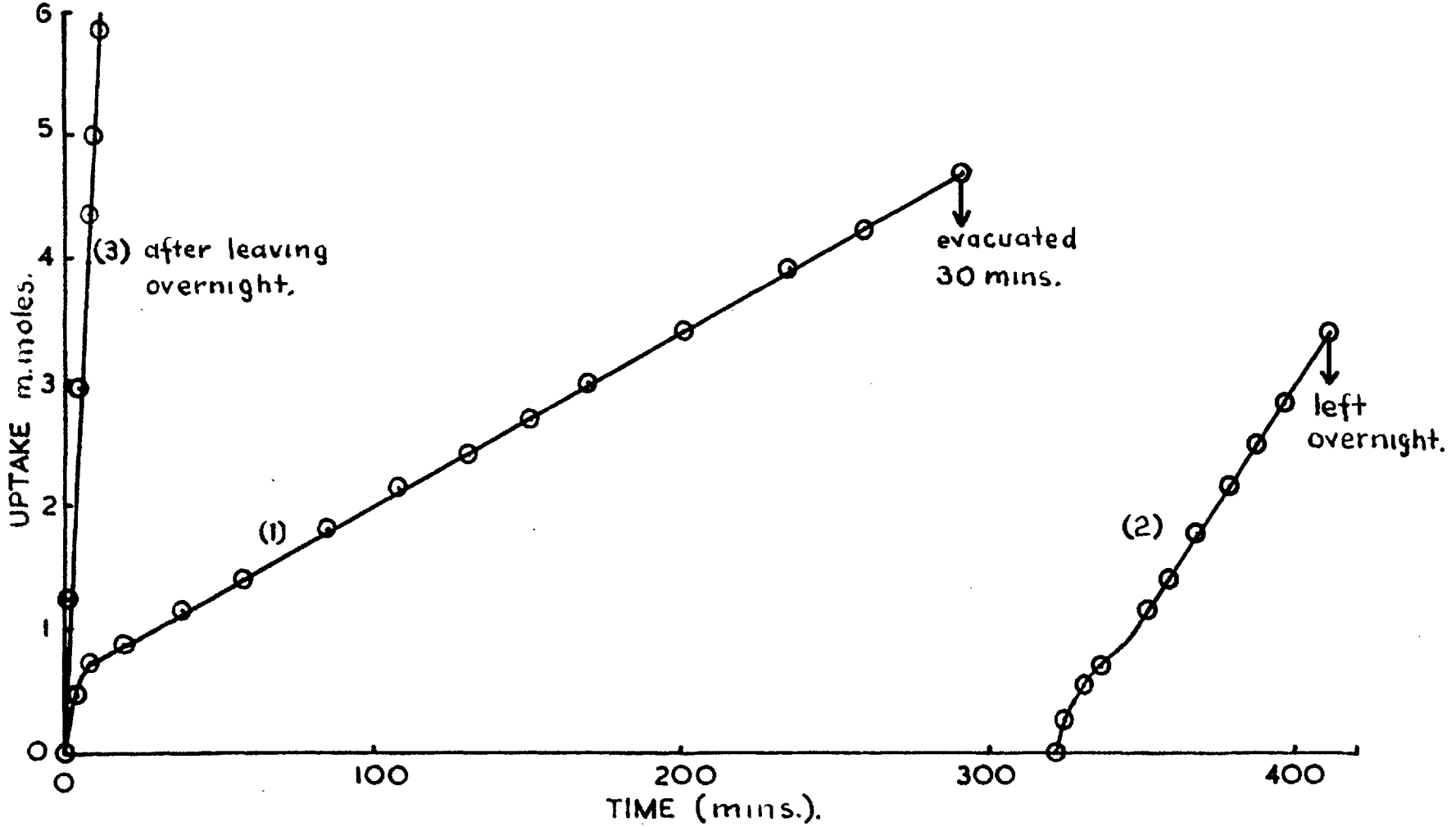
FIG. 3.21. NUCLEATION (RUN 6).



3.2.2. Linear Uptake.

After the acceleratory period OA the uptake becomes linear with time and remains so in all cases, although irreproducible rate transitions were frequently observed, some occuring spontaneously without change in experimental conditions whilst others were apparently related to variations in pressure or temperature effected during runs. These rate transitions occurred suddenly giving an increase or decrease in rate and were often of such a magnitude as to make reproducibility of results completely impossible. In the early stages after the point A had been passed, rate transitions induced by varying experimental conditions appeared to be more liable to catastrophic changes than at greater thicknesses of nitride. For example in run 15, after nucleation, the rate became linear, with a value of 0.016 mmoles $min.^{-1}$ under a pressure of 40.63 cm.Hg at 100°C and remained so for 300 minutes, but on pumping to high vacuum for 30 minutes and repeating the rate determination under identical conditions a value of 0.038 mmoles $min.^{-1}$ was obtained, which was constant for at least 80 minutes. The residual nitrogen was then allowed to react at constant volume overnight, as the temperature of the reaction vessel dropped to room temperature. On the following day the experimental conditions were reproduced exactly, and the rate was found to have increased to 0.463 mmoles $min.^{-1}$ remaining strictly linear over 30 minutes, Fig. 3.22.

FIG. 3.22. (RUN 15.)



However, as the crust thickened, and in some cases reaction was followed up to crust thicknesses of more than 2 cm., it appeared that a comparatively constant steady state was attained. Rate transitions (both increases and decreases), were still observed although smaller in magnitude. The transitions were always sharp, even when relatively small, and uptake remained linear both before and after.

Table 3.14. summarizes various attempts to isolate the effect of various parameters, temperature, pressure, evacuation etc., to discover the causes of irreproducibility, but no obvious pattern could be found.

Table 3.14.

Sequence of rate determinations	Operation	T_c °C	P_c cm.	Rate mmoles $min.^{-1}$
1.	Residual gas pumped away overnight.	40.1	20.42	0.100
2.	Repeated 1. Pressure raised quickly.	40.1	20.42	0.185
3.	Pressure allowed to decrease while reacting.	40.1	40.54	0.555
4.	Repeated 1. Pressure allowed to decrease while reacting then raised again.	40.1	20.42	0.197
5.	Repeated 1. Residual gas pumped away for 15 mins.	40.1	20.42	0.204
6.	Repeated 1. Residual gas pumped away again for 15 mins.	40.1	20.42	0.272
7.	Repeated 1.	40.1	20.42	0.309

Table 3.14. continued.

Sequence of rate determinations	Operation	T_c °C	P_c cm.	Rate mmoles $min.^{-1}$
	Pressure maintained constant while temperature lowered to 21°C then raised to 40.1°C then lowered to 0°C.			
8.		0.0	20.42	0.450
	Temperature raised again to 40.1°C.			
9.	Repeated 1. Residual gas allowed to sorb completely, then pressure raised again.	40.1	20.42	0.328
10.	Repeated 1. Residual gas again allowed to sorb, then pressure and temperature raised.	40.1	20.42	0.364
11.		100.0	20.42	0.270
	Temperature lowered to 20°C, maintaining constant pressure then temperature raised to 100°C.			
12.	Repeated 11. Repeated operation 11.	100.0	20.42	0.151
13.	Repeated 11. Residual pressure allowed to decrease slowly, maintaining constant temperature then pressure raised again.	100.0	20.42	0.138
14.	Repeated 11. Residual gas pumped away and temperature dropped overnight to 20°C then raised and pressure restored.	100.0	20.42	0.152
15.	Repeated 11. Pressure held constant while temperature dropped to 40°C.	100.0	20.42	0.267

Table 3.14. continued.

Sequence of rate determinations	Operation	T_c °C	P_c cm.	Rate mmoles $min.^{-1}$
16.	Repeated 1. Residual gas pumped away, then temperature cycled 4 times during one hour, while pumping between 100°C and 30°C.	40.1	20.42	0.493
17.	Repeated 11. Residual gas pumped away and temperature dropped to 20°C for 2 days.	100.0	20.42	0.227
18.	Repeated 11.	100.0	20.42	0.315

However, it appears that pressure decreases at constant temperature, brought about by uptake at constant volume and pressure increases, by gas introductions, showed smaller variations (2, 4 and 5) (13 and 14) than temperature changes at constant pressure (11, 12 and 13). Rapid pressure changes brought about by pumping for 15 minutes produced quite large rate increases (5, 6, 7).

Nitridation, when followed to its conclusion, proceeded completely throughout the bulk of the lithium; in one case run 14, as much as 19 g. of lithium was nitrided.

3.2.3. Dependence of Rate on Pressure.

In examining the effect of pressure on the rate, two constant temperatures were employed, 40°C and 100°C and the rate determined at pressures ranging from 4 to 40 cm.Hg, in a random manner.

The results exhibited large scatter without apparent consistency, but trends could be found if the results were examined in the numerical sequence in which they were carried out. Thus one series, in numerical order, followed a reasonably smooth curve until a rate transition occurred, then the next series would follow a similar curve shifted either above or below the first curve. After this a further series would be obtained and another transition, and so on. The empirical plots, for a typical series between rate transitions, from which rates at various pressures, were determined have been plotted in Fig. 3.23. Thus a family of rate curves were found at both temperatures, Figs. 3.24. and 3.25. See Table 3.15.

Table 3.15. Dependence of rate on pressure.

Run	Sequence of determination	Constant Temp. T_c °C	Constant Pressure P_c cm.	Rate mmoles $min.^{-1}$
17	3.	40.2	12.29	0.076
	4.	"	40.54	0.390
	5.	"	18.43	0.136
	6.	"	24.41	0.213
	7.	"	32.49	0.333

FIG.3.23. PRESSURE DEPENDENCE (RUN 17).

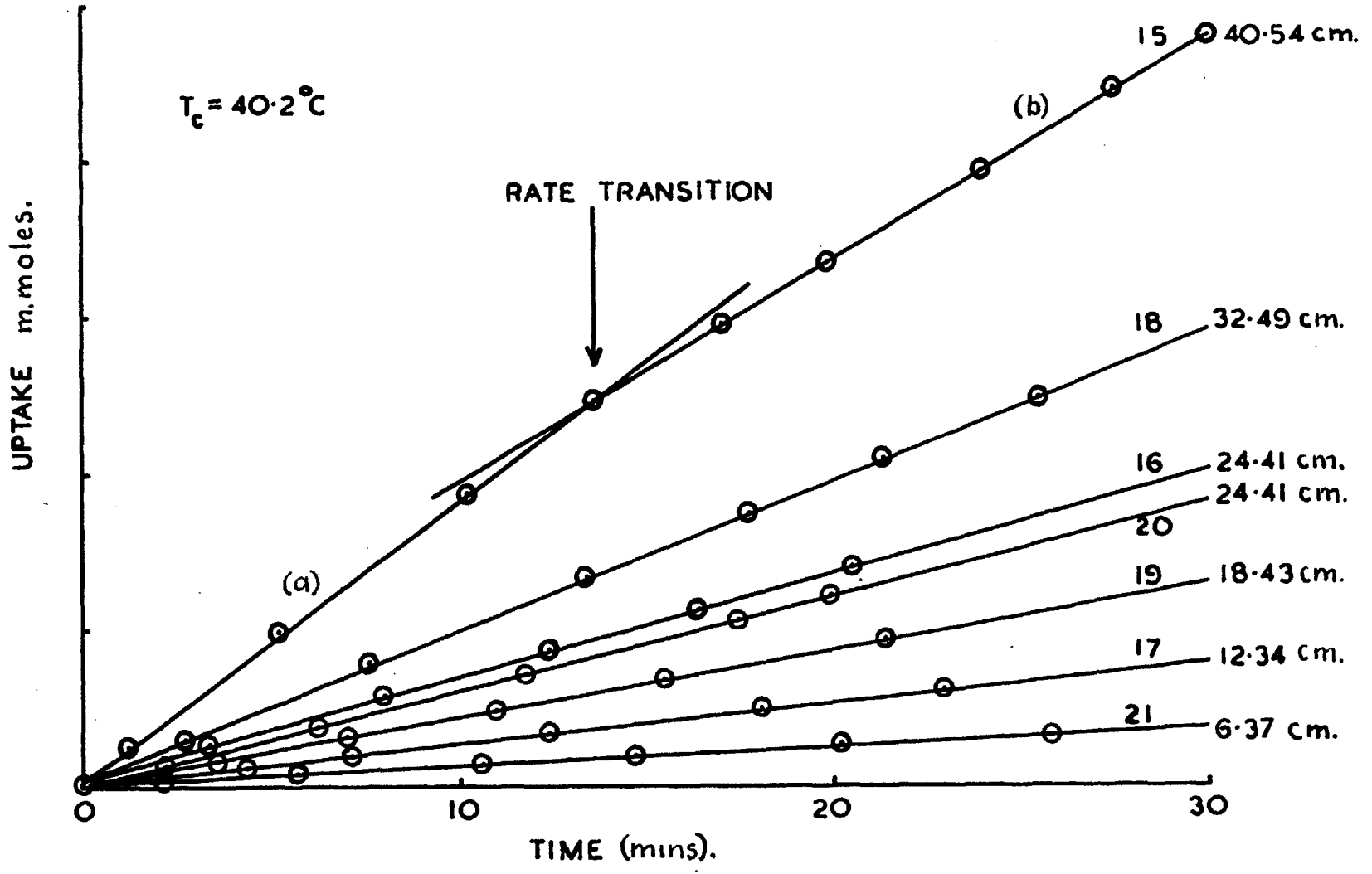


FIG. 3.24. PRESSURE DEPENDENCE (RUN 18).

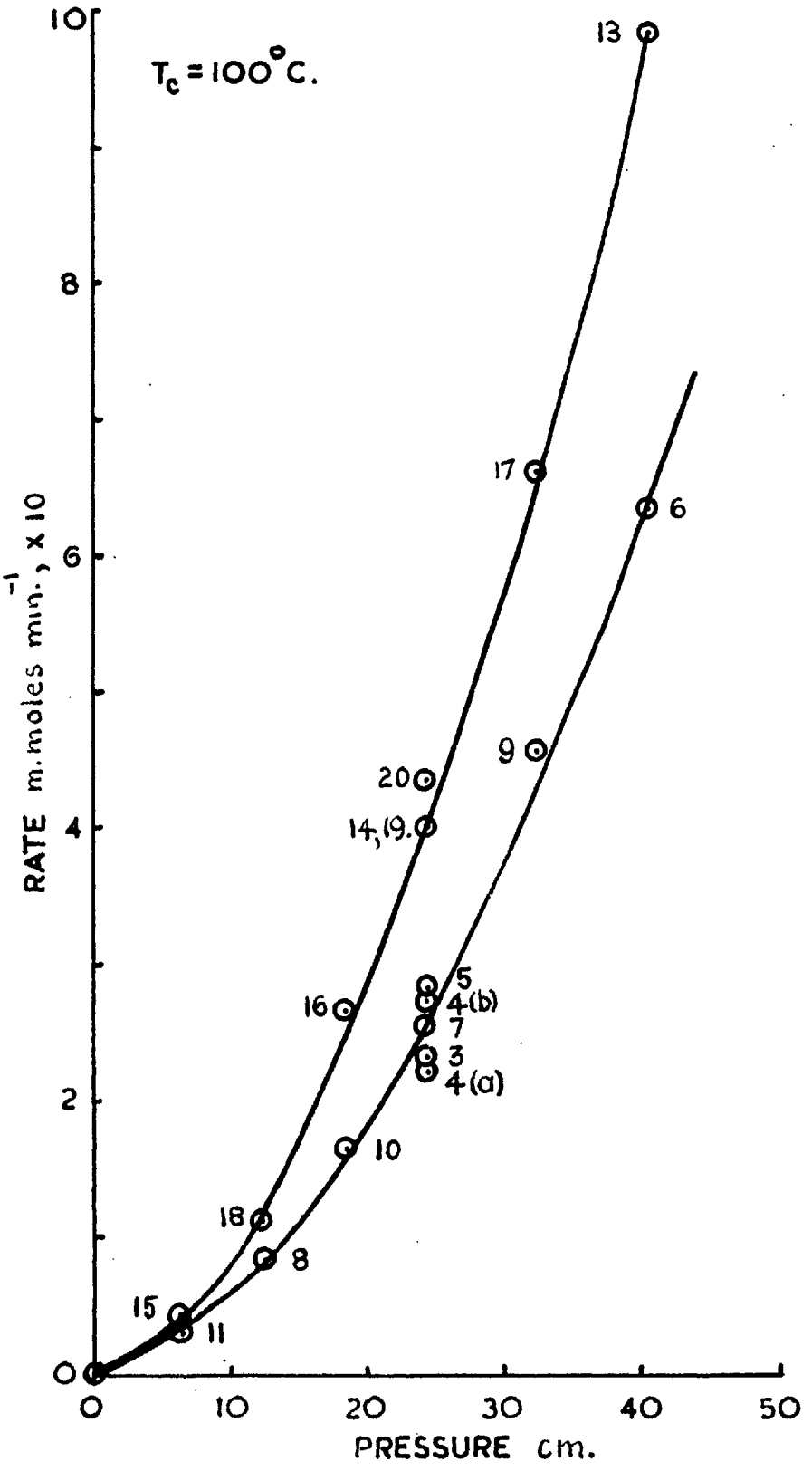


FIG. 3.25. PRESSURE DEPENDENCE (RUN 17.).

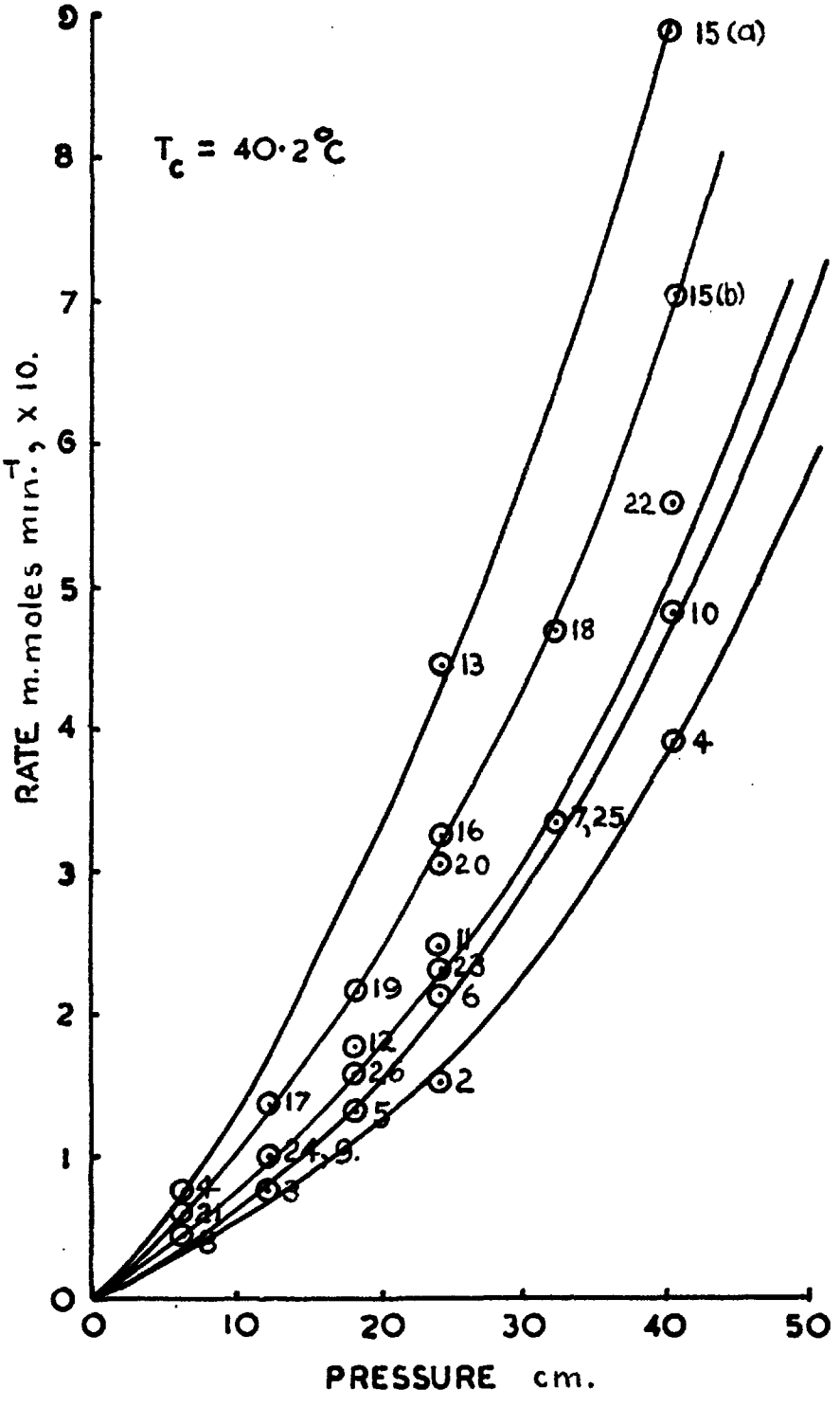


Table 3.15. continued.

Run	Sequence of determination	Constant Temp. T_c °C	Constant Pressure P_c cm.	Rate mmoles $min.^{-1}$
17	8.	40.2	6.37	0.046
	9.	"	12.34	0.098
	10.	"	40.54	0.481
	11.	"	24.41	0.247
	12.	"	18.43	0.176
	13.	"	24.41	0.445
	14.	"	6.37	0.075
	15(a).	"	40.54	0.890
		rate transition		
	15(b).	40.2	40.54	0.705
	16.	"	24.41	0.325
	17.	"	12.34	0.136
	18.	"	32.49	0.470
	19.	"	18.43	0.216
	20.	"	24.41	0.306
	21.	"	6.37	0.060
	22.	"	40.54	0.558
	23.	"	24.41	0.231
	24.	"	12.34	0.102
	25.	"	32.49	0.333
	26.	"	18.43	0.158
18	3.	100.0	24.41	0.232
	4(a).	"	24.41	0.221
		rate transition		
	4(b).	100.0	24.41	0.275

Table 3.15. continued.

Run	Sequence of determination	Constant Temp. T_c °C	Constant Pressure P_c cm.	Rate mmoles $min.^{-1}$
18	5.	100.0	24.41	0.283
	6(a).	"	40.54	0.739
		rate transition		
	6(b).	100.0	40.54	0.634
	7.	"	24.41	0.256
	8.	"	12.34	0.094
	9.	"	32.49	0.456
	10.	"	18.43	0.166
	11.	"	6.37	0.033
	12.	"	24.41	0.543
	13.	"	40.54	0.985
	14.	"	24.41	0.402
	15.	"	6.37	0.043
	16.	"	18.43	0.267
	17.	"	32.49	0.660
	18.	"	12.34	0.111
	19.	"	24.41	0.398
	20.	"	24.41	0.435

These curves now showed rates increasing with $(\text{pressure})^n$ where n was approximately 1.6, as determined from the slopes of the log (rate)/log p plots, Fig. 3.26. Values of n so obtained are given in Table 3.16.

FIG. 3.26. PRESSURE DEPENDENCE.

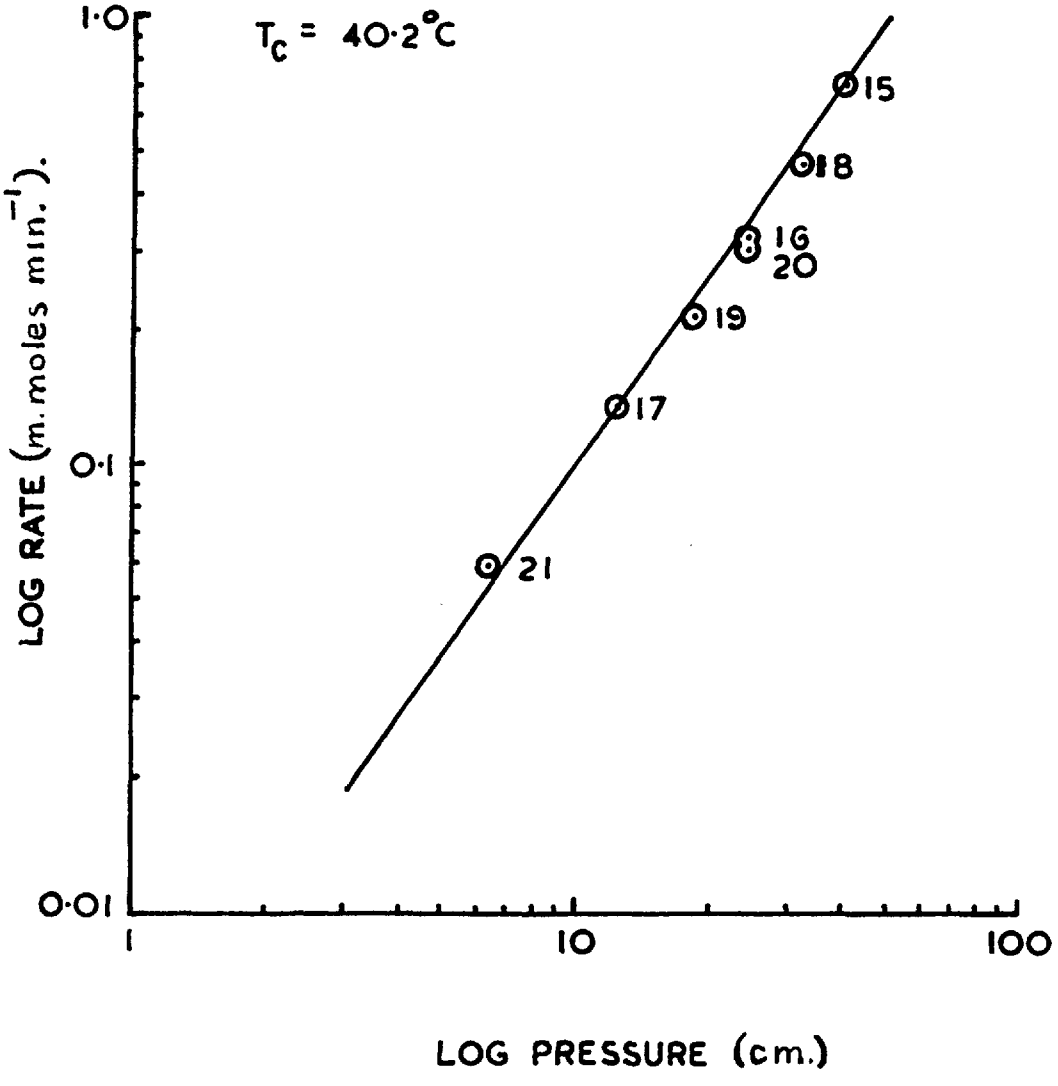


Table 3.16.

Run	Series	T_c °C	n	Average
17	5,6,7,8,9,10,11.	40.2	1.55	
	15,16,17,18,19,20,21.	40.2	1.47	
18	6(b),7,8,9,10,11.	100.0	1.67	
	13,14,15,16,17,18,19.	100.0	1.73	1.6

3.2.4. Dependence of Rate on Temperature.

The variation of rate with temperature was examined at two pressures, 24.41 cm.Hg and 12.34 cm.Hg, at three temperatures 0, 20, and 40°C in run 18. A great deal of scatter was observed, as usual, when attempting rate recoveries, for the lower pressure determinations.

Rates were also determined in run 14 at 40, 60, 80, 100, 120, 140, and 160°C at a pressure of 20.58 cm.Hg in order of increasing temperature. The results obtained are set out in Table 3.17.

Table 3.17. Dependence of rate on temperature.

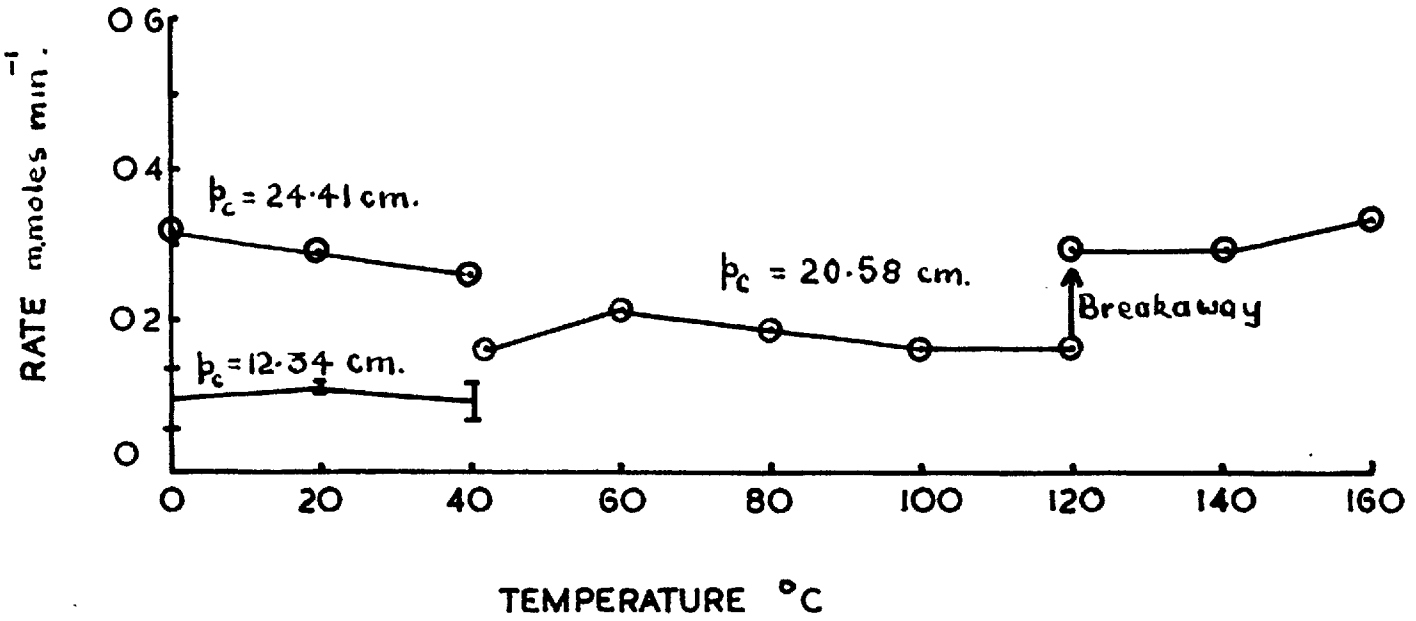
Run	Sequence	P_c cm.	T_c °C	Rate mmoles $min.^{-1}$
14	1.	20.58	42.0	0.160
	2.	"	60.4	0.214
	3.	"	80.0	0.188
	4.	"	100.0	0.162
	5.	"	120.0	0.164
		rate transition occurred		
	6.	"	120.0	0.295
	7.	"	140.5	0.294
	8.	"	160.0	0.335
18.	1.	12.34	0.0	0.088
	2.	"	19.5	0.107
	3.(a)	"	40.2	0.084
		rate transition		
	3.(b)	12.34	40.2	0.096

Table 3.17. continued.

Run	Sequence	P_c cm.	T_c °C	Rate mmoles $min.^{-1}$
18	4.	12.34	19.7	0.105
	5.	"	0.0	0.143
	6.	"	40.2	0.072
	7.	"	0.0	0.120
	8.	"	19.7	0.122
	9.(a)	"	40.2	0.106
		rate transition		
	9.(b)	12.34	40.2	0.120
	10.	"	0.0	0.055
	11.	24.41	0.0	0.312
	12.	"	19.7	0.290
	13.	"	40.2	0.258

At the lower pressure, in run 18, the spread of error of the various determinations at the three temperatures, 0°C, 19.7°C and 40.2°C is 0.099 ± 0.044, 0.1145 ± 0.0075 and 0.120 ± 0.048 mmoles $min.^{-1}$ respectively. These results are plotted in Fig. 3.27. directly against temperature and it can be seen that, taking into consideration the magnitude of indeterminacy in the rate measurements, no dependence of rate on temperature is indicated.

FIG. 3.27. TEMPERATURE DEPENDENCE (RUNS 14 and 18).



3.2.5. Appearance of Reaction Product.

The Li_3N produced was hard, brittle and reddish brown in colour. If chipped with a chisel, conchoidal fractures developed in some cases; in others, fractures developed along parallel laminated cleavage planes. The surface was covered with macroscopic cracks which tended to lie in concentric circles on the surface laced with cracks in a radial direction extending between the circular ones. These cracks appeared to be perpetuated through the bulk of the crust.

It was obvious that large stresses had developed during growth since the originally smooth metallic surface, on changing to the nitride, had become buckled as though contracted downwards by internal stresses. In some cases quite large cavities into the bulk (estimated to be as much as 1 cc. in volume), had been produced, probably due to initial preferential attack down large macroscopic grain boundaries.

The reaction was allowed to proceed to completion in run 14 and chemical analysis of the reaction product showed that total conversion to the nitride had occurred.

3.2.6. Conclusions and Discussion.

Since uptake is linear and rapid after nucleation even at great thicknesses, the rate controlling process is independent of the thickness of the nitride crust. An interstitial diffusion process in a coherent nitride crust is unlikely since this would lead to a decreasing rate as nitride thickness increased.

Frankenberger (see section 1.4.3.), has reported that Li_3N growing on solid lithium, after the formation of an initially uniform relatively impervious layer, changes to a crystalline aggregate porous to nitrogen. This view is consistent with the observation that macroscopic cracks are visible in the reaction product and is in keeping with the Pilling-Bedworth rule since the volume ratio = 0.7 for Li/Li_3N. Similar observations have been reported for the growth of thick crusts of nitride on solid Ca, at relatively low temperatures (109). However, if the metal surface were thus exposed continuously, with the growing crust offering no effective resistance to penetration of nitrogen, the rate of uptake would be constant and controlled by the chemical reaction at the interface, a process requiring an activation energy.

In the present work, however, the activation energy is around zero. It is therefore likely that the rate of uptake is controlled by some physical or mechanical process such as the rate of flow of gas through cracks and pores in

the crust, the number and effective dimensions of which remain statistically constant over a period of time. Once a crack is formed by the stresses predicted by the Pilling-Bedworth rule, it becomes self perpetuating, since crack tips are effective in relieving stresses at smaller stresses than required for the formation of new cracks; thus the number of cracks will tend to remain constant at a given temperature and pressure.

Since any form of fluid flow through a porous layer is dependent on the dimensions and number of pores, these must remain effectively constant in the present reaction. It is therefore suggested that only a certain thickness of the crust is effective in restricting the flow. At greater thicknesses, the cracks widen to such an extent that they offer no restriction to flow. In the effective region, the dimensions of the cracks are approximately constant and small enough to produce considerable hindrance to the flow of gas to the metal surface.

Cracking may be regarded as a transition from a less stable to a more stable condition; it is analogous to a phase change, a recrystallization process, and as such would normally proceed from nuclei of the new phase. The nature of the nuclei is inevitably somewhat speculative: they could be dislocations, boundaries of crystallites, independent foreign atoms, or groups of foreign atoms, (147). If as is likely, the stable phase has a higher density than

the metastable one, recrystallization will be attended by a contraction which will induce cracks. Thus according to these considerations a stationary condition would be likely where the rate of cracking equals the rate of growth.

Thus it is suggested that as each new layer of nitride is formed at the metal surface cracks existing above it in the effective portion of the crust continue into the new layer. If, however, this new layer does not immediately change from its metastable condition to the more stable form there will be a lag in crack perpetuation in the new layer, consequently some of the pores for nitrogen flow will become temporarily inoperative, and a sudden rate decrease will occur, although maintaining a linear rate, until the lag period is terminated when the rate will again increase. Thus local stress fluctuations in the crust in the vicinity of the metal interface, producing a lag in adjustment from the meta to the stable condition, would account for sudden increases or decreases in rate, although considered statistically over a sufficient period of time, approximate linearity would be likely.

The initial catastrophic increases in rate observed in the relatively thin crusts of nitride after the nucleation period, are to be expected on this reasoning since they would represent the initiation of entirely new cracks in the crust, as the stress increased with increasing thickness.

The form of the curve obtained for the pressure dependence with an exponent of approximately 1.6 is not inconsistent with the above model.

Since cracks and pores of varying size will be present in the effective region of the growing crust, some pores will exhibit streamline and others Knudsen flow.

For streamline flow under isothermal conditions, involving a compressible fluid which obeys the gas law, the rate of flow (molecules $sec.^{-1}$)

$$\frac{dn}{dt} = k_1 \frac{p_1^2 - p_2^2}{L}, \qquad (1)$$

whereas for Knudsen flow

$$\frac{dn}{dt} = k_2 \frac{p_1 - p_2}{L}, \qquad (2)$$

where p_1 is the pressure on the outer side of the effective region of the crust and p_2 (assumed to be zero here), is that at the Li/Li_3N interface. L is the thickness of the effective region, assumed constant in the present case. Since $\frac{dn}{dt}$ = the rate of uptake of nitrogen, equation (1) reduces to

$$\text{rate of uptake of } N_2 \propto p_1^2$$

and equation (2) reduces to

$$\text{rate of uptake of } N_2 \propto p_1.$$

Thus for wholly streamline flow the rate of uptake should be proportional to the square of the pressure while for wholly Knudsen flow, the rate should be directly

proportional to pressure. For a (Gaussian) distribution of pore sizes, with the maximum number in the Knudsen region, a flow rate varying with pressure having a value of the exponent between 1 or 2 may be expected.

3.3. Nitridation of Molten Lithium.

Little is known of the kinetics of oxidation or nitridation of molten metals, probably because of the difficulties of working at high temperatures, and the consequent complications ensuing from the volatility of the metal. In this regard, lithium, with the relatively low melting point of 186°C, combined with a low vapour pressure, even at temperatures well in excess of the melting point, provides ideal conditions for study. Since lithium reacts freely with nitrogen below and above the melting point, a direct comparison of the effect of both a solid and a liquid substrate upon the reaction kinetics may be made.

3.3.1. Kinetics of Nitridation.

The uptake of nitrogen, w millimoles, against time t, in minutes, is shown for two runs at 618.5°K in Fig. 3.28. The uptake decreases with time, i.e. a protective film is formed in contrast with the non protective film found with the solid metal. When w^2 is plotted against time Fig. 3.29., the plot is linear over a period of 100 minutes with some deviations at the beginning and end of the run for run 2, indicating approximate obedience to the parabolic law. For run 1, where two discontinuities were evident, the w^2/t plot exhibits linear portions of slightly different slope, between the discontinuities. However, if the whole curve is smoothed, then approximate obedience to the

parabolic relation is still maintained over the whole run.

Other kinetic laws, such as the log forms and the asymptotic equation were tested, but agreement was less good.

FIG.3.28. KINETIC PLOTS OF NITRIDATION OF MOLTEN LITHIUM.

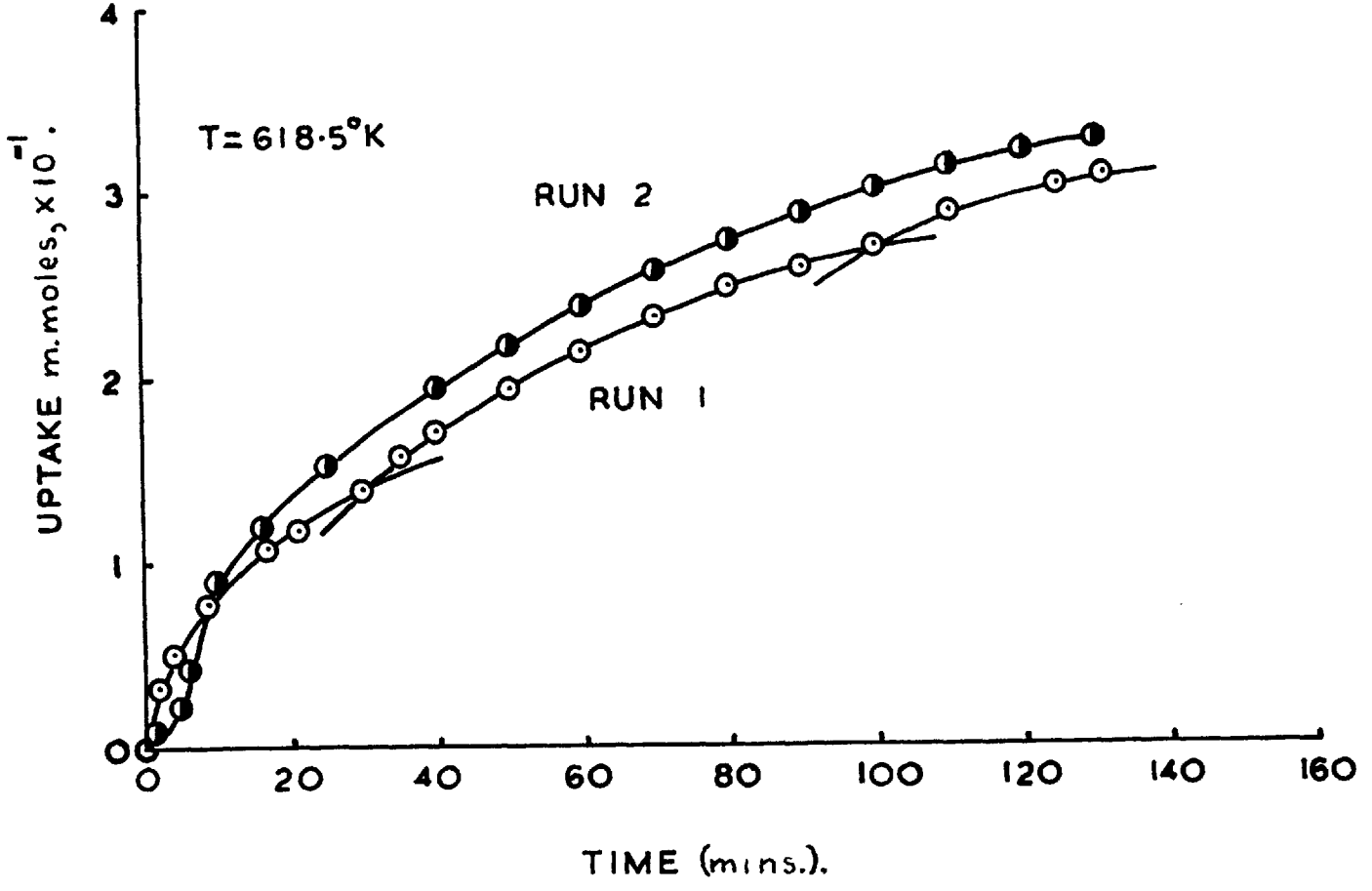
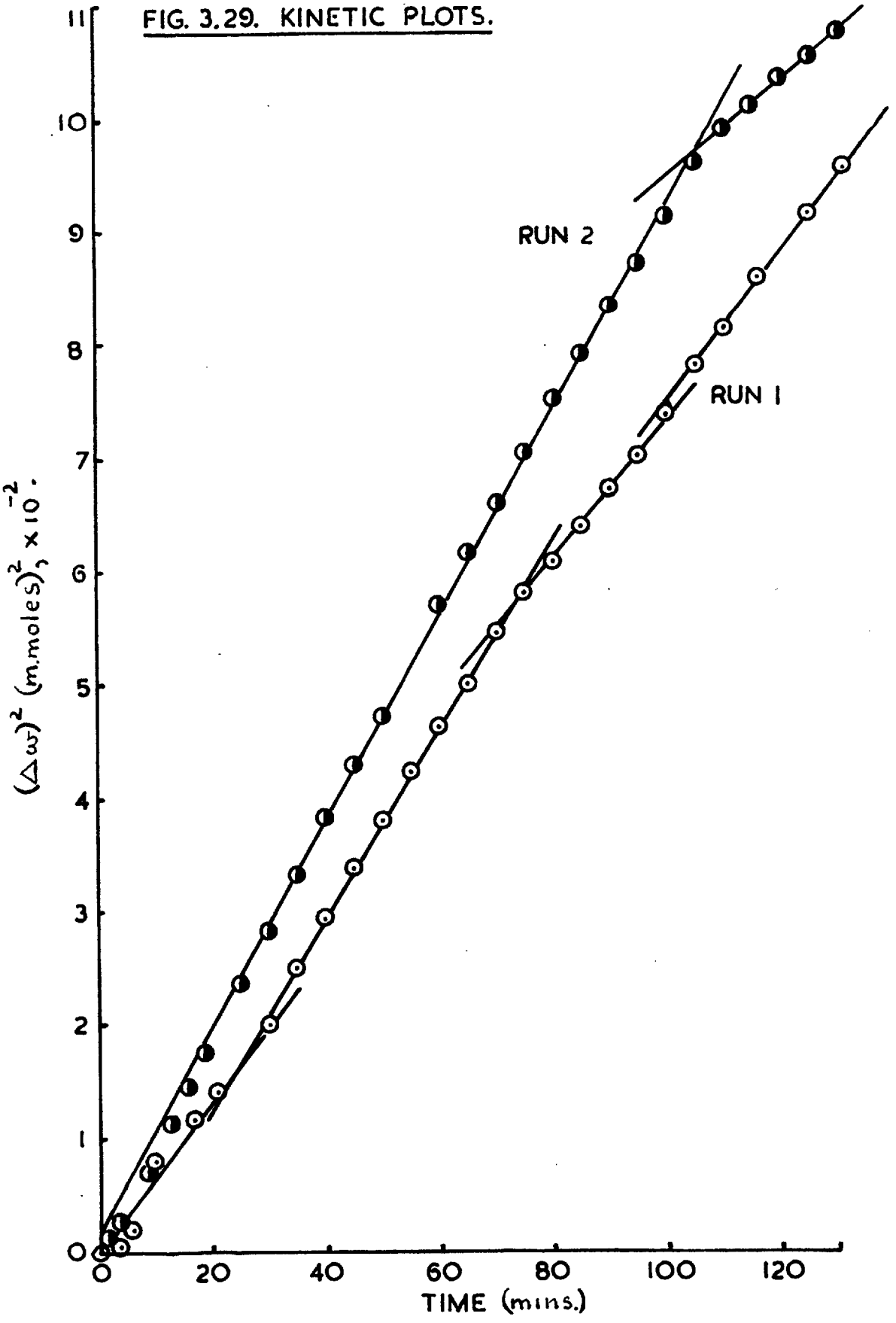


FIG. 3.29. KINETIC PLOTS.



3.3.2. Dependence of Rate on Temperature.

Activation energies were determined at a constant pressure of 10.43 cm. Hg over the range 499°K to 638°K, by determining rates over a series of both rising temperatures (run 6) and falling temperatures, (run 3, 4, 5).

All runs except the kinetic determinations were done on previously nitrided surfaces.

At the end of each constant temperature rate determination, the reaction vessel was evacuated in order to maintain conditions as invariant as possible during the period required to establish thermal equilibrium at the new temperature, often a lengthy operation (as long as 60 minutes) on account of the large heat capacity of the metal reaction vessel and contents, and the relatively poor heat transfer between the furnace and the vessel. In this manner, rates at different temperatures were obtained at virtual constant thickness of nitride film. The method adopted for decreasing temperature runs, was to allow nitridation to proceed until the rate had dropped to a relatively low, but nevertheless easily measurable value at the highest temperature. The reaction was then stopped by pumping away the residual gas. The rate was determined graphically by drawing a tangent to the last portion of the curve, since the curvature was appreciable. The temperature was then lowered to the next constant value and the curve

re-characterized. The rate was sufficiently reduced at the lower temperatures for the uptake to be small compared to that at the highest temperature. Consequently the curvature of the w/t plot at the lower temperatures was not appreciable and negligible error in the rate was introduced by regarding the lower temperature curves as linear. The uptake was followed for periods of 40 to 80 minutes. Deviations from linearity, with a slightly faster rate of uptake, were usually observed in the first 5 to 6 minutes when fresh nitrogen was added at the new constant temperature. See Fig. 3.30. This portion of the curve was attributed to diffusion of excess lithium to the Li_3N/vacuum interface during the time necessary for attaining steady state conditions between rate determinations, and was therefore neglected.

A typical set of empirical w/t plots for increasing temperature are given in fig. 3.30. (run 6).

The activation energy was calculated from the slope of the Arrhenius plot of log rate/$\frac{1}{T}$, Figs. 3.31, 3.32, and the values so obtained are listed in Table 3.18. The average value of the activation energy was 15.42 ± 0.34 kcal.mole^{-1}.

FIG.3.30. EMPIRICAL TEMPERATURE DEPENDENCE PLOTS. (RUN 6).

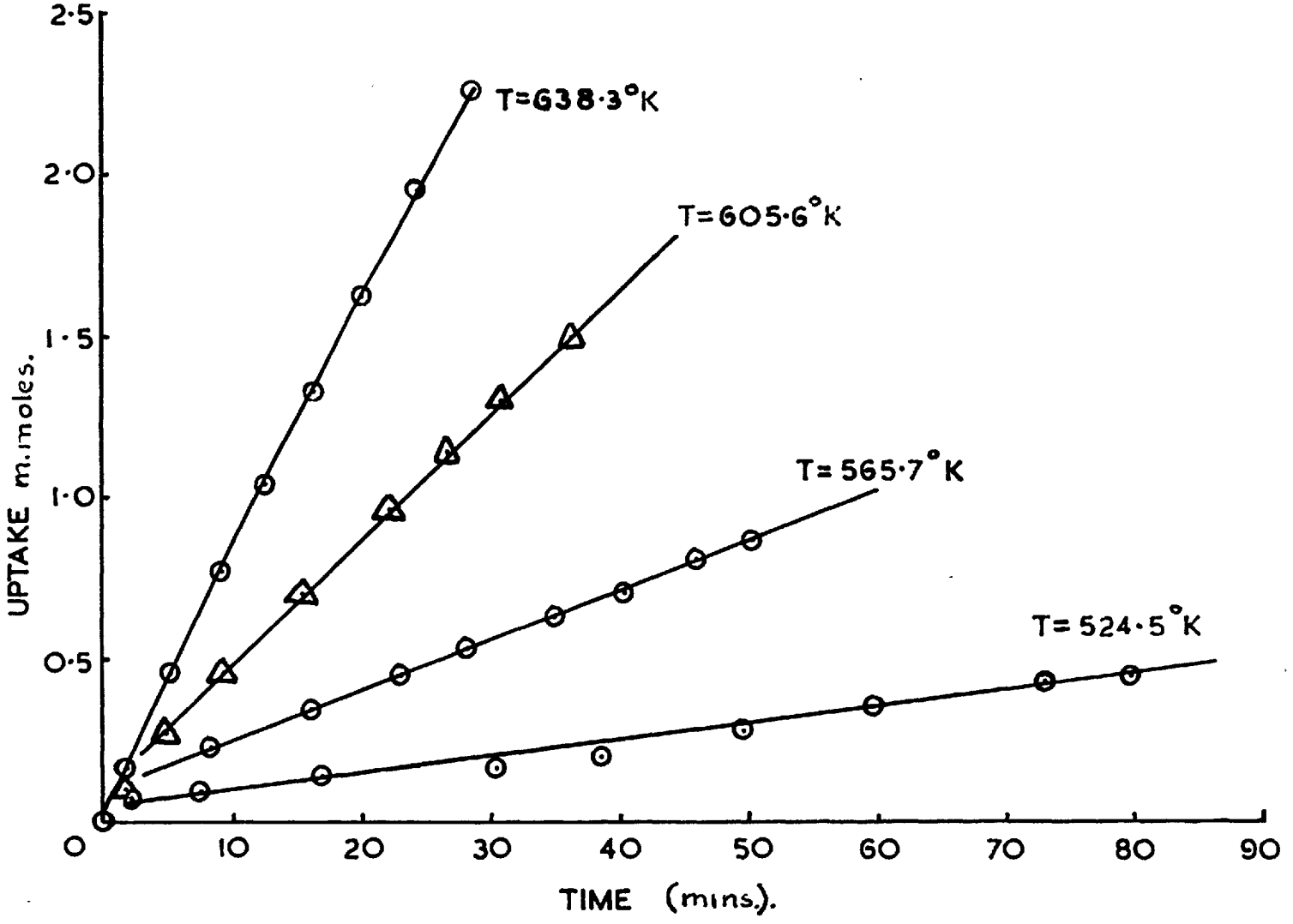


Table 3.18. Activation energy data.

Run	$T^{o}K$	Rate mmoles $min.^{-1}$	E $kcal.mole^{-1}$
3	618.5	0.1145	
	579.3	0.0306	
	548.2	0.0121	
	516.5	0.0051	
4	618.5	0.0375	
	576.9	0.0222	
	548.1	0.0121	
	512.8	0.0078	15.75*
5	624.3	0.0760	
	584.6	0.0288	
	558.5	0.0143	
	529.6	0.0093	
	499.0	0.0041	15.08
6	524.5	0.0051	
	565.7	0.0151	
	605.6	0.0380	
	638.3	0.0790	15.45

*Runs 3 and 4 were incorporated into a single Arrhenius plot.

FIG 3 31 ARRHENIUS PLOT (RUN 5) DECREASING TEMPERATURE.

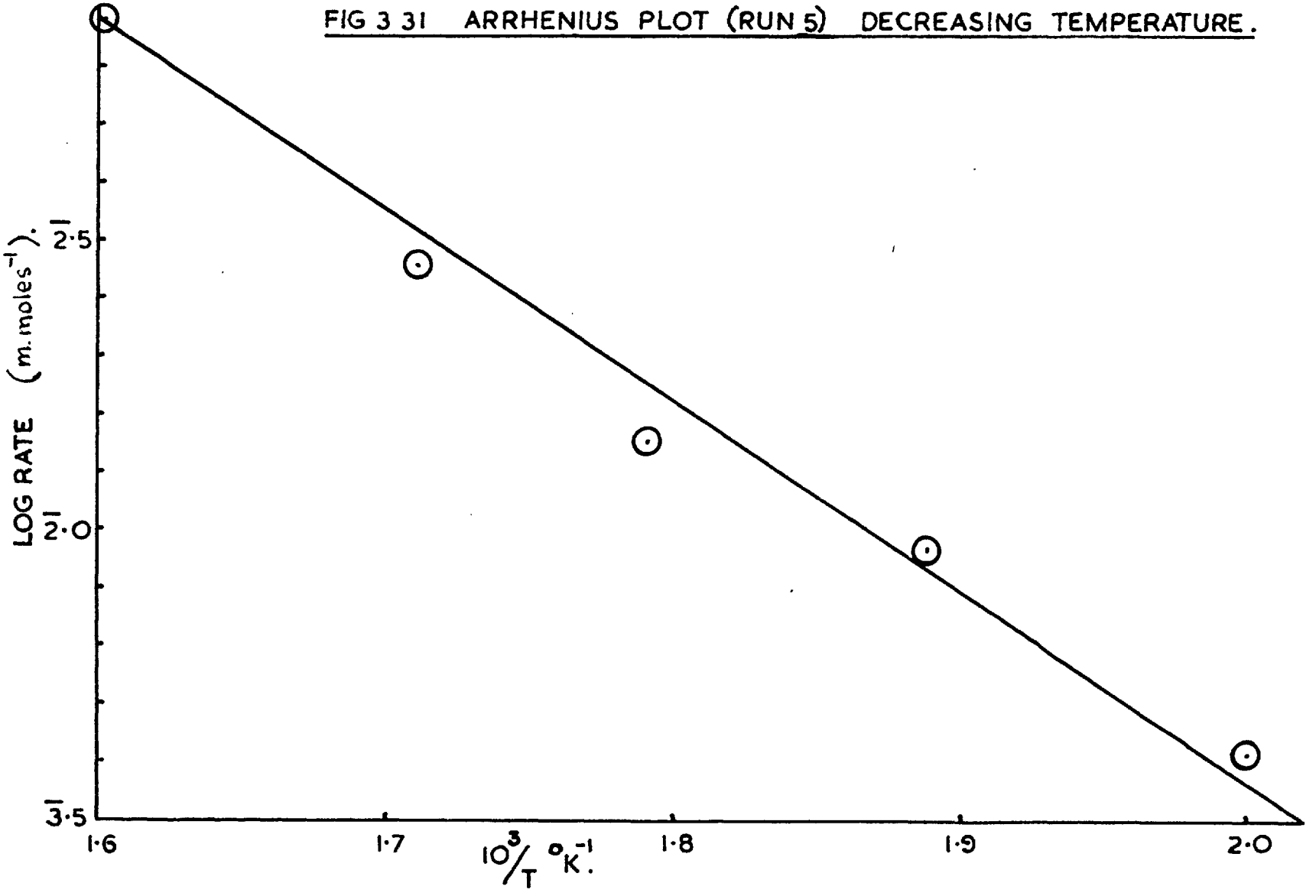
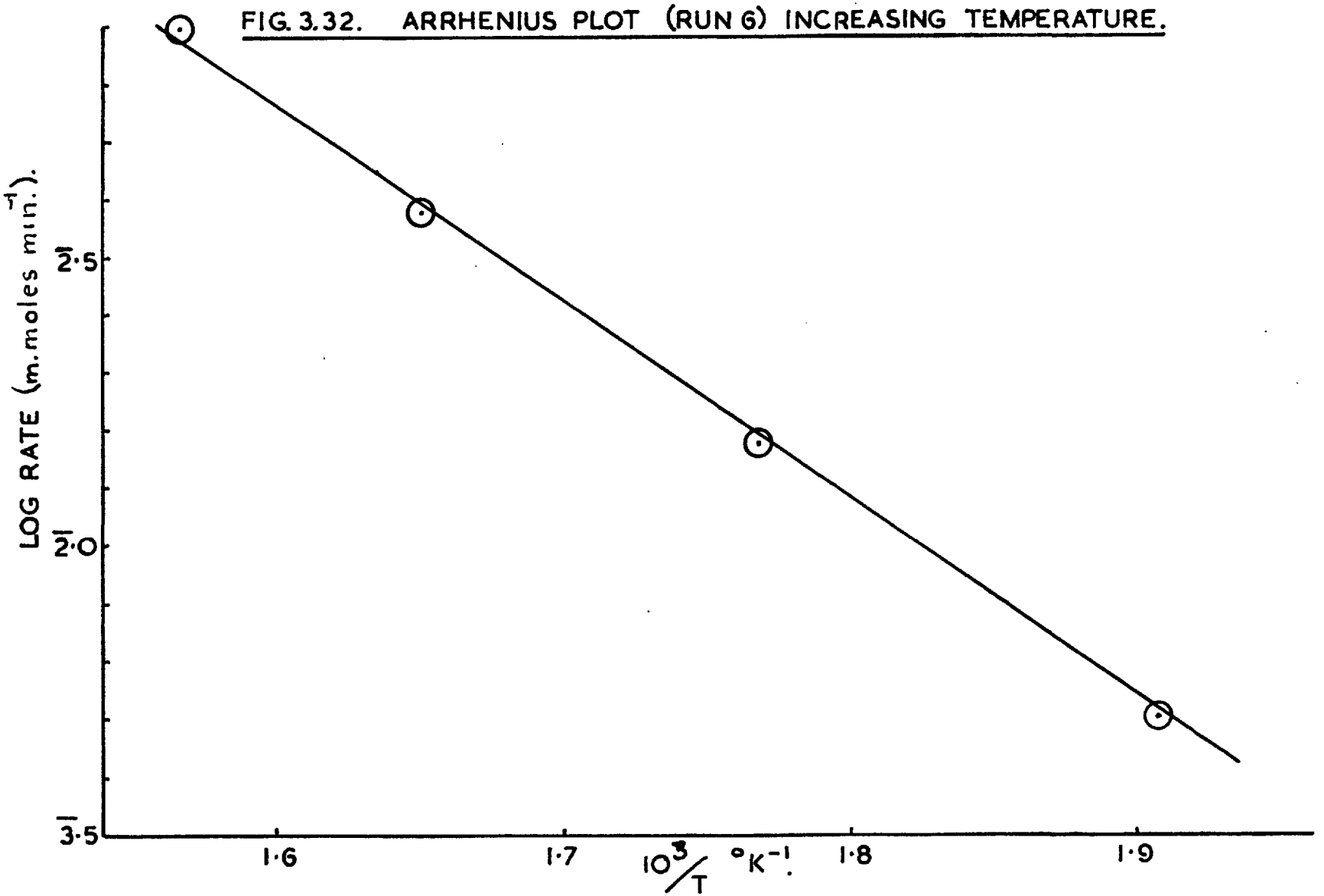


FIG. 3.32. ARRHENIUS PLOT (RUN 6) INCREASING TEMPERATURE.



3.3.3. The Dependence of Rate on Pressure.

The effect of pressure on the rate was examined over the range 10.43 cm. Hg to 44.44 cm. Hg, at three constant temperatures, 499.8°K, 516.2°K and 638.0°K. Since the determinations were carried out at large uptakes, the rates were relatively small and in all cases the curvature of the w/t plots was not appreciable.

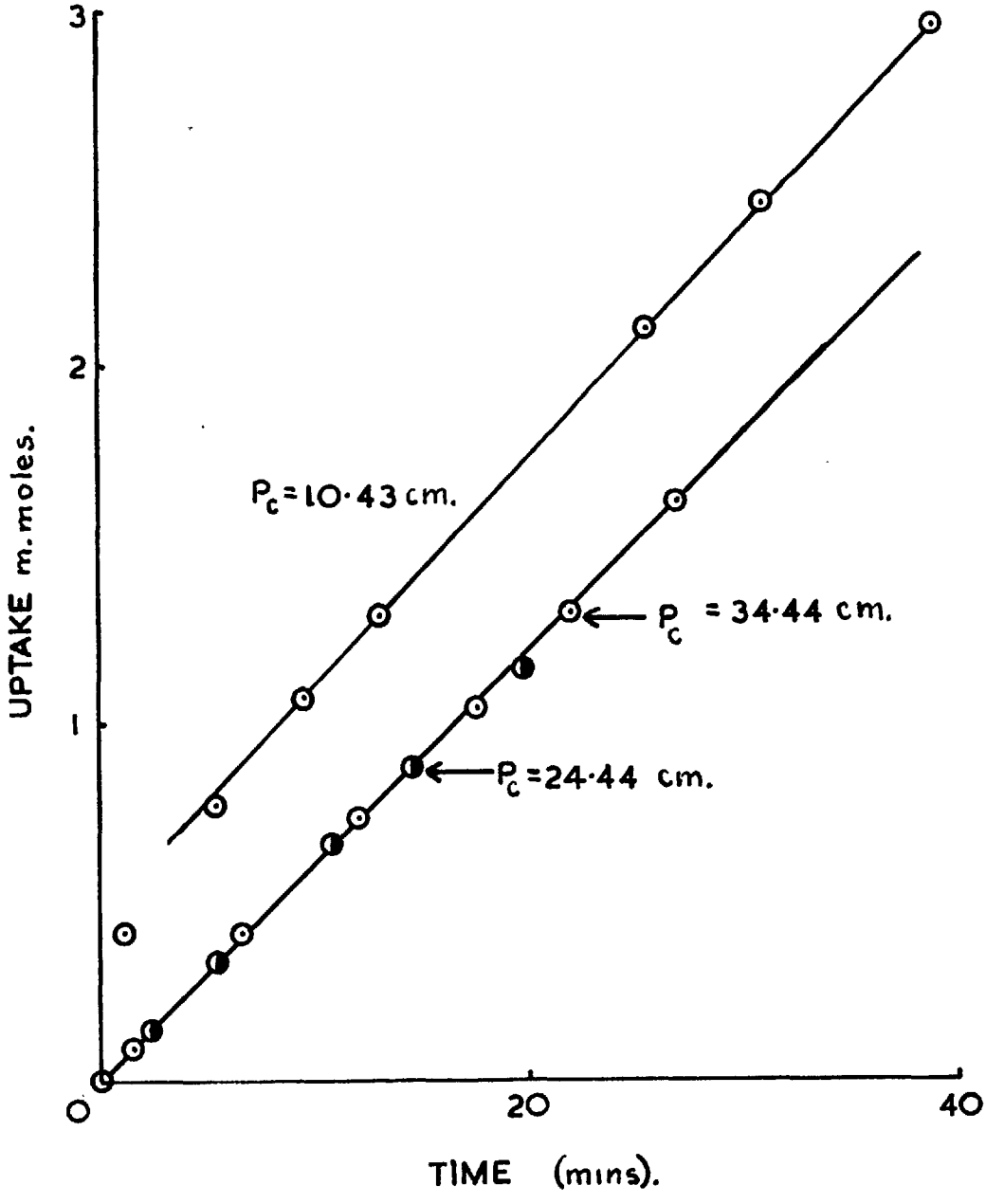
A typical set of empirical w/t plots at 638.0°K is shown in fig. 3.33., and the values of the rates so obtained are listed in table 3.19.

Within the limits of experimental error no effect of pressure on the rate was found.

Table 3.19. Pressure dependence.

Run	T°K	P cm.	Rate mmoles $min.^{-1}$
7	516.2	10.43	0.0042
		18.44	0.0043
		30.44	0.0053
8	499.8	10.43	0.0031
		18.44	0.0028
		28.44	0.0033
		44.44	0.0032
9	638.0	10.43	0.0635
		34.44	0.0600
		34.44	0.0600

FIG 3.33. PRESSURE DEPENDENCE (RUN 9.).



3.3.4. Appearance of the Reaction Product.

The surface of the crust was smooth and dull red-grey in colour. On sectioning it was noted that the crust consisted of an aggregate of small translucent ruby red crystals, closely packed with their longest axis oriented vertically to the lithium surface. The crystal habit could not be distinguished.

3.3.5. Discussion.

It is evident that the kinetics of nitridation of molten lithium are quite different from that for the solid metal. On general considerations this is to be expected. Three possible mechanisms are considered, viz. The rate controlling process is a reaction (i) occurring wholly or partly in the vapour phase, (ii) dependent on the rate of bombardment of gaseous nitrogen molecules at the reaction interface, and (iii) limited by the diffusion of a reactant through an intervening nitride crust.

The first can be eliminated because a reaction taking place in the vapour phase would be pressure dependent. This follows from kinetic theory considerations because the collision frequency between the reacting species must depend on their pressure in the gas phase - the form of the pressure dependence being determined by the particular mechanisms operating. However, in the present investigations the rate was found to be independent of the pressure.

Furthermore, the experimental activation energy for a gas phase reaction must be at least equal to the latent heat of vapourization of lithium, i.e. 38.9 kcal.mole^{-1}. The experimentally determined activation energy, however, is only 15.5 kcal.mole^{-1}.

In addition, for a vapour phase reaction, copious deposits of the reaction product on the walls of the

reaction space would be expected. In fact, the amount was negligible compared with that in the nitride crust at the lithium interface.

The second possibility is suggested from a comparison of calculated and observed rates of reaction. The number of nitrogen molecules colliding with the surface per second, for a given temperature and pressure is, from the kinetic theory of gases,

$$\mu = P\left(\frac{M}{2\pi RT}\right)^{\frac{1}{2}}$$

where μ = mass $sec.^{-1}$ striking the surface per $cm.^2$, P = pressure, M = molecular weight and the other symbols have their usual meanings.

This gives 5.6×10^{23} for the number of nitrogen molecules striking the total surface area of the nitride crust per second, at $588.2^{o}K$ and 10.43 cm. Hg. Using the experimental activation energy of 15.5 $kcal.mole^{-1}$ the calculated rate of reaction is 11.2×10^{17} compared with the experimental value of 2.7×10^{17}. For this type of calculation the agreement is good. Despite the numerical agreement, this mechanism is unlikely since the rate should again be pressure dependent.

The fact that the kinetics of the uptake obey the parabolic law approximately suggests that the rate controlling process is one of diffusion of a reactant through a relatively homogeneous layer of nitride growing at the lithium surface.

For a nitride layer growing on the mobile surface of a liquid, as contrasted with the rigid surface of a solid, the Pilling-Bedworth principle is not applicable, since stresses due to disparities between atomic volumes and substrate/epitaxial lattice parameters do not exist. It is therefore likely that growth of the nitride proceeds freely with its normal unstrained crystal structure, without the production of cracks and porosity as found for the solid metal.

It is assumed here that the crust growing on the liquid surface is virtually sealed to the sides of the metal reaction vessel and prevents access of gas directly to the liquid interface or flow of liquid metal to the surface via gaps between the crust and the walls. Now it is apparent from figs. 3.28 and 3.29 (run 1) that there are minor discontinuities, the plot between these being, however, parabolic in form. These discontinuities are probably due to cracks appearing in the peripheral region between the crust and the metal walls, thereby allowing short periods of direct access of gas to the liquid interface.

To account for the rate being independent of pressure, a reasonable assumption is that the rate controlling step is the rate of arrival, at the surface, of metal ions soluble in the uniform Li_3N layer that diffuse outwards from the liquid interface, under a chemical potential gradient.

This diffusion process depends only on the steady state conditions at the liquid interface, and is therefore independent of pressure, although dependent on temperature.

The value of 15.42±0.34 kcal.mole^{-1} obtained for the experimental activation energy compares reasonably well with the value of 16.98±0.90 kcal.mole^{-1} obtained by Longton (106), for a slightly higher range of temperature and pressure.

This energy term comprises the heat of solution of lithium in the Li_3N lattice and the energy of activation of diffusion, or mobility, within the Li_3N lattice, but separation of these two terms can not be made without further assumptions.

REFERENCES

1. Pauling, L., J. Am. Chem. Soc. 1927, 49, 765.
2. Hermann, G. and Wagener, S., The oxide coated cathode. Chapman and Hall, London, 1951, 1.c. Chap.2.
3. Hart, R.K., Proc.Roy.Soc., 1956, A236, 68.
4. Tamman, G., and Koster, W., Z. anorg.Chem. 1922, 123, 196.
5. Evans, U.R., Trans. Electrochem.Soc. 1924, 46, 247.
6. Dunn, J.S., Proc.Roy.Soc., 1926, A111, 210.
7. Vernon, W.H.J., Akeroyd, E.I. and Stroud, E.G., J. Inst. Met., 1939, 65, 301.
8. Lustman, B and Mehl, R., Trans.Amer.Inst.Min.Met.Eng., 1941, 143, 246.
9. White, A.H. and Germer, L., Trans. Electrochem.Soc., 1942, 81, 305.
10. Uhlig, H.H. and Brenner, A., Acta.Met., 1955, 3, 108.
11. Tylecote, R., J. Inst.Metals, 1950, 78, 327.
12. Lustman, B., Trans. Electrochem.Soc., 1942, 81, 359.
13. Winterbottom, A., J. Iron and Steel Inst. 1950, 165, 9.
14. Vernon, W., Calnan, E., Clews, C. and Nurse, T., Proc. Roy.Soc. 1953, A216, 375.
15. Davies, D., Evans, U and Agar, J., Proc.Roy.Soc., 1954, A225, 443.
16. Scheuble, W., Z. Physik. 1953, 135 125.
17. Steinheil, A., Ann.Physik., 1934, 19, 455.
18. Waber, J., Sturdy, G. and Wise, E., J. Amer.Chem.Soc., 1953, 75, 2269
19. Waber, J., Sturdy, G., Wise, E. and Tipton, C., J. Electrochem.Soc., 1952, 99, 121.

20. Mott, N.F., Trans. Farad.Soc., 1947, 43, 429.

21. Mott, N.F. and Cabrera, N., Reports on Progress in Physics. 1948-49, XII, 163.

22. Roberts, M.W. and Tompkins, F.C., Proc.Roy.Soc., 1959, A251, 369.

23. Rhodin, T.N., Jr., J. Amer.Chem.Soc., 1950, 72, 5102.

24. Trapnell, B.M.W. and Lanyon, M.A.H., Proc.Roy.Soc., 1955, A227, 387.

25. Bloomer, R.N., Nature, 1957, 179, 493.

26. Champion, F.A., Trans. Farad.Soc., 1945, 41, 593.

27. Bengough, G.D., Stuart, J.M. and Lee, A.R., Proc.Roy.Soc., 1927, A116, 425.

28. Idem, Ibid, 1928, A121, 88.

29. Idem, Ibid, 1930, A127, 42.

30. Bengough, G.D., Lee, A.R. and Wormwell, F., Proc.Roy.Soc., 1931, A131, 494

31. Idem, Ibid, 1931, 134, 308.

32. Evans, U.R., Nature, 1949, 164, 909.

33. Evans, U.R., The corrosion and oxidation of metals, Butler and Tanner Ltd., Frome and London, 1960, p.840.

34. Evans, U.R., Trans. Amer. Electrochem.Soc. 1947, 91, 547.

35. Tamman, G., Z. anorg.Chem., 1920, 111, 78.

36. Pilling, N.B. and Bedworth, R.E., J. Inst.Met., 1923, 29, 529.

37. Gulbransen, E.A. and Andrew, K.F., J. Electrochem.Soc. 1951, 98, 241.

38. Evans, U.R., Trans. Electrochem.Soc., 1924, 46, 247.

39. Wagner, C., Z. phys.Chem., 1933, B 21, 25.

40. Wagner, C., Atom Movements., Amer.Soc.Metals, Cleveland, Ohio, 1950, p.153.

41. Lustman, B., Metal.Progr., 1950, 57, 629.

42. Levesque, P. and Cubicciotti, D., J. Amer.Chem.Soc., 1951, 73, 2028.

43. Dunn, J.S. and Wilkins, F.J., Rev. of Oxidation and Scaling of Heated Solid Metals., D.S.I.R., 1935, p.67.

44. Kubaschewski, O. and Hopkins, B.E., Oxidation of Metals and Alloys. Butterworths 1953.

45. Pfeil, L.B., J. Iron and Steel Inst., 1929, 119, 501.

46. Himmel, L., Mehl, R.F. and Birchenall, C.E., J. Metals, 1953, 7, 827.

47. Bardeen, J., Brattain, W.H. and Shockley, W., J. Chem. Phys., 1946, 14, 714.

48. Vermilyea, D.A., Acta.Met. 1957, 5, 492.

49. Mallett, M.W., Albrecht, W.M. and Bennett, R.E., J. Electrochem.Soc., 1957, 104, 349.

50. Charles, R.G., Barnartt, S and Gulbransen, E.A., Trans. Met.Soc., A.I.M.E., 1958, 212, 101.

51. Waber, J.T., J. Chem.Phys. 1952, 20, 734.

52. Tylecote, R.F., J. Inst.Met., 1952-53, 81, 681.

53. Campbell, W.E. and Thomas, U.B., Trans. Electrochem.Soc., 1947, 91, 623.

54. Evans, U.R., The corrosion and oxidation of metals., Butler and Tanner Ltd., From and London, 1960, p.832.

55. Uhlig, H.H., Acta Met. 1956, 4, 541.

56. Bardolle, J. and Bénard, J., Rev. Métallurg, 1952, 49, 613.

57. Gulbransen, E., McMillan, W.R. and Andrew, K.F., Journal of Metals, 1954, 200, 1027.

58. Frenkel, J., Z. fur Physik. 1926, 35, 652.

59. Wagner, C. and Schottky, W., Z. für phys.Chem. 1930, (B) 11, 163.

60. Wagner, C., Z. für phys.Chem., 1936, (B) 32, 447.

61. Idem, Ibid, 1933, (B) 22, 181.

62. Mott, N.F. and Gurney, R.W., Electronic Processes in Ionic Crystals, Clarendon Press Oxford, 1940, p.28.

63. Ref. 62, p.63.

64. Lennard-Jones, J.E., Trans. Faraday Soc., 1932, 28, 333.

65. Mott, N.F., Trans. Faraday Soc., 1940, 36, 472.

66. Hauffe, K. and Ilschner, B., Z. Electrochem.Ber. Bunsenges.Physik.Chem. 1954, 58, 382.

67. Dushman, S., Elements of Quantum Mechanics, p.67.

68. Gwathmey, A.T., and Cunningham, R.E., Adv. in Cat., Vol. 10, 1958, 57.

69. Fishbeck, K. and Salzer, F., Metallwirtschaft, 1935, 14, 753.

70. Uhlig, H.H. and Pickett, J.J. unpublished data referred to in ref.55.

71. Uhlig, H.H. and Brasunas, A.S., J. Electrochem.Soc., 1950, 97, 448.

72. Ref. 62, pp. 80-88.

73. Uhlig, H.H., J. Appl.Phys. 1951, 22, 1399.

74. Hirschberg, R. and Lange, E., Naturwissenschaften, 1952, 39, 187.

75. Torrey, H. and Whitmer, C., Crystal Rectifiers, McGraw Hill, New York, 1948, p.22.

76. Ref. 62, p.176.

77. Hauffe, K., J. Chim.Phys., 1956, 53, 855-70.

78. Hauffe, K., Kinetics of High Temperature Processes. Ed. Kingery, 1959.

79. Hoar, T.P. and Price, L.E., Trans. Far.Soc., 1938, 34, 867.

80. Wagner, C. and Grunewald, K., Z. phys.Chem. 1938, B40, 455.

81. Ref. 33, p.846.

82. Ref. 33, p.833.

83. Ref. 33, p.836.

84. Mellor, J.W., Comprehensive Treatise of Inorganic Chemistry.

85. Liquid Metals Handbook. Atomic Energy Commission, June 1952.

86. Thorpe, J.F., Dictionary of Applied Chemistry. Longmans.

87. Holt, W. and Sims, W.E., J. Chem.Soc., 1894, 65, 432.

88. Pierron, P., Bul.Soc.Chim., 1939, 6, 235.

89. Tyzack, C. and Longton, P.B., U.K.A.E.A. Industrial Group. Progress Report R and DB(C)TN-131. (Declassified reprint) XMPDC/P-5. 1955.

90. Cathcart, J.V., Hall, L.L. and Smith, G.P., Acta Met., 1957, 5, 245.

91. Cathcart, J.V. and Smith, G.P., J. Electrochem.Soc., 1960, 107, 141.

92. Herrington, B.L., J. Phys.Chem. 1934, 38, 675.

93. Moyer, J.W., Phys.Rev., 1951, 83, 877.

94. Howland, W.H. and Epstein, L.F., Ind.Eng.Chem., 1957, 49, 1931.

95. Tyzack, C., Steele, B. and Longton, P.B., U.K.A.E.A. Industrial Group. 1954, Progress Report R and DB(C)TN-79 (Declassified reprint).

96. Ouvrard, L., Comptes R ndue, 1892, 114, 120.

97. Guntz, A., Ibid, 1896, 123, 995.

98. Delandres, Ibid, 1895, 121, 886.

99. Gregg, S.J. and Jepson, W.B., J. Chem.Soc., 1960, 712.

100. Dafert, F.W. and Miklauz, Monatsh, 1910, 31, 981.

101. Inorganic Syntheses. Vol. IV, p.1.

102. Belyaev, A.I., Firsanova, L.A., and Pomerantsev, I.N. Sbornik.Nauch. Trudov.Mosk.Inst. Tsvetnykh Metal i Zolata, 1955, No. 25, 172-9.

103. Besson, J. and Müller, W., Compt.Rend., 1958, 247, 2370.

104. Frankenberger, W., Z. Electrochem., 1926, 32, 481.

105. Soliman, A., J. App.Chem.(London), 1951, 1, 98.

106. Longton, P.B., U.K.A.E.A. Industrial Group. Progress Report No. IGR-TN/C.276, 1955.

107. Sieverts, A. and Brandt, R., Z. f.angen.Chem., 1916, 29, 402.

108. Von otto Ruff and Hartmann, H., Z. anorg.Chem., 1922, 121, 167.

109. Antropoff, A. von and Germann, Z. phys.Chem., 1928, 137, 209.

110. Sthapitanonda, P. and Margrave, J.L., J. Phys.Chem., 1956, 60, 1628.

111. de Graff, J.E. and Hamaker, H.C., Physica, 1942, 9, 297.

112. Trapnell, B.M.W., Proc.Roy.Soc., 1953, A218, 566.

113. Bloomer, R.N., Brit. J. Appl.Phys., 1957, 8, 321.

114. Gulbransen, E.A. and Andrew, K.F., J. Electrochem.Soc., 1950, 97, 383.

115. Cubicciotti, D., J. Amer.Chem.Soc., 1950, 72, 2084.

116. Rhodin, T.N., Int.Conf.on Structure and Props. of Thin Films, Lake George, N.Y., September 1959.

117. Sack, H., Z. Electrochem. 1959, 63, 806-7.

118. Wagener, S., J. Phys.Chem., 1956, 60, 567.

119. Finch, G.I. and Quarrell, A.G., Proc.Roy.Soc., 1933, 141, 398.

120. Boussin, M.L., Crall, L. and Caillat, R., Rév.Mét., 1957, 54, 185.

121. Gulbransen, E.A., Trans. Electrochem.Soc., 1945, 87, 589.

122. Leontis, T.E. and Rhines, F.N., Trans. Amer.Inst.Min. and Met.Eng., 1946, 166, 265.

123. Terem, H.N., C.R. Acad.Sci.(Paris), 1948, 226, 905.

124. Makolkin, I.A., Zh.Prik.Khim., 1951, 24, 460.

125. Murgulescu, I.G. and Cismaru, D., Rev.Chim.(Acad.R.P.R.) 1958, 3, 177.

126. Gregg, S.J. and Jepson, W.B., J. Inst.Met., 1958-59, 87, 187.

127. Fassell, W.M., Gulbransen, L.B., Lewis, J.R. and Hamilton, J.H., J. Metals (N.Y.), 1951, 3, 522.

128. Cubicciotti, D., J. Am.Chem.Soc., 1952, 74, 557.

129. Wagener, S., Nature (Lond.), 1954, 173, 684.

130. Arizumi, T., and Kotani, S., J. Phys.Soc.(Japan), 1952, 7, 300.

131. Solomon, Rev.Sci.Inst., 1950, 21, 570.

132. Handbook of Chemistry and Physics.(40th Ed.) 1958-59, Chemical Rubber Publishing Co. (Cleveland, Ohio).

133. Gordon, A.R., J. Chem.Phys., 1936, 4, 100-2.

134. Dushman, S., Scientific foundations of Vacuum Technique Chapman and Hall (Lond.), 1949.

135. International Critical Tables. McGraw Hill (New York and London).

136. Ref. 132.

137. Bennett, M.J. and Tompkins, F.C., Trans. Far.Soc., 1957, 53, 185.

138. Wyckoff, Crystal Structures.

139. Bennett, M.J. and Tompkins, F.C., In press.

140. Adda, Y., Compt.Rend., 1956, 242, 1?6.

141. Gulbransen, E.A. Ind. and Eng. Chem., 1949, 41, 1385.

142. Huddle, R.A.U., Nuclear and Sci. Congress (Cleveland 1955), paper No. 108.

143. Frank, F.C., and van der Merwe, J.H., Proc.Roy.Soc., 1949, A198, 205.

144. van der Merwe, J.H., Disc. Far.Soc. No. 5, 1949, 201.

145. Blackman, M. and Smollett, M., Proc.Phys.Soc.Lond., 1951, A64, 683.

146. Pashley, D.W., Adv. in Physics, 1956, 5, 173.

147. de Boer, J.H., Disc. Far.Soc., 1957, 23, 171.